Minutes of the meeting of the Departmental Research Project Monitoring Committee (DRPMC) held on 16.01.2024 at 10:00 am in the office of the Dean Faculty of Sciences, University of Jammu, Jammu.

PRESENT:

1. Prof. Anju Bhasin (Convener)
2. Prof. H.N. Sheikh, HOD (HOD Chemistry)
3. Prof. Kamal K. Kapoor (Member)
4. Prof. P.K. Srivastava (Member)
5. Dr. Monika Gupta (Member)
6. Prof. Satya Paul (Special Invitee)
7. Prof. D.S. Sambyal (Special Invitee)

Item No. 1: To consider the progress report of Research & Seed Grant assigned to the following faculty members of the Department of Chemistry:

(i) Prof. K.K. Kapoor (Rs. 2.0 lakh)
(ii) Prof. H.N. Sheikh (Rs. 2.0 lakh)
(iii) Dr. Monika Gupta (Rs. 2.0 lakh)
(iv) Dr. Ashwani Kumar (Rs. 2.0 lakh)

Resolution: The faculty members presented the progress report before the committee members and submitted the hard copy of the same after the discussions and deliberations. The committee members were satisfied with the progress reports of all the projects and appreciated the scientific outcome, especially the sanction of projects by JKSTIC (Prof. K.K. Kapoor, Prof. H.N. Sheikh & Dr. Ashwani Kumar) and submission of SERB-SURE Project to DST, GoI by Dr. Monika Gupta.

Item No. 2: To consider the request of Principal Investigators (PIs) to extend the date of submission of final utilization certificate.

Resolution: The Principal Investigators (PIs) requested to extend the date of submission of final utilization certificate by two months, i.e. March 20, 2024, to enable the PIs to spend the unutilized grant. The DRPMC resolved that the request of PIs be kindly considered for extension by the Dean Research Studies.

The meeting ended with a vote of thanks.

1. _____ 2. _____ 3. _____ 4. _____

5. _____ 6. _____ 7. _____

Office : 2453969
University : 2435248 } Extension : 2617, 2618
: 2435259

Post Graduate Department of Chemistry
University of Jammu
('A+' Grade University- Accredited by NAAC)
Baba Saheb Ambedkar Road, Jammu - 180 006

No. PGD/Chem/ *Dated* 15-01-2024

NOTICE

Due to unavoidable circumstances, meeting of the Department Research Project Monitoring Committee (DRPMC), scheduled for 15-01-2024 at 4.00 pm, will be held on 16-01-2024 at 10.00 am in the Office of the Dean Faculty of Science to discuss progress report of Research and Seed Grant assigned to following faculty members of the department of Chemistry.

1. Prof. K.K. Kapoor
2. Prof. H.N.Sheikh
3. Dr. Monika Gupta
4. Dr. Ashwani Kumar

The concerned faculty members are requested to submit and present progress report in the meeting

The members of the DRPMC are request to make it convent to attend the meeting.

1. Prof. Anju Bhasin (Convener)
2. Prof. H. N. Sheikh (HOD)
3. Prof. K.K. Kapoor
4. Prof. P.K. Srivastava
5. Dr. Monika Gupta
6. Prof. Satya Paul (Special Invitee)
7. Prof. D.S.Sambyal (Special Invitee)

15-01-2024

Prof. H.N. Sheikh
Head of the Department

Copy to:

Prof. Anju Bhasin Dean Faculty of Science for information please

Office : 2453969
University : 2435248 } Extension :
: 2435259 } 2617, 2618

Post Graduate Department of Chemistry
University of Jammu
('A+' Grade University- Accredited by NAAC)
Baba Saheb Ambedkar Road, Jammu - 180 006

No. PGD/Chem/24/ 72-73 *Dated* 11-01-24.

NOTICE

As desired by Dean Faculty of Science, a meeting of the Department Research Project Monitoring Committee (DRPMC) will be held on 15-01-2024 at 4:00 pm in the Office of the Dean Faculty of Science to discuss progress report of Research and Seed Grant assigned to following faculty members of the department of Chemistry.

1. Prof. K.K. Kapoor
2. Prof. H.N.Sheikh
3. Dr. Monika Gupta
4. Dr. Ashwani Kumar

The concerned faculty members are requested to submit and present progress report in the meeting

The members of the DRPMC are request to make it convent to attend the meeting.

1. Prof. Anju Bhasin (Convener)
2. Prof. H. N. Sheikh (HOD)
3. Prof. K.K. Kapoor
4. Prof. P.K. Srivastava
5. Dr. Monika Gupta
6. Prof. Satya Paul (Special Invitee)
7. Prof. D.S.Sambyal (Special Invitee)

Prof. H.N. Sheikh
Head of the Department

Copy to:

Prof. Anju Bhasin Dean Faculty of Science for information please

Progress Report of Research & Seed Money Grant

Amount Rs. 2 lakh

Received under

Quality Assurance Fund (DIQA)

Progress report of the project entitled ***" Designing of recyclable titania based nanomaterials and their applications in synthesis of heterocycles"*** supported by research & seed money grant assistance, cost Rs. 2 lakh, for formulation of research proposal under Quality Assurance Fund (DIQA) of University of Jammu, Jammu.

This project has following outcomes:

1) Research & Seed money grant assistance helped in the procurement of chemicals for carrying out primary research proposal investigation.
2) This grant was further utilized in the preparation of recyclable titania based nanomaterials.
3) First of all undoped Titania (TiO_2) and Copper Nickel co-doped Titania (Cu-TiO2-Ni) are synthesized using a straightforward co-precipitation method. Finally, PolyVinyl alcohol and copper nickel co-doped titania nano-composite was prepared. It was fully characterized by various characterization techniques such as FEG-SEM, HR-TEM, FTIR, TGA, XPS, XRD, Elemental mapping, PL, UV, BET etc. FEG-SEM (Fig. 1) indicates morphology as 3D porous architectures. HR-TEM (Fig. 2) indicates average particle size to be 17 nm. EDX and elemental elements indicate the presence of different types of elements present. **(Fig. 3)**

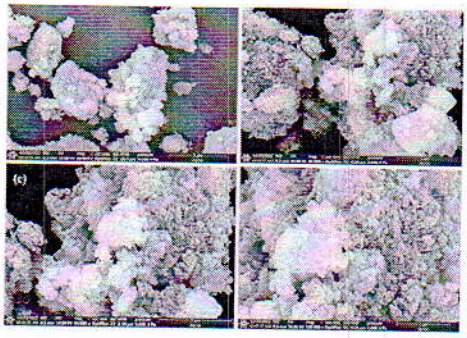

FEG-SEM images **(Fig.1)**

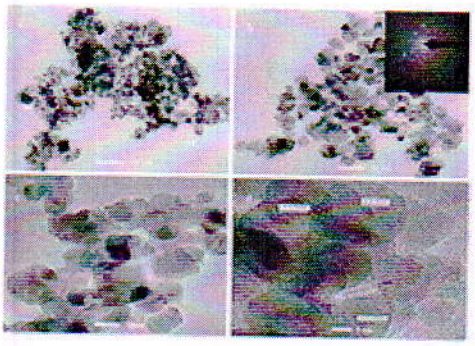

HR-TEM images **(Fig.2)**

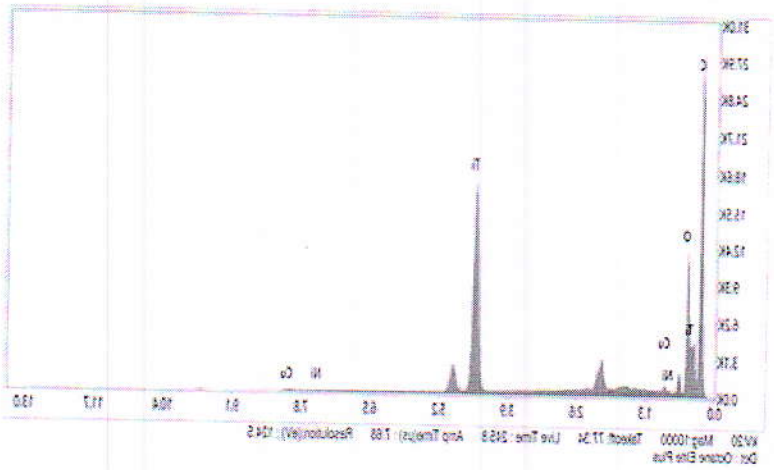

Fig. 3: EDX and elemental mapping

4) Applications of the developed catalyst were explored in the synthesis of heterocycles such as 2-aryl benzimidazoles **(Scheme1)** & 2-aryl benzothiazoles **(Scheme2).**

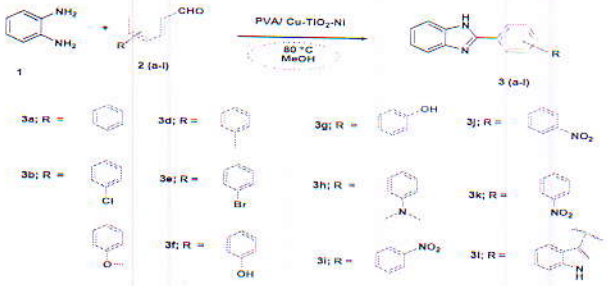

Scheme1: Synthesis of benzimidazole derivatives

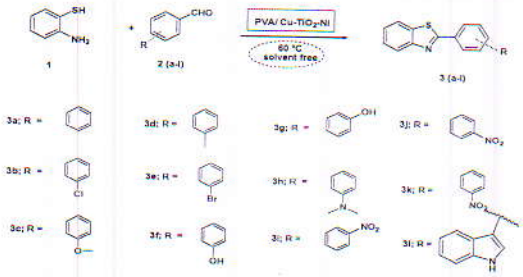

Scheme2: Synthesis of benzothiaziole derivatives

5) Synthesized products were also characterized using 1H &13 CNMR, IR studies.

6) Another application was studied in the optical properties of the developed catalyst. The results showed that the addition of Cu-TiO_2-Ni to PVA improved the material's Ultraviolet–visible spectroscopy (UV) absorption properties. The nanocomposite's photoluminescent activity was evaluated. The photoluminescence (PL) spectra of the PVA/Cu-TiO2-Ni nanocomposite indicated that when the sample was excited at 425 nm, the emission wavelength was around 665 nm **(Fig.4)**

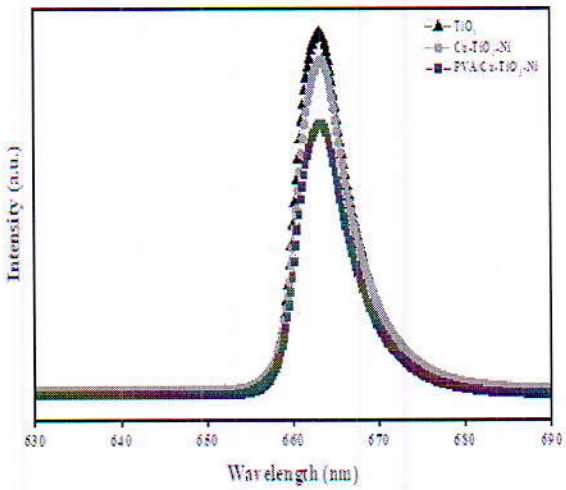

7) Prepared catalyst was found to be recyclable for five consecutive runs what made the process cost-effective and fall in the domain of **Green Chemistry**. Recycled catalyst was also compared with fresh catalyst by using FTIR **(Fig. 5)**

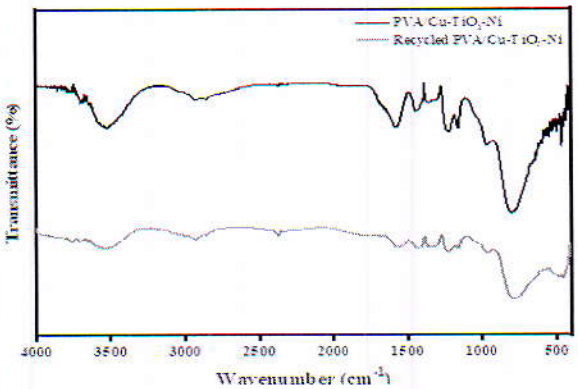

Fig. 5: Comparison of fresh and recycled catalyst

8) Papers are published in International Journal of Repute such as in ***Applied Organometallic Chemistry, ACS Sustainable Chemistry and Engineering (Accepted)***.

9) Research and seed money grant assistance also helped in preparing a complete research proposal.

Objectives and research methodology followed during this research proposal helped me in developing a complete research proposal and which I submitted to funding agency SERB-SURE amounting to Rs. approx. 30 lakh in 2023.

Thanks,

(15.01.24)

Dr. Monika Gupta
(Sr. Assistant Prof.)
PG Department of Chemistry,
University of Jammu,
Jammu.

LIST OF PUBLICATIONS

INTERNATIONAL

2023

1. Ankush Mahajan, **Monika Gupta**, "PVA and copper nickel co doped titania nanocomposite: Designing, characterization, optical properties and catalytic applications in the synthesis of aryl derivatives of benzothiazole and benzimidazole" ***Applied Organometallic Chemistry DOI:10.1002/aoc.7195, 2023, e7195*** **[IMPACT FACTOR: 3.9].**

2024

2. Ankush Mahajan, Ankit Mahajan, Aleksey Kuznetzov, **Monika Gupta,** "Cu@Ag-CeO2/Chitosan Nanocomposite: Green Catalyst for synthesis of 4-Arylidene-Isoxazolidinones & Amidoalkyl Naphthols with DFT and Antimicrobial Studies" ***ACS Sustainable Chemistry and Engineering*** **(Accepted) [IMPACT FACTOR: 8.1].**

Utilization

S.No.	Heads	Amount Sanctioned	Utilized	Unutilized
1	Consumables	1,30,000/-	1,28,668/-	1332/-
2	Equipment	50,000/-	48,800/-	1200/-
3	Contingent grant	20,000/-	18,943/-	1057/-
	Total	**2,00,000/-**	**1,96,411/-**	**3,589/-**

(Dr. Monika Gupta)

OFFICE OF DEAN RESEARCH STUDIES
UNIVERSITY OF JAMMU

ORDER

Based on the recommendations of the Committee constituted for the purpose vide order No. RA/3977-92 dated 05.12.2022 and also on the recommendations of the Dean of the Faculty concerned, sanction is hereby accorded to the payment of Rs. 200,000/- as financial assistance in favour of Prof./Dr. Monika Gupta, Department of Chemistry as per the details given below out of the **Research & Seed Grant** for Professor / Associate / Assistant Professor, under the Head **'Quality Assurance Fund (DIQA)'** as per order No. Fin./2022-23/3338-42 dated 16.09.2022:-

a) Hiring of Services / Honorarium for experts	:	–
b) Equipment (Repair) or any accessory, if needed, to the existing equipment	:	–
c) Purchase of Minor Equipment	:	50,000/-
d) AMC's of existing Equipment	:	–
e) Consumables/Chemicals/Glassware etc.	:	1,30,000/-
f) Contingency	:	20,000/-
g) Field work	:	–
h) Any other item		–
Total	:	2,00,000/-

You are required to meet the said expenditure as per University norms. The Principal Investigator (PI) shall submit the bills for pass & payment as per the existing GFR/GeM guidelines to the Grant Section. The quantum of assistance sanctioned is required to be exhausted/utilized within a period of one year starting from the date of issue of order. Utilization certificate will be submitted after completion of the project.

A detailed report of project shall mandatorily be submitted by PI to the office of the Dean Research Studies with a clear statement on whether the said project has enabled the PI to put up a bigger proposal for funding to any national funding agency.

No. RA/23/6078-85
Dated: 20/01/2023

20/1/23
Assistant Registrar (R&A)

Copy to:

1. Special Secretary to the Hon'ble Vice-Chancellor.
2. Sr. P.A. to DAA/DRS/Registrar/DIQA.
3. Dean of the Faculty concerned.
4. HOD concerned.
5. Principal Investigator.
6. Joint Registrar (Finance).
7. Deputy Registrar (Grants).

DEAN RESEARCH STUDIES
UNIVERSITY OF JAMMU

No. DRS/22/ 3026-3076
Dated: 26/09/2022

ll Heads/Rectors/Director,
niversity of Jammu, Jammu.

ef: - **Order No. Fin./2022-23/3246-52 dated 15.09.2022 & Order No. Fin./2022-23/3338-42 dated 16.09.2022.**

ir/Madam,

ou are requested to apprise the faculty members of your Department/Directorate/Offsite Campus send well formulated Research proposals to the Assistant Registrar (Research and Award) for onsideration of the Authorities, latest by **28.10.2022** in respect of following: -

a. ***Seed Grant for Assistant Professors:***

"Seed Grant for research shall be provided from UoJRF only to Assistant Professors with work experience upto five years from date of joining in University of Jammu. The assistance shall be to the tune of Rs. 1,00,000/- for faculty of Sciences/Life Sciences/Mathematical Sciences and Rs. 50,000/- for faculty from streams other than those mentioned above, to be spent in one year. Further, to apply for seed grant, the Assistant Professor shall be required to submit publications of atleast last three years along with his/her CV and the proposal for research."

b. ***Research & Seed Grant to Assistant Professor, Associate Professor & Professor of University of Jammu:***

Research Grant shall be provided to all faculty members as per the following: -

Faculty of Sciences: Maximum limit – Rs.2.00 lac (Per Annum for each selected person)
Faculty of Social Sciences: Maximum limit – Rs.1.50 lac (Per Annum for each selected person)
Other Faculties: Maximum limit – Rs.1.00 lac (Per Annum for each selected person)

Dean Research Studies

py to: -

1. Special Secretary to the Vice-Chancellor for the kind information of the Vice-Chancellor.
2. All Campus Deans.
3. Sr. P.A to DAA/Registrar.
4. Sr. P.A to Joint Registrar (Finance)
5. Dy. Registrar (Grants).
6. Assistant Registrar (R&A).
7. Guard File.

Received: 17 April 2023 | Revised: 27 June 2023 | Accepted: 3 July 2023
DOI: 10.1002/aoc.7195

RESEARCH ARTICLE

Applied Organometallic Chemistry WILEY

PolyVinyl alcohol and copper nickel co-doped titania nanocomposite: Designing, characterization, optical properties, and catalytic application in the synthesis of aryl derivatives of benzothiazole and benzimidazole

Ankush Mahajan | **Monika Gupta**

Department of Chemistry, University of Jammu, Jammu, India

Correspondence
Monika Gupta, Department of Chemistry, University of Jammu, Jammu 180006, Jammu and Kashmir, India.
Email: monika.gupta77@rediffmail.com; drmonikagupta@jammuuniversity.ac.in

Funding information
University of Jammu

The paper examines the properties and potential applications of a nanocomposite material composed of polyvinyl alcohol (PVA) and copper nickel co-doped titanium dioxide (Cu-TiO_2-Ni). The material was synthesized using a simple precipitation process, and its properties were characterized using various analytical techniques, including powder X-ray diffraction, Fourier transform infrared spectroscopy, thermogravimetry analysis, field emission scanning electron microscopy, and high-resolution tunnelling electron microscopy; Brunauer–Emmett–Teller (BET) surface area was investigated. The results showed that the addition of Cu-TiO_2-Ni to PVA improved the material's Ultraviolet–visible spectroscopy (UV) absorption properties. Additionally, the PVA/Cu-TiO_2-Ni nanocomposite material exhibited potential for use in a range of applications, including catalysis. Its utility in synthesizing aryl derivatives of benzothiazole and benzimidazoles, which are crucial intermediates in the fine chemical, agrochemical, and pharmaceutical industries and material science, was evaluated. It was found to offer several advantages, including a quick reaction time, simple workup, and good to excellent isolated yields. These characteristics make this protocol both practical and economically intriguing.

KEYWORDS
2-aryl benzimidazole, 2-aryl benzothiazole, copper and nickel, Doped titania, PVA

1 | INTRODUCTION

Nanocomposites are a new type of composite that contain at least one phase with dimensions ranging from 1 to 100 nm.[1–3] Nanocomposites have gained significant attention due to their improved performance characteristics compared with traditional composite materials.[4–7] Polymer nanocomposites show immense potential as lightweight functional materials for the future.[8–10] Inorganic nanofillers are now widely used in the fabrication of polymeric nanocomposites.[11–13] Because of their ability to combine the benefits of polymers and filler components, polymer-based nanocomposites have received a lot of attention.[14–19] Because of their optical, electrical, mechanical, and magnetic properties, polymeric nanocomposites have a wide range of applications.[20–25]

Polyvinyl alcohol (PVA) is a water-soluble polymer with numerous technological, pharmaceutical, and biomedical applications.[26–28] It is a synthetic polymer that can be used in nanocomposites as a dispersant or

binder.[29–31] PVA, when used as a dispersant, aids in the even distribution of nanoparticles within a matrix material such as plastic or resin.[32] PVA, as a binder, can help to hold nanoparticles together and improve the overall strength and properties of the nanocomposite.[33,34] PVA-based nanocomposites have been investigated for a variety of applications, including catalysis.[35–37]

Titanium oxide, or titania, is a substance that happens to exist naturally. It is a white, flavourless powder that is insoluble in most acids and water.[38,39] Titania is a popular material used in many different applications, including UV protection,[40] self-cleaning surfaces,[41] water treatment,[42] and as an active ingredient in paints, coatings, and ceramics.[43] Titania is a photocatalyst, which means it may speed up chemical processes when exposed to light. In many different sectors, including paper,[44] plastics, and cosmetics, it is extensively utilised as a white pigment.[45,46] Moreover, titanium is used as a catalyst in a variety of chemical processes, including photo-Fenton reactions,[47] hydrogenation,[48] and selective oxidation.[49] As a catalyst in the manufacturing of fine chemicals and the purification of exhaust emissions, TiO_2 is used to selectively oxidise alcohols, turning them into aldehydes and ketones.[50,51] Moreover, it serves as a catalyst in the manufacture of hydrogen fuel cells and the biofuel conversion of biomass.[52,53]

Doping a metal is the process of adding impurities to it in order to change its characteristics.[54–57] Metal's characteristics may be enhanced using it for a variety of purposes.[58,59] Doping, for instance, may be used to increase a metal's conductivity for use in electrical devices or its optical characteristics for use in optical devices.[60] Moreover, new electrical and optical characteristics that are not present in the undoped metal may be created by doping.[61,62] It is also crucial to remember that doping may be used to modify the conductivity of nonmetals like semiconductors.[63] The catalytic activity of metals and metal oxides is also enhanced by doping.[64,65] A metal or metal oxide may have its electrical structure changed by doping it with additional elements, which can then alter the material's catalytic activity.[66,67] Titania (TiO_2) doping with metal ions like iron, nickel, or cobalt is one instance.[68–70] The photocatalytic activity of TiO_2 may be increased as a result of the dopants' creation of additional active sites on its surface.[71] A more durable surface that is less prone to sintering or deactivation may be produced through doping, which can also be utilised to increase the stability of catalysts.[72,73] By generating new active sites that are selective for certain kinds of reactants, doping may also be utilised to modify the selectivity of catalysts for particular processes.[74,75]

Catalysis plays a vital role in many areas[76,77] including energy production, environmental remediation,[78] and pharmaceutical synthesis.[79–81] It enables more efficient and sustainable chemical transformations by reducing energy consumption, increasing reaction rates, and improving selectivity.[82,83] Catalysis for C–C coupling reactions refers to the use of catalysts to facilitate the formation of carbon–carbon bonds. C–C coupling reactions are crucial in organic synthesis as they allow the construction of complex organic molecules. It is extremely frequent to find heterocycle skeletons in many natural products, such as pharmaceuticals.[84] A group of substances known as benzothiazoles includes the chemical molecule 2-phenylbenzo[*d*]thiazole.[85] It is made up of a phenyl group, a six-membered ring with one carbon atom, and a benzo[*d*]thiazole ring, a five-membered ring with one sulphur atom.[86,87] It is a flexible molecule with a variety of possible uses.[87] It is a flexible molecule with a variety of possible uses e.g. In organic electronics and optoelectronics, i.e. in the area of organic field-effect transistors[88] and organic light-emitting diodes.[89] It has been employed as a semiconductor material in organic field-effect transistors since it was discovered to have strong electron mobility. Since it has been discovered to have anticancer[90,91] properties in certain studies and to prevent the proliferation of cancer cells,[92] it also has prospective uses in medicinal chemistry.[93]

The chemical molecule 2-phenyl-1*H*-benzo[*d*]imidazole (PBI) is a member of the imidazole class of substances. It is made up of a phenyl group, a six-membered ring with one carbon atom, and a benzo[*d*] imidazole ring, a five-membered ring with two nitrogen atoms.[94] PBI and its derivatives are adaptable substances with several possible uses. It has been researched both as a ligand in the production of metal nanoparticles and in the area of asymmetric catalysis. It has been discovered that this ligand enhances the enantioselectivity and catalytic activity of certain processes due to its electron-donating characteristics. Optoelectronics and organic electronics properties of the material have been explored.[95] In organic solar cells, organic field-effect transistors, and organic light-emitting diodes, PBI has been employed as an active ingredient.[96,97] In perovskite solar cells, PBI has also been employed as a hole-transporting substance.[98] Due to their capacity to interact with biological systems and prospective applications in medicinal chemistry,[99,100] they are also being researched as possible drug candidates.

Motivated by these factors, we herein report the synthesis and characterization of PVA and copper nickel co-doped titania (Cu-TiO_2-Ni) nanocomposite and, thereafter, their application as a nanocatalyst in the synthesis of aryl derivatives of benzothiazoles and benzimidazoles.

2 | EXPERIMENTAL

2.1 | Synthesis of PVA/Cu-TiO_2-Ni nanocomposite

2.1.1 | Preparation of Cu-TiO_2-Ni

Here, undoped Titania (TiO_2) and Copper Nickel co-doped Titania (Cu-TiO_2-Ni) are synthesised using a straightforward coprecipitation method. Hydrolysis of the isopropoxide chain was accomplished by adding the proper amounts of water. As a starting precursor, $Ti\{OCH(CH_3)_2\}_4$ titanium (IV) isopropoxide was used. To dissolve 5 mL of $Ti\{OCH(CH_3)_2\}_4$, 100 mL of isopropyl alcohol $(CH_3)_2CHOH$ was usually used. The TiO_2 precursor solution was added, along with 4% $CuCl_2$ and 4% $NiCl_2$, and the mixture was continuously stirred at room temperature for 1 h. Four hundred millilitres of deionized water were abruptly added to the stock solution after stirring. The resulting solution was aged for 3 h, centrifuged, and repeatedly washed with ethanol and deionized water. It was then allowed to dry at room temperature overnight. Afterward, Cu-TiO_2-Ni nanoparticles were created when the powder was heated at 450°C for 2 h in a muffle furnace.

2.1.2 | Preparation of PVA and Cu-TiO_2-Ni nanocomposite (PVA/Cu-TiO_2-Ni)

Cu-TiO_2-Ni nanoparticles (500 mg) were initially dispersed in 100 mL of deionized water for a few minutes using sonication. They were then forcefully agitated for 1 h to achieve a uniform suspension. PVA aqueous solutions (5 mL) with a Cu-TiO_2-Ni:PVA weight ratio of 1:0.050 were then added to the Cu-TiO_2-Ni suspensions, followed by 1 h of magnetic stirring at room temperature. Following that, 5 mL of ethanol was progressively added to the mixture. The phase separation happens when ethanol is dropped. The samples were washed multiple times with ethanol to remove excess PVA before being dried under vacuum at ambient temperature. The dried PVA coated Cu-TiO_2-Ni nanoparticles were then thermally treated in a muffle furnace at 180°C for 2 h.

2.2 | Procedure for the preparation of 2-aryl benzothiazoles

A mixture of 2-thiophenol (125 mg, 1.0 mmol) and benzaldehyde (106 mg, 1.0 mmol) and PVA/Cu-TiO_2-Ni nanocomposite (10 mg) was magnetically mixed at 60°C for the appropriate time. Thin layer chromatography was used to monitor the progress of the reaction. After completion, the reaction is quenched with water, and the resultant solid product was filtered, dried, and recrystallised with Ethanol (EtOH) to yield compounds.

2.3 | Procedure for the preparation of 2-aryl benzothiazoles

A mixture of 1,2-phenylenediamine (108 mg, 1.0 mmol) and benzaldehyde (106 mg, 1.0 mmol) in methanol (3.0 mL) was mixed, and PVA/Cu-TiO_2-Ni nanocomposite (10 mg) was added. The reaction was agitated for an adequate amount of time at 80°C. Following the completion of the reaction (as monitored by thin layer chromatography), the solvent was evaporated under vacuum and then dried to provide crude product, which was purified by column chromatography using hexane/ethyl acetate as the eluent to yield pure products.

3 | RESULTS AND DISCUSSION

3.1 | Characterization

3.1.1 | Fourier transform infrared analysis (FTIR)

Fourier transform infrared spectroscopy (FTIR) is a technique employed to examine the molecular vibrations and chemical composition of a substance. In the instance of PVA/Cu-TiO_2-Ni nanocomposite, FTIR may be used to identify the different functional groups present in the material and to assess its purity. Titania peaks linked with Ti–O bonds and vibrations of hydroxyl groups are two of the most prevalent peaks detected in FTIR spectra. The FTIR spectra of undoped, Cu-TiO_2-Ni, and PVA/Cu-TiO_2-Ni materials are shown in Figure 1. The spectrum shows many absorption bands with distinct intensity variations. The area from 3553 cm^{-1} broad absorption band may correlate to OH stretching vibrations linked to Titania's anatase phase. Moisture absorption is the primary basis of these OH bonds. The peak at 2921 cm^{-1} may be attributed to CH_2 asymmetric stretching in PVA. The absorption bands situated at 1635 cm^{-1} are ascribed to the C–O and C–C stretching modes. The existence of a well-defined signal at 1458 cm^{-1} confirms the interaction of the nanoparticles surface with the O–H groups of the PVA. Moreover, the signal at 1328 cm^{-1} might be attributed to the coordination of PVA molecules with TiO_2 surfaces. The band corresponding to the CH_2 asymmetric stretching vibration emerges at around 969 cm^{-1}. The interacting absorption bands at 788 cm^{-1} correspond to the stretching vibrations of the C–O–C group and the

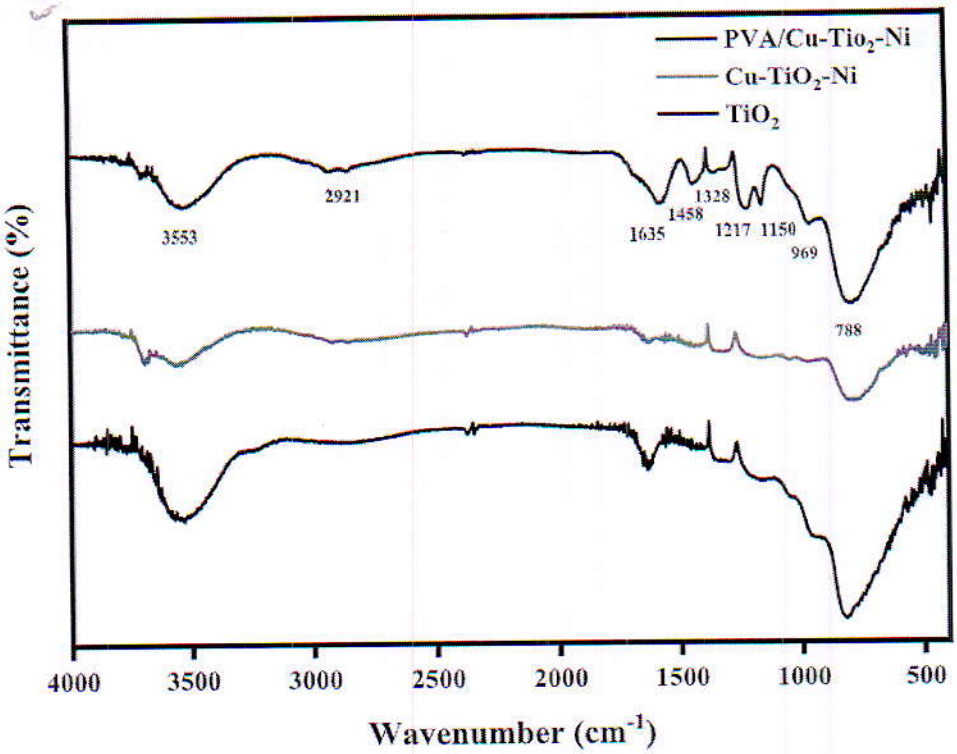

FIGURE 1 Fourier transform infrared spectra of TiO_2, Cu-TiO_2-Ni, and PVA/Cu-TiO_2-Ni.

flexion vibrations of the anatase phase. Moreover, the absorption band in the 400 to 600 cm^{-1} range is ascribed to the transverse optic vibration of the anatase Titania Ti–O bonds as well as bending vibration. However, no distinct absorption band attributable to Cu or Ni is seen. This finding supports the presence of Cu atoms in the host Titania matrix.

3.1.2 | Powder X-ray diffraction (PXRD)

Figure 2 shows the X-ray diffraction patterns of nano-TiO_2 powder before modification. The following signals at (101), (103), (004), (112), (200), (105), (211), (204), (220), (215), and (224) planes confirm that only the anatase crystal phase is formed, which confirms with the JCPD 89-4921 standard. Additionally, the peaks of Cu and Ni were not detected owing to the low content and indicate the complete assimilation of Cu and Ni. In addition to this, a small shift in 2θ is observed in the plane (101) of pure TiO_2 (25.29°) and Cu, Ni co-doped TiO_2 (25.57°). This small shifting may be considered as a confirmation that Cu and Ni are incorporated in the crystal lattice of pure TiO_2. It may also be concluded that the incorporation of both ions, that is, Cu and Ni, did not alter the crystal structure of synthesized nano-TiO_2 (anatase) to rutile. Moreover, the crystal structure of PVA/Cu-TiO_2-Ni is found to be similar to that of Cu-TiO_2-Ni.

The particle size of the nanoparticles was calculated using the Debye–Scherer equation[101]:

$$D = \frac{0.9\lambda}{\beta \mathrm{Cos}\theta}.$$

β is the full line width at half maximum, D is the crystallite size, θ is the Bragg's diffraction angle, and λ is the wavelength = 1.5406 A.

The average size of the PVA/Cu-TiO_2-Ni powder for 2θ = 25.303° is estimated to be around 15 nm.

3.1.3 | Thermogravimetry analysis (TGA)

Thermogravimetry analysis (TGA) is a widely utilized technique for polymer-based nanocomposites, specifically for examining their thermal stability. Thermogravimetry involves monitoring the sample's mass as a function of temperature. Thermogravimetry analysis of the synthesized nanocomposite PVA/Cu-TiO_2-Ni has been given in Figure 3. The analysis finds the degradation of the nanocomposite with temperature (thermal stability). The nanocomposite is quite stable up to 800°C having loss of only 10% which has been recorded in two steps having 3.1% loss up to 400°C and 7% loss from 400°C to 800°C.

3.1.4 | Field emission scanning electron microscopy (FE-SEM)

Figure 4 shows the field emission scanning electron microscopy (FE-SEM) study of the PVA/Cu-TiO_2-Ni

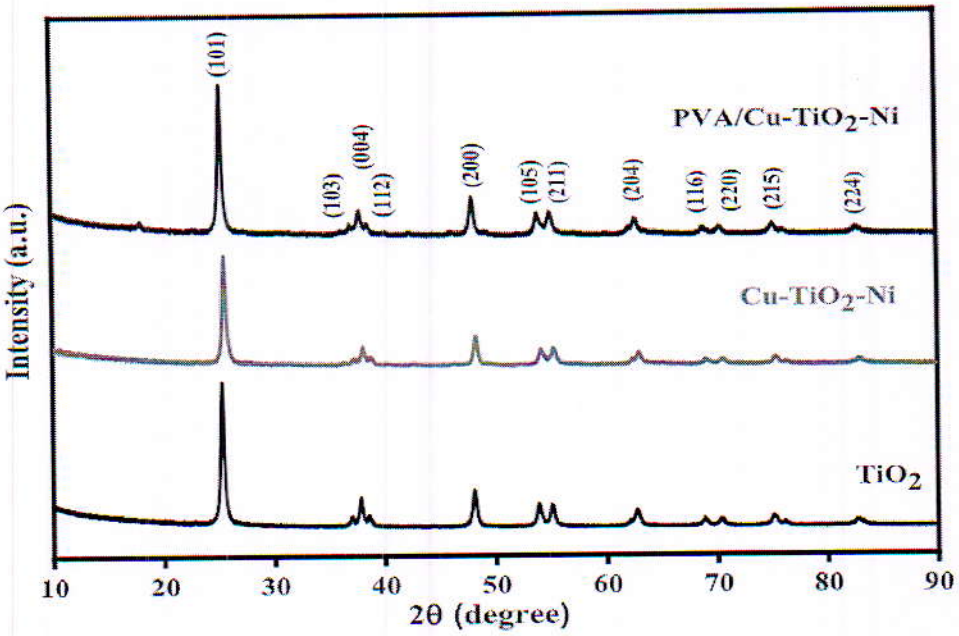

FIGURE 2 X-ray diffraction of TiO_2, Cu-TiO_2-Ni, and PVA/Cu-TiO_2-Ni.

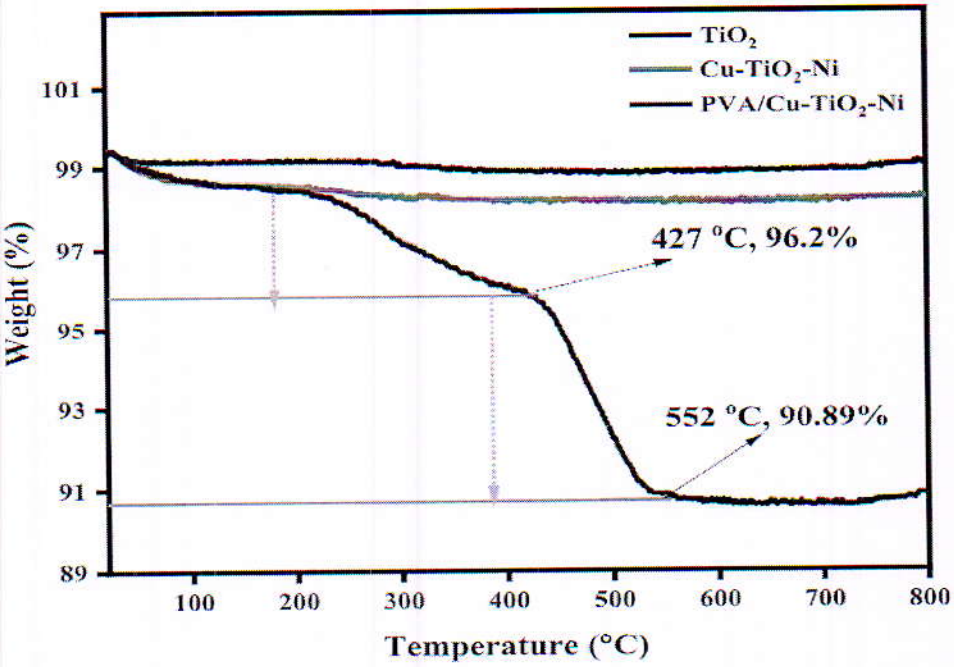

FIGURE 3 Thermogravimetric analysis of TiO_2, Cu-TiO_2-Ni, and PVA/Cu-TiO_2-Ni.

nanocomposite, which shows that the particles have a spherical-like shape. Moreover, the particles were tiny and agglomerated in a regular pattern. The Cu-TiO_2-Ni trapped in the polymer matrix appeared as a heavily agglomerated core of PVA with a shell of Cu-TiO_2-Ni in the SEM picture. There was also no pore between the particles. FE-SEM confirms the nanocomposite is in a well-mixed manner and also helps to substantiate as a good catalyst. Cu-TiO_2-Ni particles were found to be clear and freely bound by PVA, providing a high surface area. The structural properties of TiO_2 can be improved by the incorporation of nickel and copper, exhibiting good dispersion and uniformity on the surface of the obtained nanocomposite by becoming rougher and more porous. The synergistic effects of polymer support interfaces, and charge transfer between metal and metal oxide may lead to enhanced catalytic properties. These nanoparticles aggregate and connect to each other to build 3D porous architectures, which is quite favourable for the diffusion in the inner pores.

3.1.5 | EDX and elemental mapping

All the required elements (Ti, Cu, Ni, C, and O) confirm the presence of organic PVA in PVA/Cu-TiO_2-Ni as well

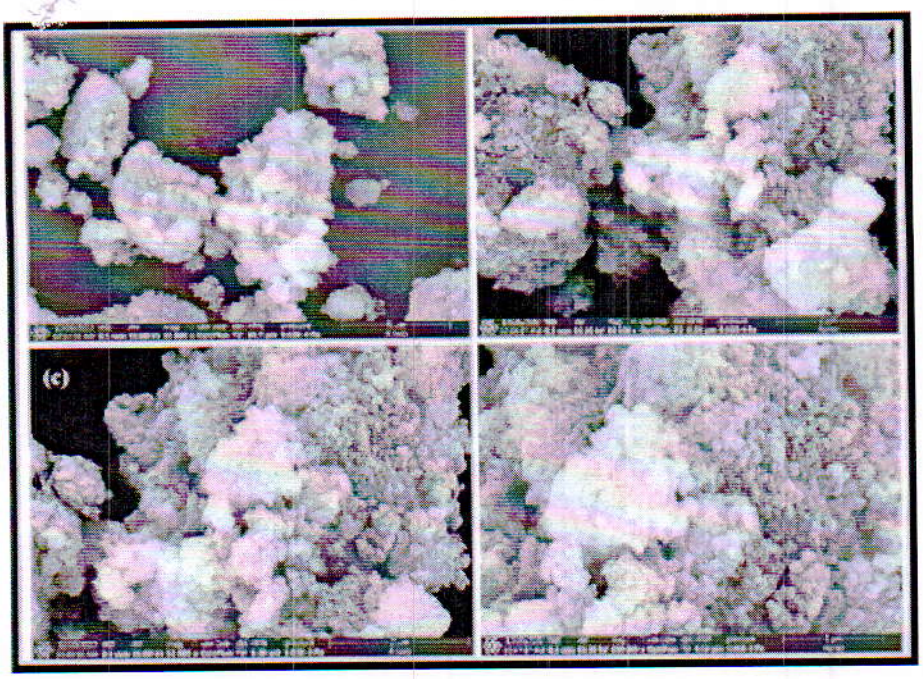

FIGURE 4 Field emission scanning electron microscopy images of PVA/Cu-TiO_2-Ni at different magnification at (a) 20,000×, (b) 50,000×, (c) 65,000×, and (d) 100,000×.

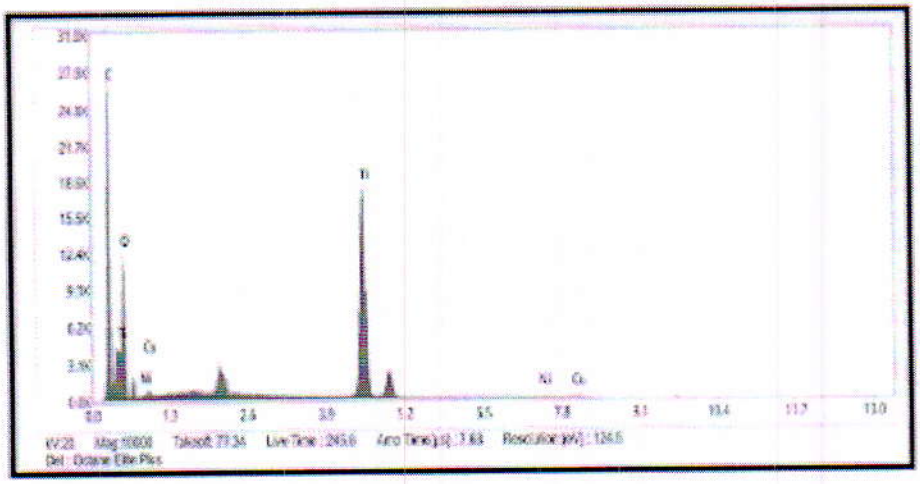

FIGURE 5 Energy dispersive X-ray spectrum of PVA/Cu-TiO_2-Ni.

as of titania, copper, and nickel as shown by energy dispersive X-ray (EDX) in Figure 5.

Table 1 provides a list of results of the elemental analysis of PVA/Cu-TiO_2-Ni nanocomposite. The presence and distribution of elements of the prepared nanocomposite was also confirmed by the elemental mapping technique. The images confirmed the uniform distribution of Cu, Ni, and TiO_2 over the PVA. Figure 6 shows elemental maps for C, O, Ni, Cu, and Ti.

TABLE 1 Energy dispersive X-ray analysis of PVA/Cu-TiO_2-Ni.

Element	Weight %	Atomic %	Error %
C K	59.25	71.55	9.63
O K	26.76	24.25	10.81
Ti K	13.39	4.06	1.80
Ni K	0.28	0.07	9.05
Cu K	0.32	0.07	9.60

3.1.6 | High-resolution tunnelling electron microscopy (HR-TEM)

High-resolution tunnelling electron microscopy (HR-TEM) images of the nanocomposite at various magnifications are given in Figure 7. The size differences between the nanoparticles are readily apparent. Due to the edges of one nanoparticle being fused with the edges of another nanoparticle, they are not precisely spherical. This is because of the annealing process's Ostwald ripening.[102] Core of PVA with the shell of Cu-TiO_2-Ni can be clearly seen. It was also observed that the average particle size was around 17 nm (Figure 8).

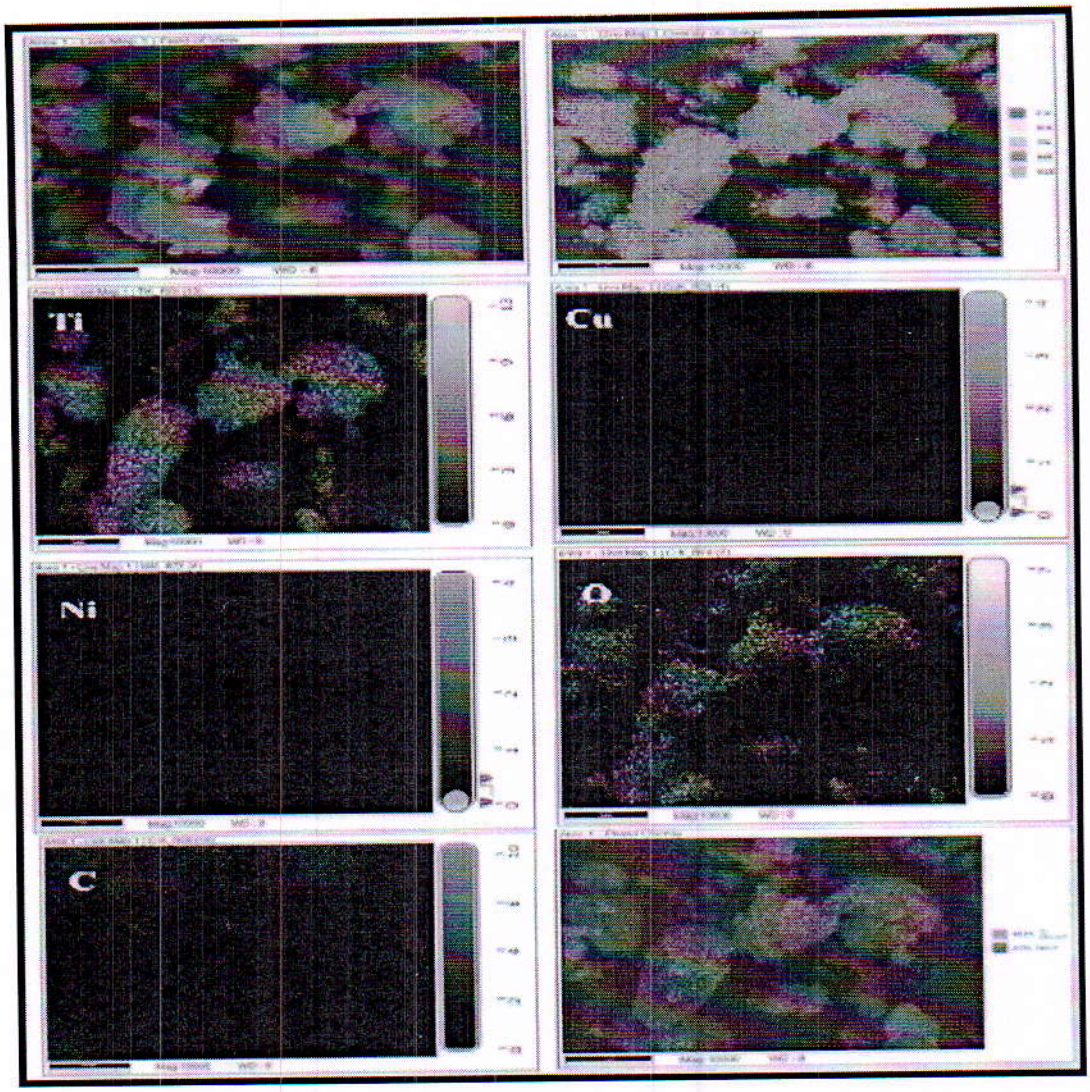

FIGURE 6 Elemental mapping of PVA/Cu-TiO_2-Ni.

3.1.7 | Brunauer Emmett Teller (BET) analysis

The N_2 adsorption/desorption isotherm of TiO_2 (Figure 9a), Cu-TiO_2-Ni (Figure 9b), and PVA/Cu-TiO_2-Ni nanocomposite (Figure 9c) was investigated. The isotherms were identified to be as Type IV hysteresis loop, which are the characteristic of mesoporous materials, representative of narrow slit-like pores, particles with internal voids of irregular shape and broad size distribution. (i.e., small particles filled in the gaps between larger particles leading to a more uniform and smoother surface). The BET surface areas of TiO_2, Cu-TiO_2-Ni, and PVA/Cu-TiO_2-Ni were measured to be 10, 30, and 29 $m^2\ g^{-1}$, respectively. The total pore volume of TiO_2, Cu-TiO_2-Ni, and PVA/Cu-TiO_2-Ni nanocomposite was found to be 0.01, 0.06, and 0.05 $cm^3\ g^{-1}$, respectively, and the mean diameter of the pore was 6.5, 8.7, and 8.2 nm, respectively, for TiO_2, Cu-TiO_2-Ni, and PVA/Cu-TiO_2-Ni (Table 2).

3.2 | Optical properties

3.2.1 | Photoluminescence

The nanocomposite's photoluminescent activity was evaluated. The photoluminescence spectra of the PVA/Cu-TiO_2-Ni nanocomposite indicated that when the sample was excited at 425 nm, the emission wavelength was around 665 nm (Figure 10).

3.2.2 | UV–Vis spectrum

Figure 11 shows the Ultraviolet-visible (UV-Vis) spectroscopy DRS spectra of the pure TiO_2, Cu-TiO_2-Ni, and PVA/Cu-TiO_2-Ni samples. As can be observed from the spectra, a strong absorption peak at around 350 nm is ascribed to the TiO_2 system, which decreases after nanocomposite formation. In addition, the nanocomposite

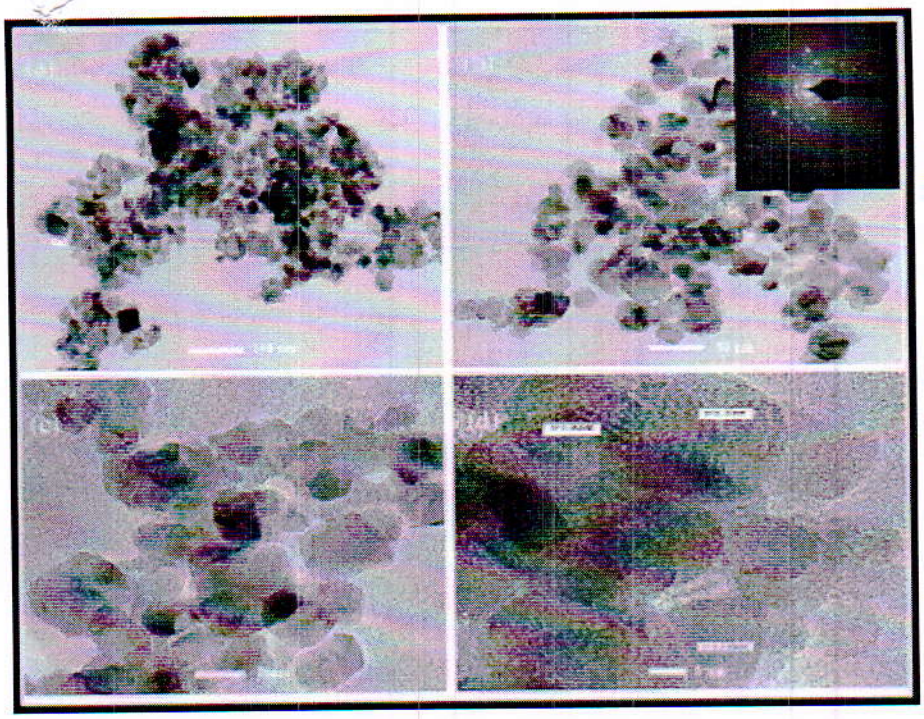

FIGURE 7 High-resolution tunnelling electron microscopy images of PVA/Cu-TiO_2-Ni at (a) 100, (b) 50, (c) 20, and (d) 5 nm (Inset) selected area electron diffraction pattern.

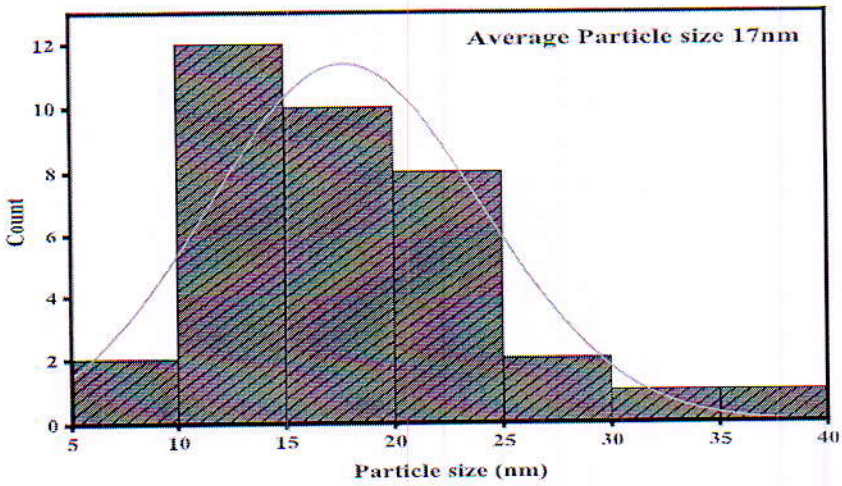

FIGURE 8 Average particle size distribution.

formation also results in a shift of adsorption edge to higher wavelength region (red shift), which is characteristic for the TiO_2 system after metal doping. The band gap energy is calculated. The absorption, $F(R)$, is related to the reflectance R in diffuse reflectance spectroscopy (DRS) mode by the Kubelka–Munk equation[103] which is given by

$$F(R) = \frac{(1-R)^2}{2R},$$

where R is the reflectance of the sample.

Figure 12 depicts the Kubelka–Munk plot. For direct band gap determination, $[F(R)\ h\upsilon]^2$ is plotted against energy, and the linear part of the curve was extrapolated to $[F(R) * h\upsilon]^2 = 0$ (Figure 13), where h is a Planck's constant and υ is the ratio of speed of light (c) to the wavelength (λ).

This gives rise to a band gap value of 2.6 eV for PVA/Cu-TiO_2-Ni, whereas band gap corresponding to Cu-TiO_2-Ni gave a band gap of 2.5 which is smaller than the band gap of TiO_2 (2.9 eV).

3.2.3 | Synthesis of 2-aryl benzothiazole

Initially, the reaction between 2-aminothiophenol and benzaldehyde was selected for the synthesis of 2-phenyl-

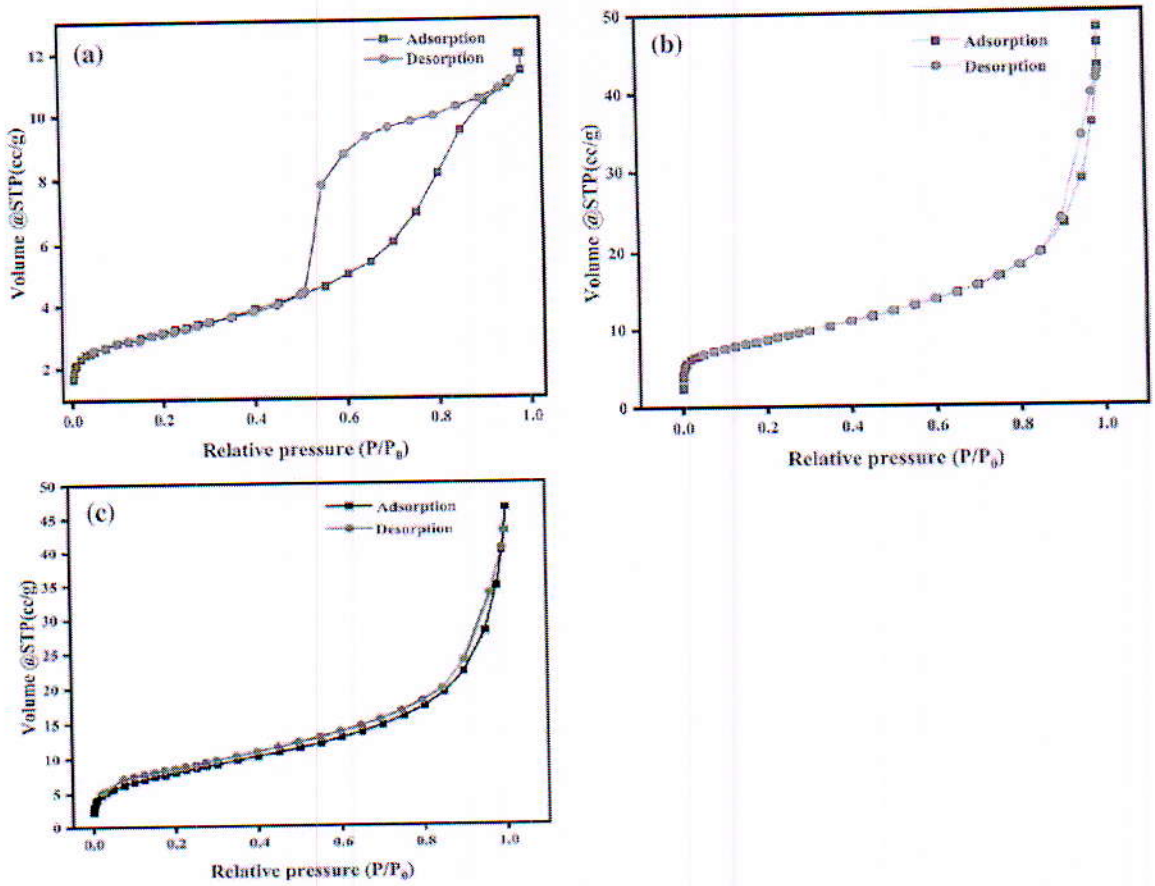

FIGURE 9 Adsorption–desorption spectrum of (a) TiO_2, (b) Cu-TiO_2-Ni, and (c) PVA/Cu-TiO_2-Ni.

TABLE 2 BET analysis of TiO_2, Cu-TiO_2-Ni, and PVA/Cu-TiO_2-Ni.

	BET surface area (m^2 g^{-1})	Total pore volume (cm^3 g^{-1})	Mean pore diameter (nm)
TiO_2	10.7	0.01	6.5
Cu-TiO_2-Ni	30.2	0.06	8.7
PVA/Cu-TiO_2-Ni	29.0	0.05	8.2

Abbreviations: Cu-TiO_2-Ni, copper nickel co-doped titanium dioxide; PVA, polyvinyl alcohol; TiO_2, titanium dioxide.

1,3-benzothiazole as a model reaction for optimizing the reaction conditions (Scheme 1). The role of the catalyst, reaction temperature, solvent, and reaction time were all thoroughly investigated. The model reaction was carried out with varying amounts of catalyst (5, 10, 15, and 20 mg of PVA/Cu-TiO_2-Ni); it was discovered that 15 mg of catalyst was sufficient. With more catalyst, there was no substantial increase in yield. The model reaction was carried out solvent-free at room temperature, 40°C, 60°C, 80°C, and 100°C using PVA/Cu-TiO_2-Ni as the nano catalyst, and it was discovered that the reaction completed without any solvent at 60°C, yielding 95% of the required product after recrystallization with ethanol in 15 min. It was investigated whether solvents could play an important role in this reaction.

It was observed that the solvent-free reaction gave the highest yield (95%) in 15 min compared with the other solvents used in the reaction (for more information, see Tables S1–S4). Finally, after optimising reaction conditions, the synthesis of 2-aryl benzothiazole derivatives using a variety of substrates, including aromatic aldehydes, was performed to study the scope of catalysts, as shown in Table 3. Aromatic aldehydes with different functional groups on the phenyl ring, as well as heterocyclic aldehydes, gave good to excellent amounts of products (spectral data are given in Figures S1–S8).

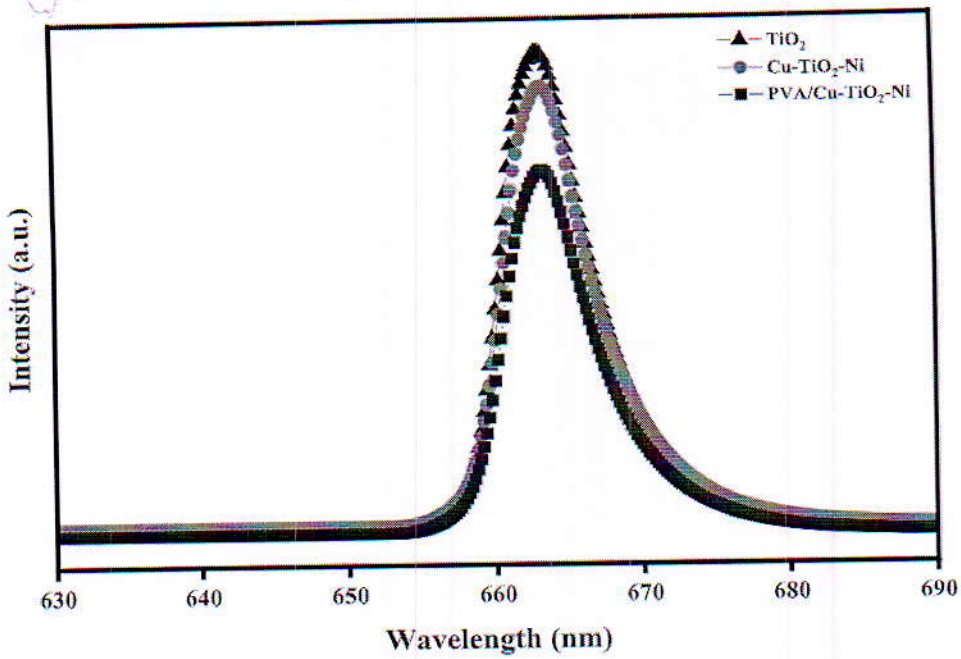

FIGURE 10 Photoluminescence spectra of TiO_2, Cu-TiO_2-Ni, and PVA/Cu-TiO_2-Ni.

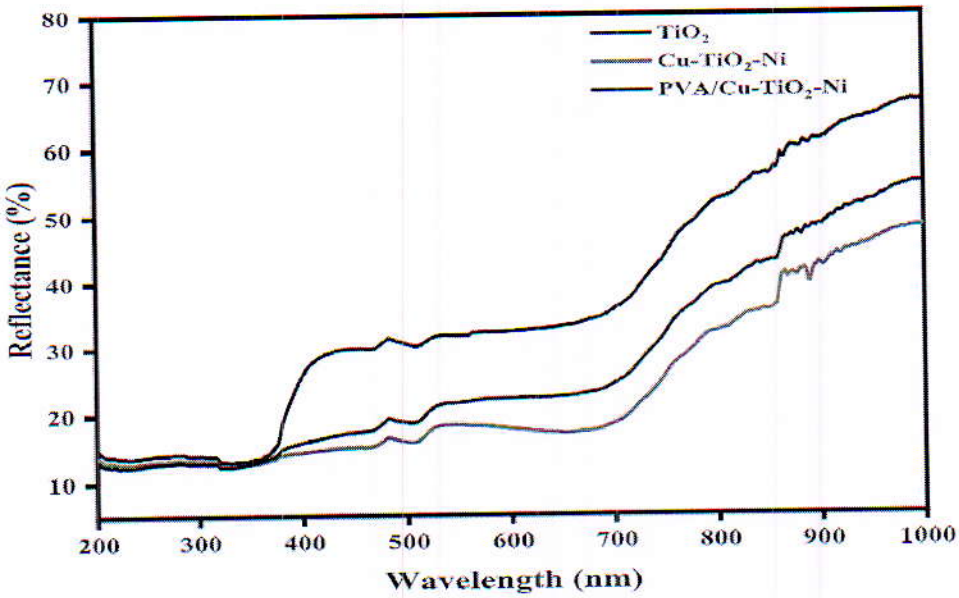

FIGURE 11 Diffuse reflectance spectrum of TiO_2, Cu-TiO_2-Ni, and PVA/Cu-TiO_2-Ni.

3.2.4 | Plausible mechanism

A plausible reaction mechanism for 2-aminothiophenol synthesis is given in Scheme 2. In the first step, 2-aminthiophenol (1) and benzaldehyde (2) react to generate a Schiff base intermediate. The amino group of 2-aminthiophenol and the carbonyl group of benzaldehyde form the imine linkage in the presence of a nanocatalyst PVA/Cu-TiO_2-Ni. This results in an unstable intermediate Schiff base (3) that is vulnerable to ring closure. The next step is the ring closure of the intermediate Schiff base, which leads to the formation of a thiazole ring. The thiazole ring is formed by the attack of the sulphur atom of the thiol group on the carbon atom of the imine group. This forms a cyclic intermediate, which undergoes proton transfer to form the thiazole ring which then reacts with the thiol group and undergo cyclization to create the intermediate benzothiazoline (4). The final step involves the aromatization of the thiazole ring to form the 2-phenylbenzothiazole (5). The aromaticity of the benzene ring is restored by the elimination of a proton from the thiazole ring.

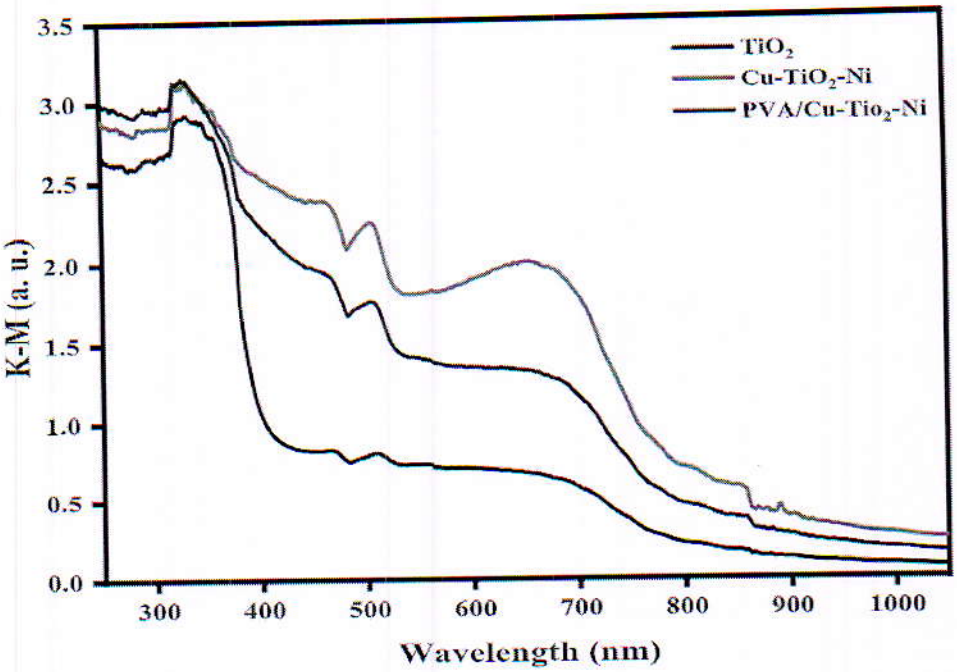

FIGURE 12 Kubelka–Munk plot of TiO_2, Cu-TiO_2-Ni, and PVA/Cu-TiO_2-Ni.

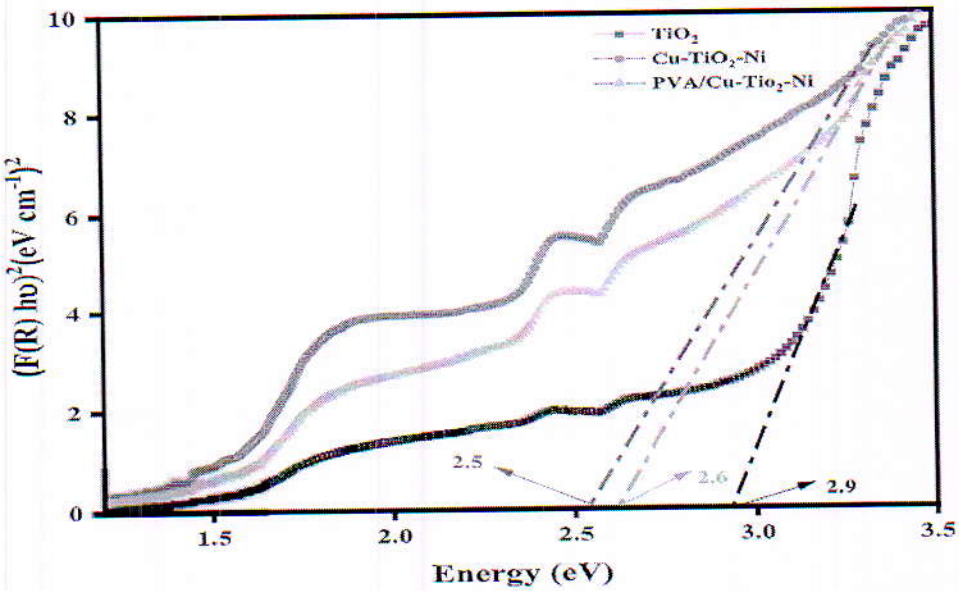

FIGURE 13 Band gap (direct) determination by plotting $[F(R) * h\nu]$ 2 versus energy of TiO_2, Cu-TiO_2-Ni, and PVA/Cu-TiO_2-Ni.

3.2.5 | Synthesis of 2-aryl benzimidazole

Initially, the reaction between o-phenyldiamine and benzaldehyde was selected for the synthesis of 2-aryl benzimidazole as a model reaction for optimising the reaction conditions in a methanol as solvent at 80°C (Scheme 3).

The role of the catalyst, reaction temperature, solvent, and reaction time were all thoroughly investigated. The model reaction was carried out with varying amounts of catalyst (5, 10, 15, and 20 mg of PVA/Cu-TiO_2-Ni); it was discovered that 10 mg of catalyst was sufficient. With more catalyst, there was no substantial increase in yield. The model reaction was carried out in methanol (at room temperature, 40°C, 60°C, 80°C, and 100°C) using PVA/Cu-TiO_2-Ni as the nano catalyst, and it was discovered that the reaction completed with methanol as the solvent at 80°C, yielding 90% of the required product after purification in 40 min.

It was found that solvents play an important role in this reaction. We investigated the effect of solvent on the

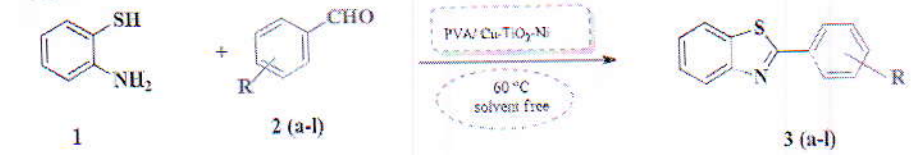

SCHEME 1 Synthesis of 2-aryl benzothiazole catalysed by PVA/Cu-TiO_2-Ni.

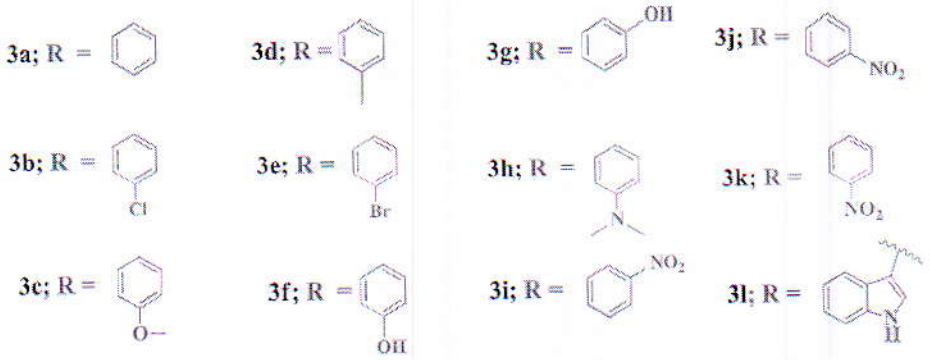

TABLE 3 Substrate scope for the synthesis of 2-aryl benzothiazole[a] catalysed by PVA/Cu-TiO_2-Ni.

Entry	Benzaldehyde	Time (min)	Yield (%)[b]	Product	Obs. M. pt. (°C)/Lit. M. Pt. (°C)
1 (3a)	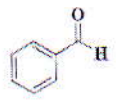	15	95	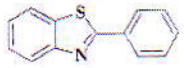	102–104/ 98.1–100.7[104]
2 (3b)	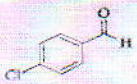	10	90		108–109/ 110.3–112.5[104]
3 (3c)	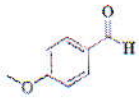	12	95	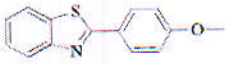	118–120/ 123–125[105]
4 (3d)	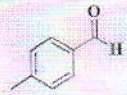	25	85		90–92/ 87–89[105]
5 (3e)	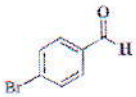	12	82	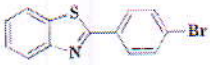	100–101 105.3–107.1 [104]
6 (3f)	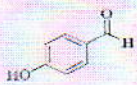	30	75	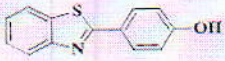	222–224 227–228[106]
7 (3g)	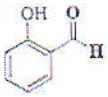	35	80	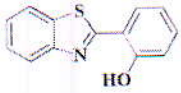	131–133/ 131–132[106]
8 (3h)		25	80	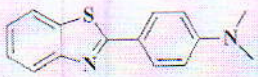	168–170/ 167–169[105]

TABLE 3 (Continued)

Entry	Benzaldehyde	Time (min)	Yield (%)[b]	Product	Obs. M. pt. (°C)/Lit. M. Pt. (°C)
9 (3i)	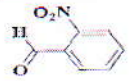	15	85	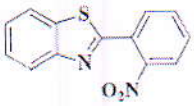	123–125/ 122–123[107]
10 (3j)	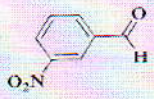	20	80		180–182/ 181–182[108]
11 (3k)		10	80	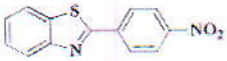	222–224/ 226–228[109]
12 (3l)	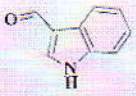	40	55	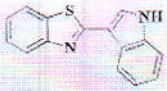	142–144/ 144–146[110]

[a]Reaction conditions: Benzaldehyde (1 mmol), 2-aminothiophenol (1 mmol), and nanocatalyst (15 mg) at 60°C.
[b]Isolated yield refers to yield obtained after recrystallisation.

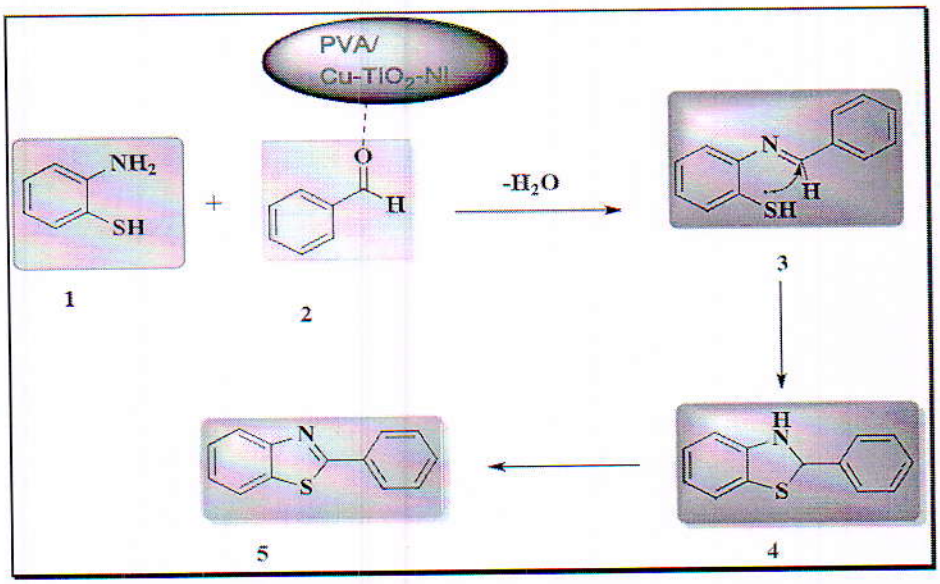

SCHEME 2 Plausible mechanism for the synthesis of 2-aryl benzothiazole catalysed by PVA/Cu-TiO_2-Ni.

synthesis of 2-aryl benzimidazoles using PVA/Cu-TiO_2-Ni nanocatalyst. It shows that only methanol gave the highest yield (90%) in 40 min compared with the other solvents used in the reaction (see Tables S5–S8). Finally, after optimising reaction conditions, the synthesis of 2-aryl benzimidazole derivatives using a variety of substrates, including aromatic aldehydes, was performed to study the scope of catalysts, as shown in Table 4. Aromatic aldehydes with different functional groups on the phenyl ring, as well as heterocyclic aldehydes, gave good to excellent amounts of products (spectral data are provided in Figures S9–S16).

3.2.6 | Plausible mechanism

Scheme 4 describes the plausible mechanism for the practical and environmentally friendly way to synthesize 2-aryl benzimidazoles. By condensation of 2-phenyldiamine (1) with benzaldehyde (2), a Schiff base intermediate (3) is generated in the first step. The Schiff base intermediate then undergoes intramolecular cyclization to form the benzimidazole ring (4). This cyclization occurs through nucleophilic attack of the nitrogen atom in the amino group on the carbon atom of the imine group. The imine nitrogen lone pair attacks the carbon,

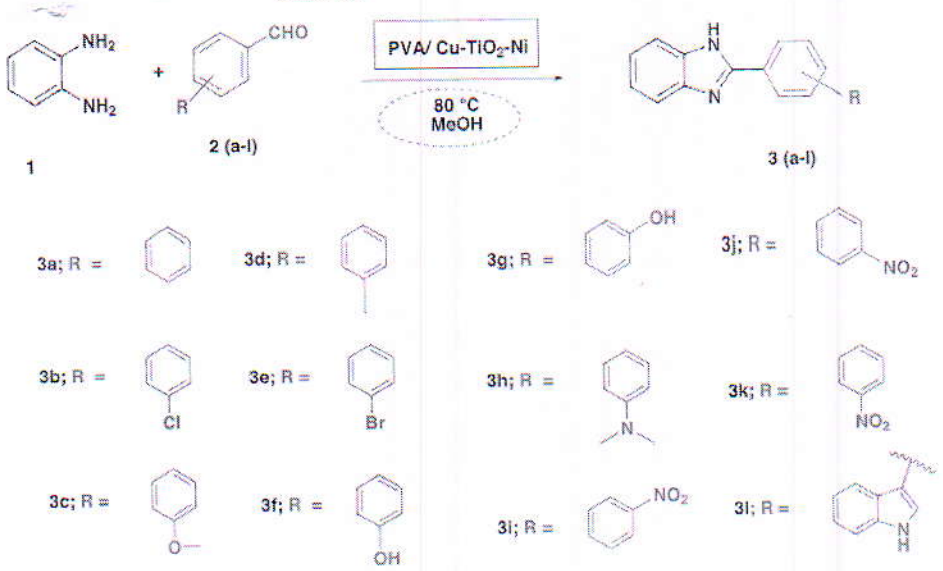

SCHEME 3 Synthesis of 2 aryl benzimidazole catalysed by PVA/Cu-TiO_2-Ni.

leading to the formation of a cyclic intermediate (4). Finally, with the loss of a water molecule, the intermediate (4) was readily oxidized by air; the product is formed by the elimination of a proton from the C-2 position of the imidazole ring, leading to the formation of the double bond between the carbon and nitrogen atoms, which yield the desired product (5).

3.3 | TON and TOF of the catalyst

The catalyst turnover number (TON) and the turnover frequency (TOF) are two important quantities used for comparing catalyst efficiency in heterogeneous catalysis. The TON is determined as the number of molecules that experience transformation by ratio of active sites to products in the presence of 1 g catalyst. Also, the TOF is calculated as TON / degradation time.[115] Hence, TON for the synthesis of 2-phenyl benzothiazole and 2-phenyl benzimidazole with the amount of the loading PVA/Cu-TiO_2-Ni nanocatalyst is calculated to be 3.2×10^{-5} and 3.1×10^{-5}, respectively. The TOF of PVA/Cu-TiO_2-Ni nanocatalyst was found to be up to 2.1×10^{-6} and 7.7×10^{-7} min^{-1} for the synthesis of 2-phenyl benzothiazole and 2-phenyl benzimidazole, respectively.

3.4 | Hot filtration test

The hot filtration test is employed to determine whether the nanocatalyst PVA/Cu-TiO_2-Ni is required for the synthesis of aryl derivatives of benzothiazole and benzimidazole or not. During this test, the catalyst was removed from the model reactions of benzaldehyde with 2-aminothiophenol to give 2-aryl benzothiazole and also other reaction of benzaldehyde with o- phenylenediamine to give 2-aryl benzimidazole after 8 and 20 min, respectively, by filtering it while it is still hot, and the reaction was monitored for continued activity. It was found that the reaction comes to an end after filtration, which proves that the nanocatalyst was important for the reaction.

3.5 | Recyclability of PVA/Cu-TiO_2/Ni nanocomposite

Recyclability and reusability are one of the most important criteria for the reaction to be in the domain of 'Green Chemistry'. To demonstrate the reusability and recyclability of the nanocatalyst, model reactions of benzaldehyde with 2-aminothiophenol to give 2-aryl benzothiazole and also other reaction of benzaldehyde with o-phenylenediamine to give 2-arylbenzimidazole were investigated alternately for five cycles; the reaction mixture was dissolved in ethyl acetate, and the catalyst was separated by filtration after each cycle, washed with ethanol, and dried in an oven at 70°C for 60 min prior to use. The model reaction proceeded with recovered PVA/Cu-TiO_2-Ni even after five cycles without any extension of the reaction time or marked loss in yield. Infrared spectrum of recycled catalyst is given in Figure 14.

3.6 | Comparison of catalytic activity

Comparison of the catalytic activity of PVA/Cu-TiO_2-Ni with the recently published work has been described in Table 5.

TABLE 4 Substrate scope for the synthesis of 2-aryl benzimidazole[a] catalysed by PVA/Cu-TiO_2-Ni.

Entry	Benzaldehyde	Time (min)	Yield (%)[b]	Product	Obs. M. pt. (°C)/Lit. M. Pt. (°C)
1 (3a)	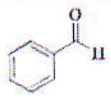	40	90	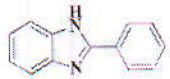	290–292/ 293–295[111]
2 (3b)	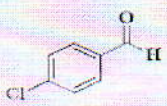	35	95	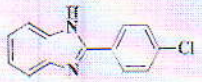	293–295/ 290–291[111]
3 (3c)	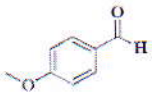	40	95		222–224/ 222–225[111]
4 (3d)	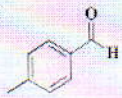	45	85	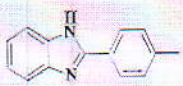	275–277/ 274–276[111]
5 (3e)	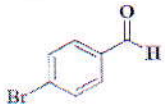	35	80	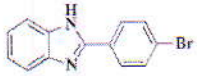	298–300/ 299[112]
6 (3f)	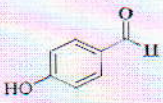	50	85	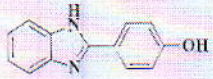	234–236/ 235–237[113]
7 (3g)	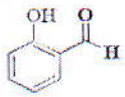	45	80	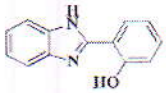	222–224/ 218–220[113]
8 (3h)		50	90	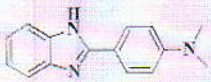	285–287/ 287–289[111]
9 (3i)	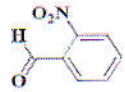	30	82	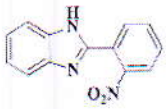	211–212/ 210–212[113]
10 (3j)	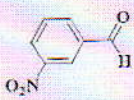	35	80	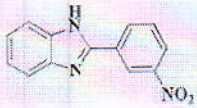	208–210/ 205–207[111]
11 (3k)		38	90	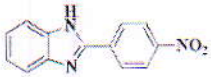	305–307/ 308–310[113]

(Continues)

TABLE 4 (Continued)

Entry	Benzaldehyde	Time (min)	Yield (%)[b]	Product	Obs. M. pt. (°C)/Lit. M. Pt. (°C)
12 (3l)	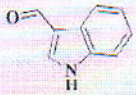	70	70	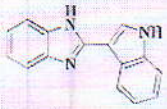	220–221/ 223–224[114]

[a]Reaction conditions: Benzaldehyde (1 mmol), o-phenyldiamine (1 mmol), and nanocatalyst (10 mg) at 80°C.
[b]Isolated yield refers to yield obtained after purification.

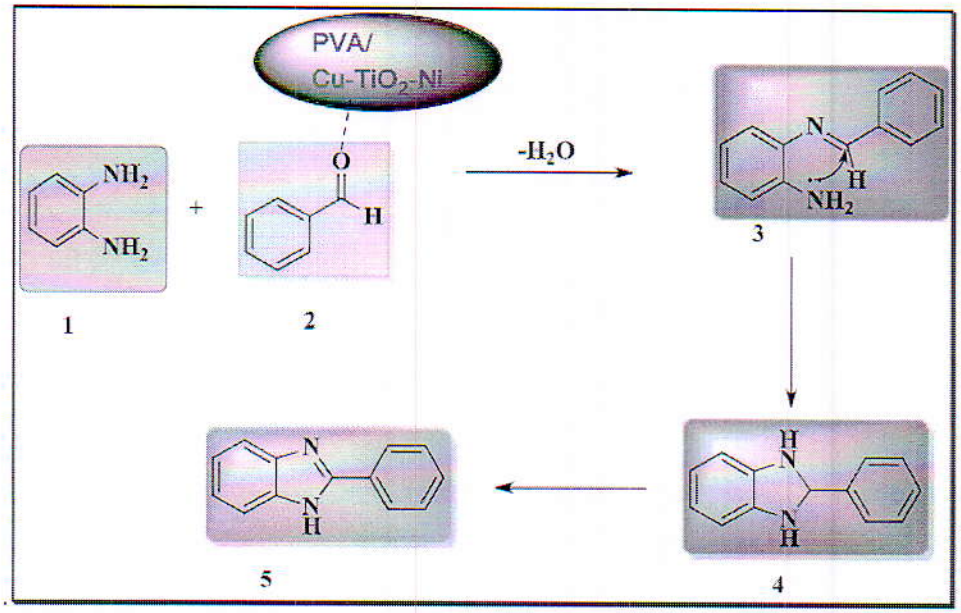

SCHEME 4 Plausible mechanism for the synthesis of 2-aryl benzimidazole catalysed PVA/Cu-TiO_2-Ni.

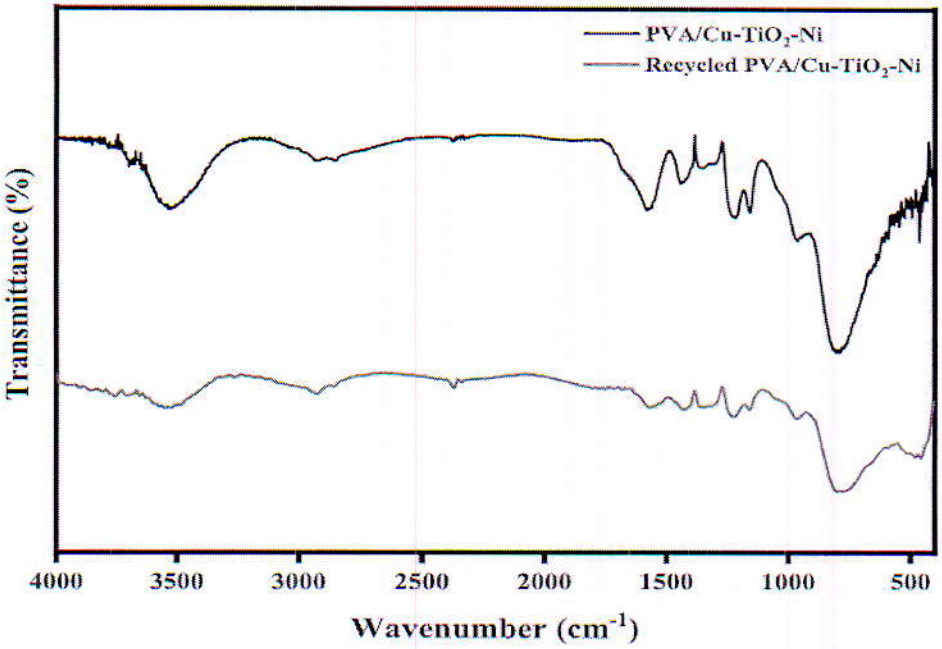

FIGURE 14 Fourier transform infrared spectroscopy showing recyclability of PVA/Cu-TiO_2-Ni.

TABLE 5 Comparison of catalytic activity of designed catalyst with some recent published work.

Product	Catalyst	Reaction time	Reaction conditions	Yield (%)	References
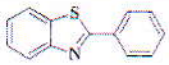	Bail gel	6 h	Solvent-free, 130°C	94	Nguyen et al.[116]
	Pentafluorophenyl ammonium triflate	5 h	H_2O, 60°C	88	Datta[117]
	Camphor sulfonic acid	1 h	EtOH:H_2O, room temperature	93	Kaur et al.[118]
	Alkyl carbonic acid	12 h	CH_3OH,70°C	87	Xiao et al.[119]
	This work	15 min	Solvent-free, 60°C	95	This work
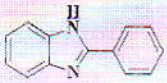	PS-Iron (III)–salen complex	20 h	70°C	90	Balinge et al.[120]
	SO_3H-Fe_3O_4@SiO_2	45 min	Ultrasonicate, EtOH, 50°C	79	Azarifar et al.[121]
	Cu@βCD-PEG-mesoGO	2 h	H_2O, 85°C	93	Bahadorikhalili et al.[122]
	Ferrites@wool-SO_3H	7 h	Toluene, reflux	75	Shaabani et al.[123]
	This work	40 min	80°C	90	This work

4 | CONCLUSIONS

In conclusion, we have successfully synthesized and characterized our efficient polymer-based nanocomposite using various techniques such as FTIR, PXRD, FE-SEM, EDX, elemental mapping, and HR-TEM. The surface area of the nanocomposites has been determined, and its optical properties, including the band gap, have been investigated. The nanocomposite has been successfully applied as a catalyst for the synthesis of 2-aryl benzothiazole and 2-aryl benzimidazole, demonstrating improved efficiency. Notably, the catalyst is cost-effective, readily available, and yields excellent results. It aligns with the principles of 'Green Chemistry' due to its recyclability, which has been tested for up to five consecutive runs.

AUTHOR CONTRIBUTIONS

Ankush Mahajan: Conceptualization; formal analysis; methodology; writing—original draft. **Monika Gupta:** Conceptualization; data curation; investigation; project administration; supervision; validation; writing—review and editing.

ACKNOWLEDGEMENTS

The authors are grateful to Department of Chemistry, University of Jammu, Jammu, and funding agencies for instruments like NMR (DST-PURSE), TGA (UGC-SAP), BET (RUSA 2.0), and PL (RUSA 2.0). The authors acknowledge IIT Jammu for P-XRD, IIT Roorkee for FE-SEM, EDX, and elemental mapping, and IIT Delhi for HR-TEM. The authors also acknowledge University of Jammu for providing Research and Seed Money Grant.

DATA AVAILABILITY STATEMENT

The data that support the findings of this study are available in the supplementary material of this article.

ORCID

Ankush Mahajan https://orcid.org/0000-0002-0496-1277

Monika Gupta https://orcid.org/0000-0001-5265-0388

REFERENCES

[1] S. S. Ray, *Macromol. Chem. Phys.* **2014**, *215*, 1162.

[2] N. Saba, P. M. Tahir, M. Jawaid, *Polymer* **2014**, *6*, 2247.

[3] X. Feng, L. Xia, Z. Jiang, M. Tian, S. Zhang, C. He, *Fuel* **2022**, *326*, 125051.

[4] G. Xia, Y. Zheng, Z. Sun, S. Xia, Z. Ni, J. Yao, *Environ. Sci. Pollut. Res.* **2022**, *29*, 39441.

[5] H. Yu, J. Zhu, R. Qiao, N. Zhao, M. Zhao, L. Kong, *ChemistrySelect* **2022**, *7*, e202103668.

[6] A. Maleki, J. Rahimi, *J. Porous Mater.* **2018**, *25*, 1789.

[7] R. Taheri-Ledari, W. Zhang, M. Radmanesh, S. S. Mirmohammadi, A. Maleki, N. Cathcart, V. Kitaev, *Small* **2020**, *16*, 2002733.

[8] P. Lepcio, F. Ondreas, K. Zarybnicka, M. Zboncak, O. Caha, J. Jancar, *Soft Matter* **2018**, *14*, 2094.

[9] Y. Li, X. Xia, W. Hou, H. Lv, J. Liu, X. Li, *Int. J. Nanomed.* **2023**, *18*, 1109.

[10] R. Eivazzadeh-Keihan, F. Radinekiyan, H. A. M. Aliabadi, S. Sukhtezari, B. Tahmasebi, A. Maleki, H. Madanchi, *Sci. Rep.* **2021**, *11*, 650.

[11] M. M. Shameem, S. M. Sasikanth, R. Annamalai, R. G. Raman, *Mater. Today: Proc.* **2021**, *45*, 2536.

[12] I. Armentano, M. Dottori, E. Fortunati, S. Mattioli, J. M. Kenny, *Polym. Degrad. Stab.* **2010**, *95*, 2126.

[13] A. Maleki, V. Eskandarpour, *J. Iran. Chem. Soc.* **2019**, *16*, 1459.

[14] S. Sonawane, P. Thakur, R. Paul, *Mater. Today: Proc.* **2020**, *27*, 550.
[15] M. Naffakh, A. M. Diez-Pascual, C. Marco, G. J. Ellis, M. A. Gomez-Fatou, *Prog. Polym. Sci.* **2013**, *38*, 1163.
[16] M. Aslam, M. A. Kalyar, Z. A. Raza, *Polym. Eng. Sci.* **2018**, *58*, 2119.
[17] C. Cazan, A. Enesca, L. Andronic, *Polymer* **2017**, *2021*, 13.
[18] H. Chen, C. Xu, F. Zhao, C. Geng, Y. Liu, J. Zhang, Q. Kang, Z. Li, *Appl. Surf. Sci.* **2023**, *609*, 155447.
[19] A. Maleki, F. Hassanzadeh-Afruzi, Z. Varzi, M. S. Esmaeili, *Mater. Sci. Eng. C.* **2020**, *109*, 110502.
[20] N. G. Sahoo, S. Rana, J. W. Cho, L. Li, S. H. Chan, *Prog. Polym. Sci.* **2010**, *35*, 837.
[21] S. Li, M. Meng Lin, M. S. Toprak, D. K. Kim, M. Muhammed, *Nano Rev.* **2010**, *1*, 5214.
[22] R. Sahay, V. J. Reddy, S. Ramakrishna, *Int. J. Mech. Eng.* **2014**, *9*, 25.
[23] Y. Liu, B. Fan, B. Xu, B. Yang, *Mater. Lett.* **2023**, *337*, 133979.
[24] C. Zhao, C. F. Cheung, P. Xu, *ISA Trans.* **2020**, *101*, 503.
[25] A. Maleki, A. A. Jafari, S. Yousefi, *J. Iran. Chem. Soc.* **2017**, *14*, 1801.
[26] B. Gajra, S. S. Pandya, G. Vidyasagar, H. Rabari, R. R. Dedania, S. Rao, *Int. J. Pharm. Res* **2026**, *2012*, 4.
[27] M. S. B. Husain, A. Gupta, B. Y. Alashwal, S. Sharma, *Environ. Eff.* **2018**, *40*, 2388.
[28] T. S. Gaaz, A. B. Sulong, M. N. Akhtar, A. A. H. Kadhum, A. B. Mohamad, A. A. Al-Amiery, *Molecules* **2015**, *20*, 22833.
[29] A. S. K. Kiran, J. B. Veluru, S. Merum, A. V. Radhamani, M. Doble, T. S. S. Kumar, S. Ramakrishna, *Nano* **2018**, *4*, 190.
[30] S. M. R. Shaikh, M. S. Nasser, I. Hussein, A. Benamor, S. A. Onaizi, H. Qiblawey, *Sep. Purif. Technol.* **2017**, *187*, 137.
[31] S. Morimune, T. Nishino, T. Goto, *Polym. J.* **2012**, *44*, 1056.
[32] A. Barman, A. De, M. Das, *J. Inorg. Organomet. Polym. Mater.* **2020**, *30*, 2248.
[33] N. Usawattanakul, S. Torgbo, P. Sukyai, S. Khantayanuwong, B. Puangsin, P. Srichola, *Polymer* **2021**, *13*, 1778.
[34] J. Chen, Z. Dong, M. Li, X. Li, K. Chen, P. Yin, *Adv. Funct. Mater.* **2022**, *32*, 2111892.
[35] T. A. Alrebdi, H. A. Ahmed, S. H. Alrefaee, R. A. Pashameah, A. Toghan, A. M. Mostafa, F. H. Alkallas, R. A. Rezk, *J. Mater. Res. Technol.* **2022**, *20*, 4356.
[36] N. Kakati, J. Maiti, G. Das, S. H. Lee, Y. S. Yoon, *Int. J. Hydrogen Energy* **2015**, *40*, 7114.
[37] A. A. A. Darwish, A. M. Aboraia, S. R. Alharbi, A. M. El Shafey, Z. M. Mohammedsaleh, H. A. Alrafai, T. A. Hanafy, A. M. A. Omar, *Opt. Mater.* **2021**, *120*, 111416.
[38] D. Fattakhova-Rohlfing, A. Zaleska, T. Bein, *Chem. Rev.* **2014**, *114*, 9487.
[39] A. Markowska-Szczupak, M. Endo-Kimura, O. Paszkiewicz, E. Kowalska, *Nanomaterials* **2020**, *10*, 2065.
[40] A. Fujishima, T. N. Rao, D. A. Tryk, *J. Photochem. Photobiol. C* **2000**, *1*, 1.
[41] N. T. Padmanabhan, H. John, *J. Environ. Chem. Eng.* **2020**, *8*, 104211.
[42] S. Banerjee, D. D. Dionysiou, S. C. Pillai, *Appl. Catal. B* **2015**, *176*, 396.
[43] A. J. Haider, Z. N. Jameel, I. H. M. Al-Hussaini, *Energy Procedia* **2019**, *157*, 17.
[44] D. Chen, R. A. Caruso, *Adv. Funct. Mater.* **2013**, *23*, 1356.
[45] Y. Liang, H. Ding, *J. Alloys Compd.* **2020**, *844*, 156139.
[46] P. Munafò, G. B. Goffredo, E. Quagliarini, *Constr. Build. Mater.* **2015**, *84*, 201.
[47] G. B. O. de la Plata, O. M. Alfano, A. E. Cassano, *Chem. Eng. J.* **2008**, *137*, 396.
[48] M. Anpo, *Catal. Surv Asia* **1997**, *1*, 169.
[49] G. Centi, *Appl. Catal. A: Gen.* **1996**, *147*, 267.
[50] X. Wang, H. Kawanami, S. E. Dapurkar, N. S. Venkataramanan, M. Chatterjee, T. Yokoyama, Y. Ikushima, *Appl. Catal. A: Gen.* **2008**, *349*, 86.
[51] X. Li, J.-L. Shi, H. Hao, X. Lang, *Appl. Catal. B* **2018**, *232*, 260.
[52] C. Carlucci, L. Degennaro, R. Luisi, *Catalysts* **2019**, *9*, 75.
[53] M. Zhao, S. Li, M. Wang, X. Guan, R. Zhao, *New J. Chem.* **2023**, *47*, 8737.
[54] B. Ghanbari Shohany, A. Khorsand Zak, *Ceram. Int.* **2020**, *46*, 5507.
[55] A. Jafari, S. Khademi, M. Farahmandjou, *Mater. Res. Express.* **2018**, *5*, 095008.
[56] A. Mahajan, M. Gupta, *Appl. Organomet. Chem.* **2021**, *35*, e6161.
[57] L. Kong, Y. Liu, L. Dong, L. Zhang, L. Qiao, W. Wang, H. You, *Dalton Trans.* **2020**, *49*, 1947.
[58] L. Kong, H. Sun, Y. Nie, Y. Yan, R. Wang, Q. Ding, S. Zhang, H. Yu, G. Luan, *Molecules* **2023**, *28*.
[59] G. Li, S. Huang, K. Li, N. Zhu, B. Zhao, Q. Zhong, Z. Zhang, D. Ge, D. Wang, *Appl. Catal. B* **2022**, *311*, 121363.
[60] Q. A. Alsulami, A. Rajeh, *Opt. Mater.* **2022**, *123*, 111820.
[61] S. Kment, H. Kmentova, P. Kluson, J. Krysa, Z. Hubicka, V. Cirkva, I. Gregora, O. Solcova, L. Jastrabik, *J. Colloid Interface Sci.* **2010**, *348*, 198.
[62] R. Qiu, W. Wang, Z. Wang, H. Wang, *Catal. Sci. Technol.* **2023**, *13*, 2566.
[63] S. B. Patil, P. S. Basavarajappa, N. Ganganagappa, M. S. Jyothi, A. V. Raghu, K. R. Reddy, *Int. J. Hydrogen Energy* **2019**, *44*, 13022.
[64] X. Zhang, Y. Liu, J. Deng, L. Jing, X. Yu, Z. Han, H. Dai, *Catal. Today* **2021**, *375*, 623.
[65] P. Legutko, T. Jakubek, W. Kaspera, P. Stelmachowski, Z. Sojka, A. Kotarba, *Top. Catal.* **2017**, *60*, 162.
[66] K. Guo, G. Gou, H. Lv, M. Shan, *Coatings* **2022**, *12*, 1559.
[67] Z. H. Fu, B. J. Yang, M. L. Shan, T. Li, Z. Y. Zhu, C. P. Ma, X. Zhang, G. Q. Gou, Z. R. Wang, W. Gao, *Corros. Sci.* **2020**, *164*, 108337.
[68] A. Zaleska, *Recent Pat. Eng.* **2008**, *2*, 157.
[69] T. Jafari, E. Moharreri, A. S. Amin, R. Miao, W. Song, S. L. Suib, *Molecules* **2016**, *21*, 900.
[70] R. Daghrir, P. Drogui, D. Robert, *Ind. Eng. Chem. Res.* **2013**, *52*, 3581.
[71] G. Li, N. M. Dimitrijevic, L. Chen, T. Rajh, K. A. Gray, *J. Phys. Chem. C* **2008**, *112*, 19040.
[72] J. Huo, J.-P. Tessonnier, B. H. Shanks, *ACS Catal.* **2021**, *11*, 5248.
[73] H. O. Otor, J. B. Steiner, C. Garcia-Sancho, A. C. Alba-Rubio, *ACS Catal.* **2020**, *10*, 7630.
[74] J. Sa, C. A. Agüera, S. Gross, J. A. Anderson, *Appl. Catal. B* **2009**, *85*, 192.
[75] C. Y. Toe, C. Tsounis, J. Zhang, H. Masood, D. Gunawan, J. Scott, R. Amal, *Energy Environ. Sci.* **2021**, *14*, 1140.

[76] S. Zhao, H. Li, B. Wang, X. Yang, Y. Peng, H. Du, Y. Zhang, D. Han, Z. Li, *Fuel* **2022**, *321*, 124124.

[77] A. Maleki, R. Paydar, *React. Funct. Polym.* **2016**, *109*, 120.

[78] J. Liu, X. Qu, C. Zhang, W. Dong, C. Fu, J. Wang, Q. Zhang, *J. Cleaner Prod.* **2022**, *377*, 134228.

[79] D. Chen, T. Savidge, *Science* **2015**, *349*, 936.

[80] Q. Wan, Z. Zhang, Z.-W. Hou, L. Wang, *Org. Chem. Front.* **2023**, *10*, 2830.

[81] R. Taheri-Ledari, J. Rahimi, A. Maleki, *Ultrason. Sonochem.* **2019**, *59*, 104737.

[82] A. Maleki, Z. Hajizadeh, R. Firouzi-Haji, *Microporous Mesoporous Mater.* **2018**, *259*, 46.

[83] A. Shaabani, E. Soleimani, A. Maleki, J. Moghimi-Rad, *Synth. Commun.* **2008**, *38*, 1090.

[84] W. Haifei, G. Chuliang, Z. Zhipeng, Z. Qingxia, L. Youshi, L. Jie, *Heterocycles* **2022**, *104*, 123.

[85] N. Jangir, S. Dhadda, D. K. Jangid, *ChemistrySelect* **2022**, *7*, e202103139.

[86] G. Tripathi, A. Kumar, S. Rajkhowa, V. K. Tiwari, *Green Synthetic Approaches for Biologically Relevant Heterocycles*, Elsevier **2021** 421.

[87] Z. Liu, B. Fan, J. Zhao, B. Yang, X. Zheng, *Corros. Sci.* **2023**, *212*, 110957.

[88] Y.-X. Hu, X. Xia, W.-Z. He, Z.-J. Tang, Y.-L. Lv, X. Li, D.-Y. Zhang, *Org. Electron.* **2019**, *66*, 126.

[89] R. Wang, L. Deng, M. Fu, J. Cheng, J. Li, *J. Mater. Chem.* **2012**, *22*, 23454.

[90] K. Wang, F. P. Guengerich, *Chem. Res. Toxicol.* **2012**, *25*, 1740.

[91] N. Pathak, E. Rathi, N. Kumar, S. G. Kini, C. M. Rao, *Mini-Rev. Med. Chem.* **2020**, *20*, 12.

[92] A. Irfan, F. Batool, S. A. Zahra Naqvi, A. Islam, S. M. Osman, A. Nocentini, S. A. Alissa, C. T. Supuran, *J. Enzyme Inhib. Med. Chem.* **2020**, *35*, 265.

[93] S. L. Khokra, K. Arora, H. Mehta, A. Aggarwal, M. Yadav, *Int. J. Pharm. Sci.* **2011**, *2*, 1356.

[94] Y. Bansal, R. Minhas, A. Singhal, R. K. Arora, G. Bansal, *Curr. Org. Chem.* **2021**, *25*, 669.

[95] J.-H. Zhao, Y.-X. Hu, H.-Y. Lu, Y.-L. Lü, X. Li, *Org. Electron.* **2017**, *41*, 56.

[96] A. G. Nurioglu, H. Akpinar, F. E. Kanik, D. Toffoli, L. Toppare, *J. Electroanal. Chem.* **2013**, *693*, 23.

[97] Q.-F. Li, M.-J. Li, H.-X. Lin, P.-P. Xu, Z.-B. Gu, Y.-M. Cui, *Heterocycl. Commun.* **2016**, *22*, 21.

[98] S. Zhang, K. Moudgil, E. Jucov, C. Risko, T. V. Timofeeva, S. R. Marder, S. Barlow, *Inorg. Chim. Acta* **2019**, *489*, 67.

[99] L. Shi, T.-T. Wu, Z. Wang, J.-Y. Xue, Y.-G. Xu, *Eur. J. Med. Chem.* **2014**, *84*, 698.

[100] C.-K. Ryu, R.-Y. Lee, S.-Y. Lee, H.-J. Chung, S. K. Lee, K.-H. Chung, *Bioorg. Med. Chem. Lett.* **2008**, *18*, 2948.

[101] Z. H. Mahmoud, R. A. Al-Bayati, A. A. Khadom, *J. Mol. Struct.* **2022**, *1253*, 132267.

[102] C. J. Gommes, *Nanoscale* **2019**, *11*, 7386.

[103] S. Landi, I. R. Segundo, E. Freitas, M. Vasilevskiy, J. Carneiro, C. J. Tavares, *Solid State Commun.* **2022**, *341*, 114573.

[104] Z. Yang, X. Chen, S. Wang, J. Liu, K. Xie, A. Wang, Z. Tan, *J. Org. Chem.* **2012**, *77*, 7086.

[105] X. Yu, Z. Zhang, R. Song, L. Gou, G. Wang, *Heterocycl. Commun.* **2020**, *26*, 1.

[106] M. Kodomari, Y. Tamaru, T. Aoyama, *Synth. Commun.* **2004**, *34*, 3029.

[107] M. Cellier, O. J. Fabrega, E. Fazackerley, A. L. James, S. Orenga, J. D. Perry, V. L. Salwatura, S. P. Stanforth, *Biorg. Med. Chem.* **2011**, *19*, 2903.

[108] B. Maleki, H. Salehabadi, *Eur. J. Chem.* **2010**, *1*, 377.

[109] K. S. Niralwad, B. B. Shingate, M. S. Shingare, *Bull. Korean Chem. Soc.* **2010**, *31*, 981.

[110] W. Senapak, R. Saeeng, J. Jaratjaroonphong, U. Sirion, *Mol.* **2018**, *458*, 97.

[111] R. M. Borade, S. B. Kale, S. U. Tekale, K. M. Jadhav, R. P. Pawar, *Catal. Commun.* **2021**, *159*, 106349.

[112] D. Saha, A. Saha, B. C. Ranu, *Green Chem.* **2009**, *11*, 733.

[113] R. V. Shingalapur, K. M. Hosamani, *Catal. Lett.* **2010**, *137*, 63.

[114] D. Secci, A. Bolasco, M. D'Ascenzio, F. della Sala, M. Yáñez, S. Carradori, *J. Heterocycl. Chem.* **2012**, *49*, 1187.

[115] F. Ganjali, A. Kashtiaray, S. Zarei-Shokat, R. Taheri-Ledari, A. Maleki, *Nanoscale Adv.* **2022**, *4*, 1263.

[116] T. T. Nguyen, X.-T. T. Nguyen, T.-L. H. Nguyen, P. H. Tran, *ACS Omega* **2019**, *4*, 368.

[117] A. Datta, *Orient. J. Chem.* **2021**, *37*, 95.

[118] G. Kaur, R. Moudgil, M. Shamim, V. K. Gupta, B. Banerjee, *Synth. Commun.* **2021**, *51*, 1100.

[119] X. Li, Q. Ma, R. Wang, L. Xue, H. Hong, L. Han, N. Zhu, *Phosphorus Sulfur Silicon Relat. Elem.* **2022**, *197*, 689.

[120] K. R. Balinge, S. K. Datir, V. B. Khajone, K. J. Bhansali, A. G. Khiratkar, P. R. Bhagat, *Res. Chem. Intermed.* **2019**, *45*, 155.

[121] D. Azarifar, M. Farbodmehr, O. Badalkhani, M. Jaymand, *Bull Chem Commun* **2019**, *51*, 596.

[122] S. Bahadorikhalili, L. Ma'mani, H. Mahdavi, A. Shafiee, *Microporous Mesoporous Mater.* **2018**, *262*, 207.

[123] A. Shaabani, Z. Hezarkhani, *Appl. Organomet. Chem.* **2017**, *31*, e3542.

SUPPORTING INFORMATION

Additional supporting information can be found online in the Supporting Information section at the end of this article.

How to cite this article: A. Mahajan, M. Gupta, *Appl Organomet Chem* **2023**, e7195. https://doi.org/10.1002/aoc.7195

Subject: Gupta, Monika sc-2023-05011k.R2 - Manuscript Accepted 11-Jan-2024

From: ACS Sustainable Chemistry & Engineering <onbehalfof@manuscriptcentral.com> on Thu, 11 Jan 2024 20:03:26

To: monika.gupta77@rediffmail.com

11-Jan-2024

Journal: ACS Sustainable Chemistry & Engineering
Manuscript ID: sc-2023-05011k.R2
Title: "Cu@Ag-CeO2/Chitosan Nanocomposite: Green Catalyst for synthesis of 4-Arylidene-Isoxazolidinones & Amidoalkyl Naphthols with DFT and Antimicrobial Studies"
Author(s): Mahajan, Ankush; Mahajan, Ankit; Kuznetsov, Aleksey; Gupta, Monika
Manuscript Status: Accept

Dear Dr. Gupta:

We are pleased to inform you that your manuscript has been accepted for publication in ACS Sustainable Chemistry & Engineering.

You will soon receive an email invitation from the ACS Journal Publishing Staff that contains a link to the online Journal Publishing Agreement. Please sign and submit the journal publishing agreement within 48 hours.

Your manuscript has been forwarded to the ACS Publications office. You will be contacted in the near future by the ACS Journal Publishing Staff regarding the proofs for your manuscript.

After you approve your proofs, your manuscript will be published on the Web in approximately 48 hours. In view of this fast publication time, it is important to review your proofs carefully. Once a manuscript appears on the Web it is considered published. Any change to the manuscript once it appears on the Web will need to be submitted to the journal office as additions or corrections.

Once your paper is published, you can track downloads and citations of your work by logging into the ACS Publishing Center (https://pubs.acs.org/publish/dashboard) and selecting "Published".

Thank you for selecting ACS Sustainable Chemistry & Engineering as your research publication medium.

Sincerely,

Nicholas Gathergood
University of Lincoln
School of Chemistry
Joseph Banks Laboratories
Brayford Pool, Lincoln, LN6 7TS
Email : gathergood-office@sustain.acs.org

Thank you.

Cu@Ag-CeO2/Chitosan Nanocomposite: Green Catalyst for synthesis of 4-Arylidene-Isoxazolidinones & Amidoalkyl Naphthols with DFT and Antimicrobial Studies

Journal:	*ACS Sustainable Chemistry & Engineering*
Manuscript ID	sc-2023-05011k.R1
Manuscript Type:	Article
Date Submitted by the Author:	n/a
Complete List of Authors:	Mahajan, Ankush; University of Jammu Mahajan, Ankit; University of Jammu Kuznetsov, Aleksey; Universidad Tecnica Federico Santa Maria, Chemistry Gupta, Monika; University of Jammu,

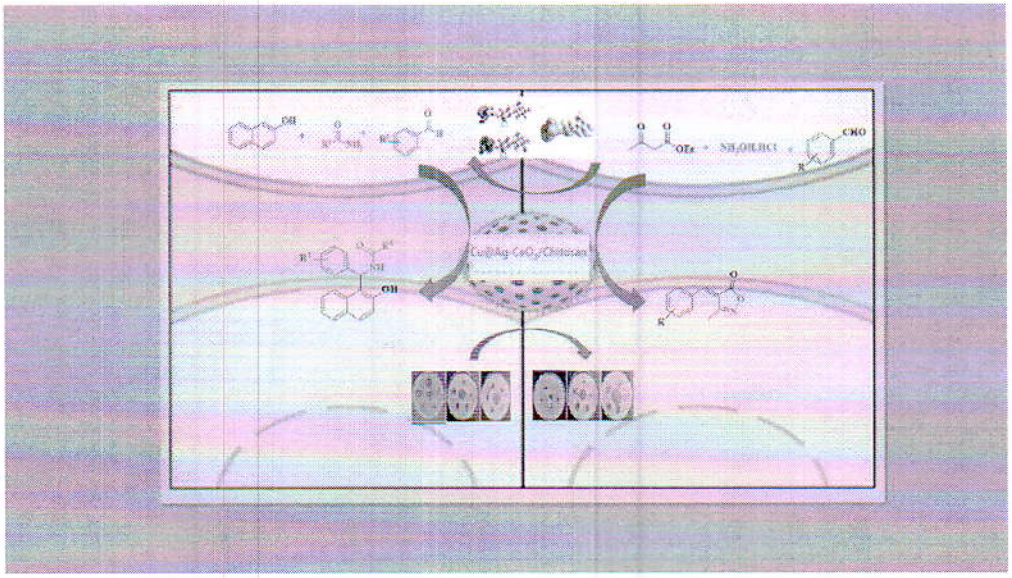

Graphical abstract

338x190mm (96 x 96 DPI)

Cu@Ag-CeO_2/Chitosan Nanocomposite: Green Catalyst for synthesis of 4-Arylidene-Isoxazolidinones & Amidoalkyl Naphthols with DFT and Antimicrobial Studies

Ankush Mahajan[a], Ankit Mahajan[b], Aleksey Kuznetsov[c] and Monika Gupta*[a]

[a] *Department of Chemistry, University of Jammu, Jammu*

[b] *School of Biotechnology, University of Jammu, Jammu*

[c] *Department of Chemistry, Universidad Técnica Federico Santa Maria 6400, Vitacura 7660251, Santiago, Chile*

Abstract

Multifunctional nanocomposite has been developed containing polymer chitosan, nano silver doped ceria and copper nanoparticles. Cu-CeO_2 catalysts have been widely used as active catalysts whereas doping of Ag to CeO_2 is known to enhance the oxygen storage capacity (OSC) of CeO_2. Various characterization tools such as Powder X-Ray Diffraction (PXRD), Fourier transform infrared spectroscopy (FTIR), Thermogravimetric analysis (TGA), Field emission Scanning Electron Microscopy (FR-SEM), EDX Elemental Mapping, High Resolution Transmission Electron Microscopy (HR-TEM), have been used for the nanocomposite characterization. Surface area was found using Brunauer–Emmett–Teller (BET). Optical properties by UV vis Diffuse reflectance spectroscopy (DRS), Photoluminescence (PL) spectroscopy has been given. Average nanocomposite particle size was found to be 4 nm. The nanocomposite optical properties were reported as well. The synergistic effects of metal-support interfaces, along with charge transfer between metal oxide and metal, have the capacity to yield noteworthy catalytic properties. The nanocomposite was used as a catalyst for the synthesis of the 4-arylidene-isoxazolidinones and amidoalkyl naphthols which are the moieties used in the various useful molecules. Its antibacterial activity for gram positive and gram-negative bacteria was evaluated. Also, Density Functional Theory (DFT) study was performed which supported the experimental findings.

Keywords: Ceria, Doping, Silver, Copper, Isoxazoles, Amidoalkyl naphthols, Antibacterial activity, DFT

Supporting information available

1. Introduction

The development of polymeric nanocomposites, containing polymer matrices and in which at least one of the filler material particle diameters is of the order of a nanometer, has received a lot of attention in the last years. [1-3] Polymer nanocomposites are commercially synthesized for a wide range of uses, including catalysis[4], antimicrobial agents[5], tissue engineering,[6, 7] recreational goods[8], aerospace components[9], vehicles[10], and so on. Catalysis plays a pivotal role in chemical reactions and constitutes a fundamental aspect of numerous synthetic processes across academia, research

purification of intermediate products, multicomponent reactions have received special attention in green synthesis.[42-44]

Isoxazole and its derivatives are important heterocycles that are utilised to make synthetic therapeutics[45-47]. Because of their anti-inflammatory[48], fungicidal[49], antioxidant[50], analgesic[51], antimicrobial[52], antiviral properties[53], etc., they are well-known in medicine and organic chemistry. Synthetic methods aimed at creating this heterocycle core are a constant source of interest, and many procedures have been developed to attain this goal.[54]A range of biologically essential natural products and strong medicines, such as nucleoside antibiotics and HIV protease inhibitors like ritonavir and lopinavir, contain compounds with 1,3-amino oxygenated functional groups.[55] By using an amide hydrolysis procedure, 1-amidoalkyl-2-naphthols can be transformed to physiologically active 1-aminomethyl-2-naphthol derivatives.[56-58] These substances' hypotensive and bradycardic actions have been studied.[59] Multicomponent condensation of aryl aldehydes, 2-naphthol, and amide in the presence of nanocatalysts can be used to make 1-amidoalkyl-2-naphthols.[60-65]

Nanoparticles exhibit a wide-ranging antibacterial effect against both gram-positive and gram-negative bacteria.[66-70] Despite not fully understanding the specific antibacterial processes of nanoparticles, various types of nanoparticles typically produce different effects. The antibacterial mechanisms of nanoparticles can be categorized into three main groups: induction of oxidative stress, release of metal ions, and non-oxidative mechanisms.[71-73] These mechanisms may occur simultaneously. In some studies, silver nanoparticles, for instance, are reported to neutralize the surface electric charge of the bacterial membrane and alter its permeability, ultimately leading to bacterial mortality.[74-76]

Thus, motivated by the above consideration, we have synthesized and fully characterized the novel Cu@Ag-CeO_2/chitosan nanocomposite and tested its catalytic activity in the synthesis of the 4-arylidene-isoxazolidinones and amidoalkyl naphthols along with its DFT studies and antibacterial activity.

2. Experimental Part

2.1. Synthesis of Cu@Ag-CeO_2/chitosan nanocomposite

2.1.1. Preparation of chitosan solution

Chitosan powder (1g) was thoroughly dissolved in a 20% v/v aqueous acetic acid solution through overnight stirring in a 100 mL round-bottomed flask.

2.1.2. Synthesis of silver doped Ceria (Ag-CeO_2)

The synthesis of silver-doped ceria (Ag-CeO_2) utilized the co-precipitation method. A mixture of ceric ammonium nitrate ($(NH_4)_2Ce(NO_3)_6$, 20 g) and silver nitrate ($AgNO_3$, 5.1g, 0.3 mol eq) was introduced into distilled water (100 mL) and stirred at 80°C for 5 hours. Following this, an aqueous

approximately 10.0 was achieved. The reaction mixture was then heated at 80°C for 3 hours. The resulting suspension underwent filtration, followed by multiple rinses with deionized water and ethanol. The prepared sample was dried overnight at 110°C and subjected to calcination for 3 hours at 400°C.

2.1.3. Preparation of silver doped ceria–chitosan nanocomposite (Ag-CeO_2/chitosan)

A 2 wt% chitosan solution was introduced into a 100 mL round-bottom flask, and 5g (10 wt.%) of nano Ag-doped CeO_2 was added to it in deionized water. The mixture was stirred continuously for 3 hours to synthesize the chitosan-silver-doped ceria nanocomposite (Ag-CeO_2/chitosan). The resulting Ag-CeO_2/chitosan mixture was subsequently dispersed in a concentrated NaOH aqueous solution, filtered, and subjected to multiple washes with water. Finally, the composite was dried at room temperature.

2.1.4. Synthesis of copper nanoparticles @ silver doped ceria and chitosan (Cu@Ag-CeO_2/chitosan)

A 0.1 M solution of copper sulphate ($CuSO_4$) was prepared in deionized water. The Ag-CeO_2/chitosan nanocomposite served as the support material. The dried Ag-CeO_2/chitosan nanocomposite was stirred for 3 hours in a 100 mL solution of $CuSO_4$ (0.1 M). Cu^{2+} ions were adsorbed onto the Ag-CeO_2/chitosan support. After filtration and drying at room temperature, the prepared nanocomposite was immersed for 1 hour in a 100 mL 0.1 M aqueous sodium borohydride solution to convert the metal ions into alloy nanoparticles. The shift in colour to black upon immersion in the $NaBH_4$ solution indicated the complete removal of Cu^{2+}, signifying the formation of Cu@Ag-CeO_2/chitosan nanocomposite. However, when exposed to open air, the reduced Cu nanoparticles immobilized in the Ag-CeO_2/chitosan oxidized. [77]

2.2. Procedure for the preparation of 4-arylidene-isoxazolidinones

A solution of ethyl acetoacetate (1 mmol), hydroxylamine hydrochloride (1 mmol), and aromatic aldehyde (1 mmol), Cu@Ag-CeO_2/chitosan (10 mg) as catalyst in Ethanol / water (10:1) was magnetically stirred at 80 °C for the required period. TLC (n-hexane/ethyl acetate: 10/3 v/v) was used to monitor the entire consumption of the starting ingredients. After the process was completed, the catalyst was removed from the reaction mixture by dissolving it in hot EtOH and filtering it out. After adding 10 ml of cold water to the filtrate, the precipitate was collected by filtration and rinsed with a cold ethanol–water mixture. The pure product was dried and identified using spectroscopic data and by comparing melting points to reported values.

2.3. Procedure for the preparation of amidoalkyl naphthols

To a mixture of aldehyde (1 mmol), 2-naphthol (1 mmol) and amide/urea (1 mmol), Cu@Ag-CeO_2/chitosan as catalyst (10 mg) was added. The reaction mixture stirred magnetically at 100 °C for appropriate time. The progress of the reaction was monitored by thin layer chromatography. After

acetate washed with water. The catalyst was separated from the filtrate. The residue was dried and recrystallized from ethanol or by column chromatography (EtOAc/Hexane 40:60).

2.4. Computational details

DFT studies were performed with the Gaussian 16 software.[78] In our study we used the Ce_3CuAgO_7 model, which was connected through the oxo-bridge to two chitosan monomer units used to model the chitosan polymer. The calculations were performed with the hybrid density functional B3LYP[79] with the SDD basis set, which is the Dunning/Huzinaga full double zeta basis set up to Ar[80] and Stuttgart/Dresden ECPs on the remainder of the periodic table[81-83], the approach furthermore referred to as B3LYP/SDD. We did the computational studies and the analyses listed below with the B3LYP/SDD approach in the gas phase. Below we consider the calculated structural parameters, Mulliken charges, and frontier molecular orbitals (FMOs) for the model studied. Avogadro, version 1.1.1, was used to visualize the structure, FMOs, and molecular electrostatic potential (MEP) plot[84, 85]

3. Results and Discussion

3.1. Characterization of Cu@ Ag-CeO_2/chitosan

3.1.1. Powder X-ray Diffraction

Figure 1 illustrates the XRD patterns of the Cu@Ag-CeO_2/chitosan catalysts. The typical peaks of fluorite CeO_2 crystal structure in 2θ degrees at 228.6, 33.1, 47.5, 56.3, 59.1, and 69.4 which can be assigned to the (111), (200), (220), (311), (222), (400), (331) and (420) planes, respectively (JCPDS 34-0394), were observed in the pattern. The peak of chitosan is also shown in the Fig. 1, and a broad peak was observed at the 2-theta value of 20-21° that can be ascribed to the characteristic peak of chitosan. The peaks of Cu could not be detected, suggesting that Cu nanoparticles were well dispersed on the support. Additionally, the peaks of Ag were not detected owing to the low Ag content of the catalyst.[86] The particle size of the nanoparticles was calculated using the Debye-Scherer equation [87] (equation 1).

$$D = \frac{0.9\lambda}{\beta Cos\theta} \qquad \text{Equation 1}$$

β is the full line width at half maximum;

D is the crystallite size;

Θ is the Bragg's diffraction angle;

λ is the wavelength = 1.5406 Å.

Crystallite size was found to be in an excellent range of 4nm.

Additionally, the sharpness of the red peak (XRD peaks of Ag-doped CeO_2 nanoparticles) as compared to black (XRD peaks of CeO_2 nanoparticles) may be attributed to the doping of Ag in the ceria lattice due to which the crystalline nature of the nanocomposite was formed and thereby

to the difference in the electron densities of the dopant and the host atoms, which mainly depends on the scattering factor, structure factor, etc.

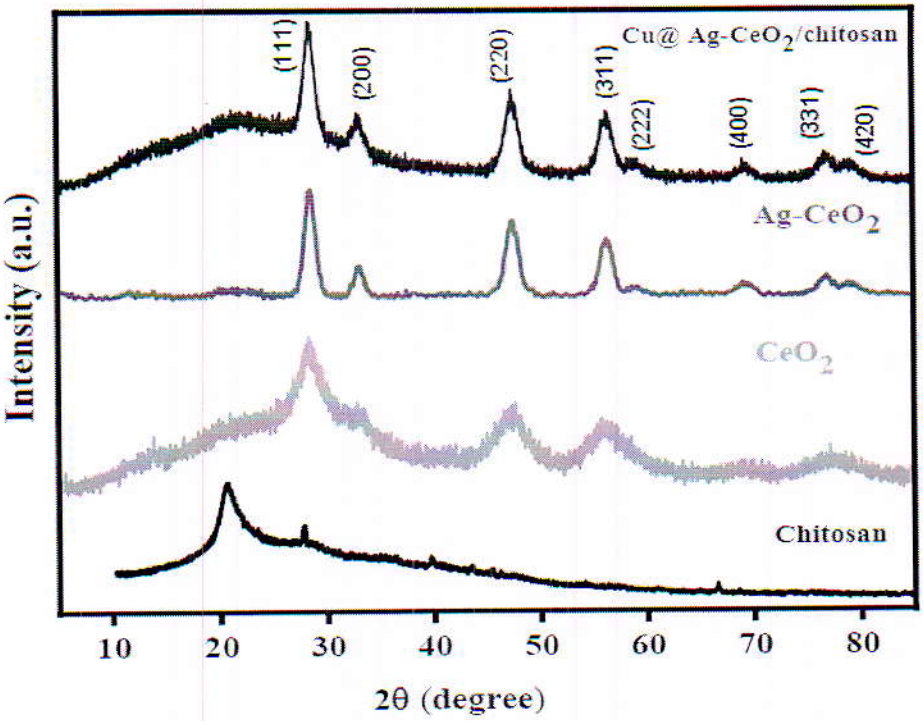

Figure 1. PXRD results for (a) Chitosan (b) CeO_2, (c) Ag-CeO_2, (d) Cu@ Ag-CeO_2/chitosan.

3.1.2. FTIR study

The main functional groups and their interactions were identified using FT-IR analysis of pure CeO_2, Ag-CeO_2, and the Cu@Ag-CeO_2/chitosan nanocomposite; the results are given in Figure. 2. In CeO_2 absorption peaks can be found at 3553 1632, 1116, 725, and 494cm^{-1}. The peak at 3553 cm^{-1} is due to stretching vibration of O-H bonds in H_2O molecules, whereas the band at 1632 cm^{-1} is due to in-plane and out-of-plane bending of O-H bonds in the adsorbed water molecule. The sharp peak at 494 cm^{-1} corresponds to the surface-bridging oxide's antisymmetric Ce-O-Ce stretching. The FT-IR findings of Cu@ Ag-CeO_2/chitosan revealed seven prominent absorption peaks at 3430, 2922, The production of Ce–O bonds is responsible for the large peaks detected at 449 and 769 cm^{-1}. The absorption peak at 1024 cm^{-1} is attributed to a weak stretch of –COO– pectin and C=O amide, indicating the presence of chitosan. At 1349 cm^{-1}, the stretching vibration of the major chains of the C=O and C–O–C groups was assigned. The stretching vibration of the C=C bond was recorded at 1663 cm-1. The stretching vibration of –C–H, =C–H, and O–H groups in chitosan is responsible for the peaks at 2922 and 3430 cm^{-1}. These results were consistent with earlier findings. [88-90]

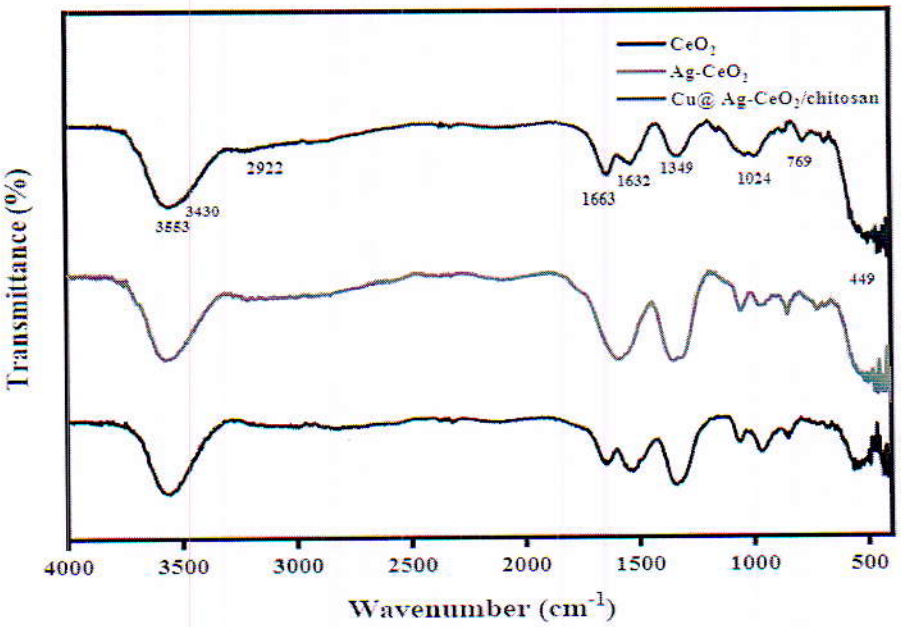

Figure 2. FTIR spectra of (a) CeO_2, (b) Ag-CeO_2, (c) Cu@Ag-CeO_2/chitosan.

3.1.3. Thermogravimetric analysis (TGA)

Figure 3 depicts a comparison among CeO_2, Ag-CeO_2, and Cu@Ag-CeO_2/chitosan. The Thermogravimetric Analysis (TGA) graph revealed the stability of the nanocomposite up to 800°C with minimal loss. In the TGA graph of Cu@Ag-CeO_2/chitosan, the initial loss may be attributed to residual water, and 87% of the catalyst remains undecomposed. Much of this loss, over 10%, occurs up to 100°C, indicating that the observed decline might be due to the presence of residual water in the catalyst. Further degradation of the nanocomposite from 200-300 °C can be due to the chitosan.

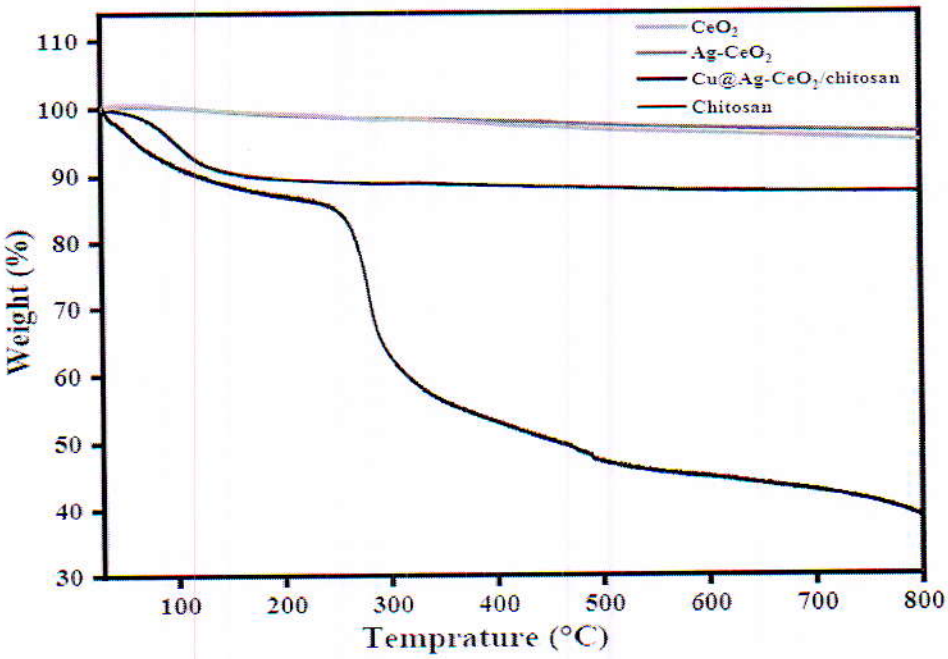

Figure 3. TGA results of (a) Chitosan (b) CeO_2, (c) Ag-CeO_2, (d) Cu@Ag-CeO_2/chitosan.

3.1.3. FE-SEM study

structure is evident. The particles are quasispherical in shape showing flocculation that are quite uniformly conglomerated.

3.1.4. EDX study

All essential elements (Ag, Ce, Cu, C, N, and O) are detected, confirming the presence of organic molecules from chitosan in Cu@Ag-CeO_2/chitosan, as well as the presence of Ag and ceria. Presence of copper was also confirmed as shown in Figure 5. Table 1 provides results of the elemental analysis of Cu@Ag-CeO_2/chitosan nanocomposite. It can be seen that 79% of particles weight is of ceria and Ag together. The presence of copper nanoparticles (around 3%) is clearly indicated as well (Table 1).

3.1.5. Elemental mapping

The elemental mapping technique was applied to the prepared nanocomposite to assess the presence and distribution of elements (see Figure 6). The images substantiate the even distribution of Cu and Ag-CeO_2 across the chitosan. Figure 6 presents elemental maps for C, O, N, Ag, Ce, and Cu, respectively.

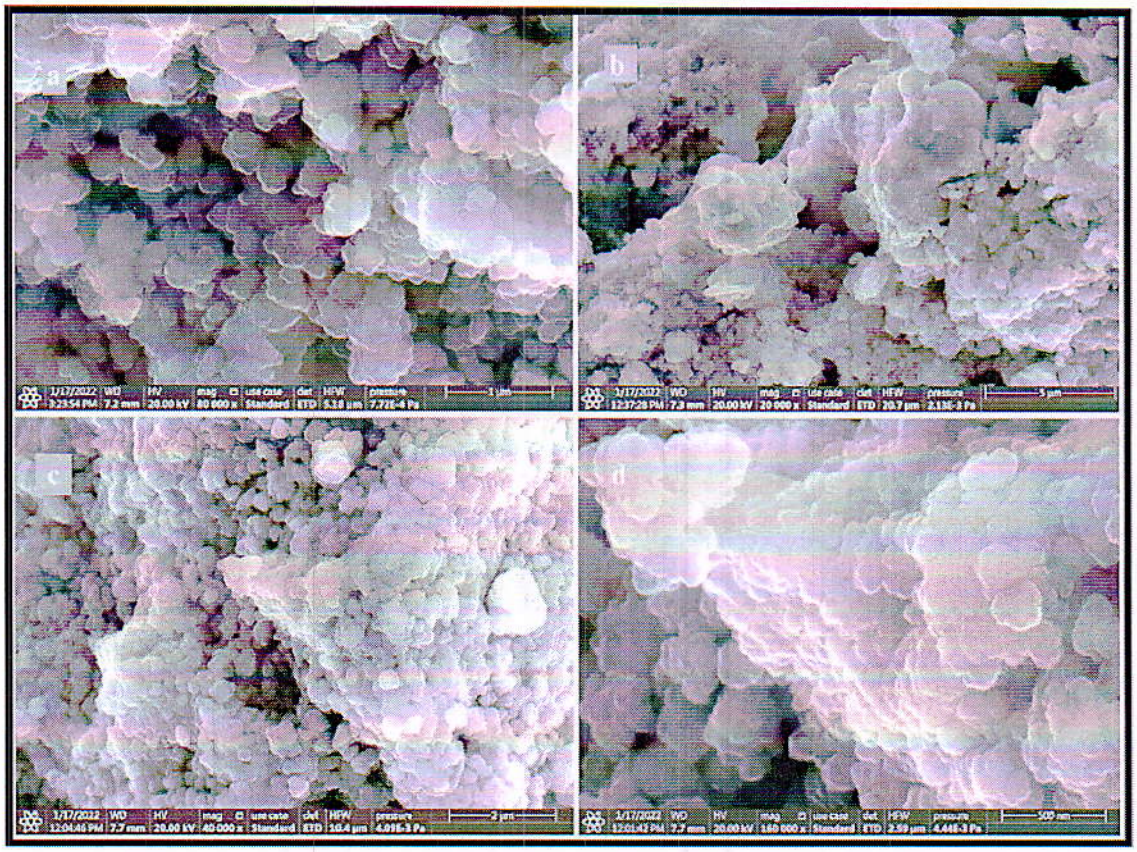

Figure 4. Field emission scanning electron microscopy (FE-SEM) images of (a) Ag-CeO_2, (b) Ag-CeO_2/chitosan, (c) Cu@Ag-CeO_2/chitosan at 2 μm, and (d) Cu@Ag-CeO_2/chitosan at 500 nm.

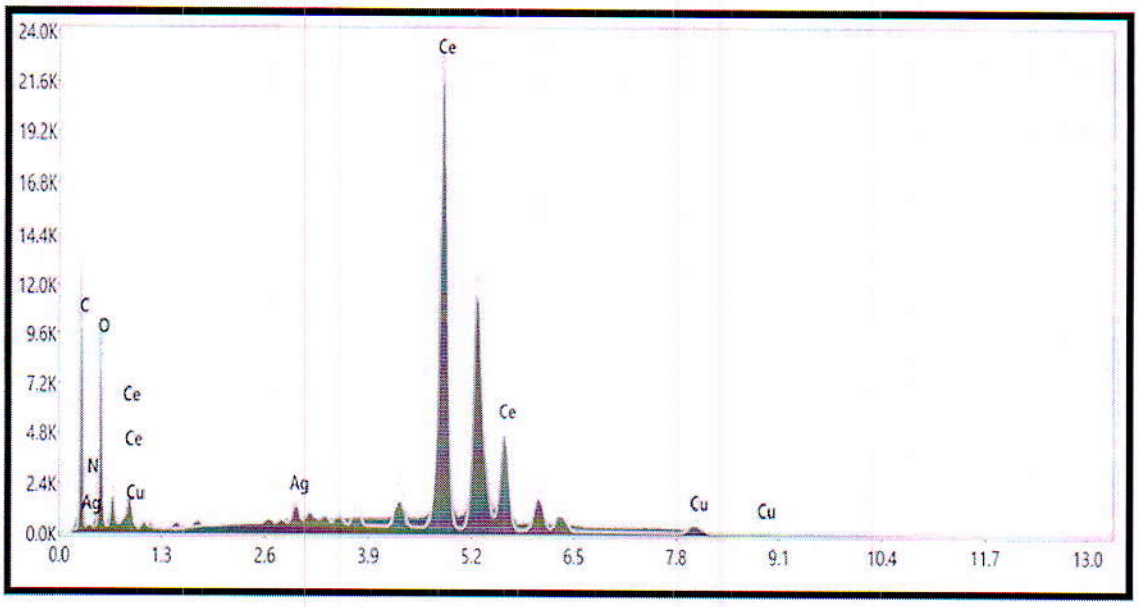

Figure 5. Energy dispersive X-ray (EDX) spectrum of Cu@Ag-CeO_2/chitosan.

Table 1. EDX analysis of Cu@Ag-CeO_2/ chitosan.

Element	Weight %	Atomic %	Error %
C K	12.8	52.2	10.3
N K	0.2	0.6	23.1
O K	5.6	17.2	10.1
Cu K	2.9	2.3	6.2
Ag L	1.6	0.7	6.1
Ce L	77.0	27.0	2.6

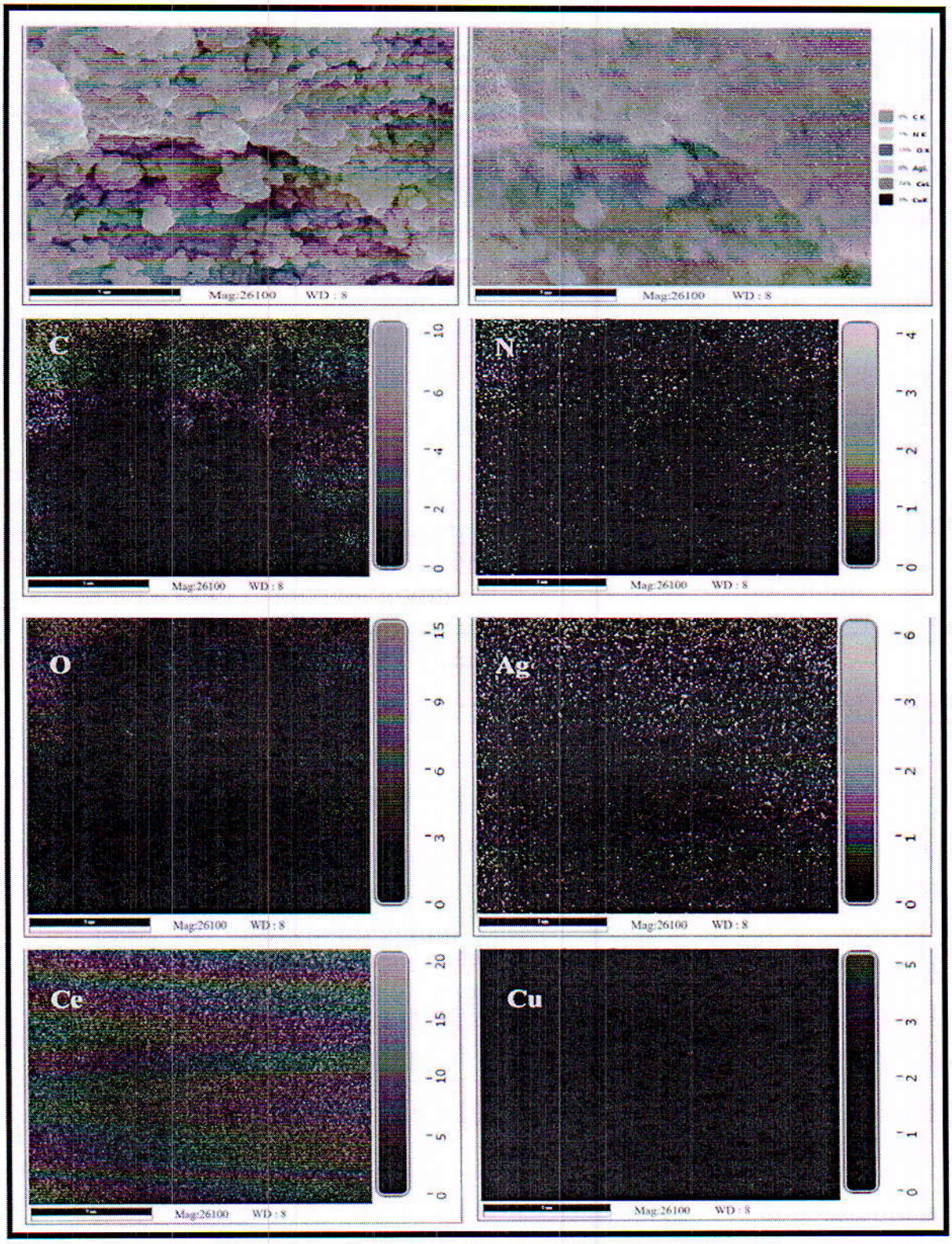

Figure 6. Elemental mapping of Cu@Ag-CeO_2/chitosan.

3.1.6. HR-TEM study

High-resolution transmission electron microscopy (HR-TEM) substantiated the formation of the nanocomposite. Ultrafine particles are observable in Figure 7, revealing two types of nanoparticles, namely Cu and Ag-CeO_2, embedded in the chitosan. The average size distribution of these nanoparticles was determined to be 4 nm, consistent with the findings from powder X-ray diffraction (P-XRD) shown in Figure 8. The selected area diffraction (SAED) pattern, as shown in the inset of Figure 7, revealed the amorphous characteristics of the catalyst.

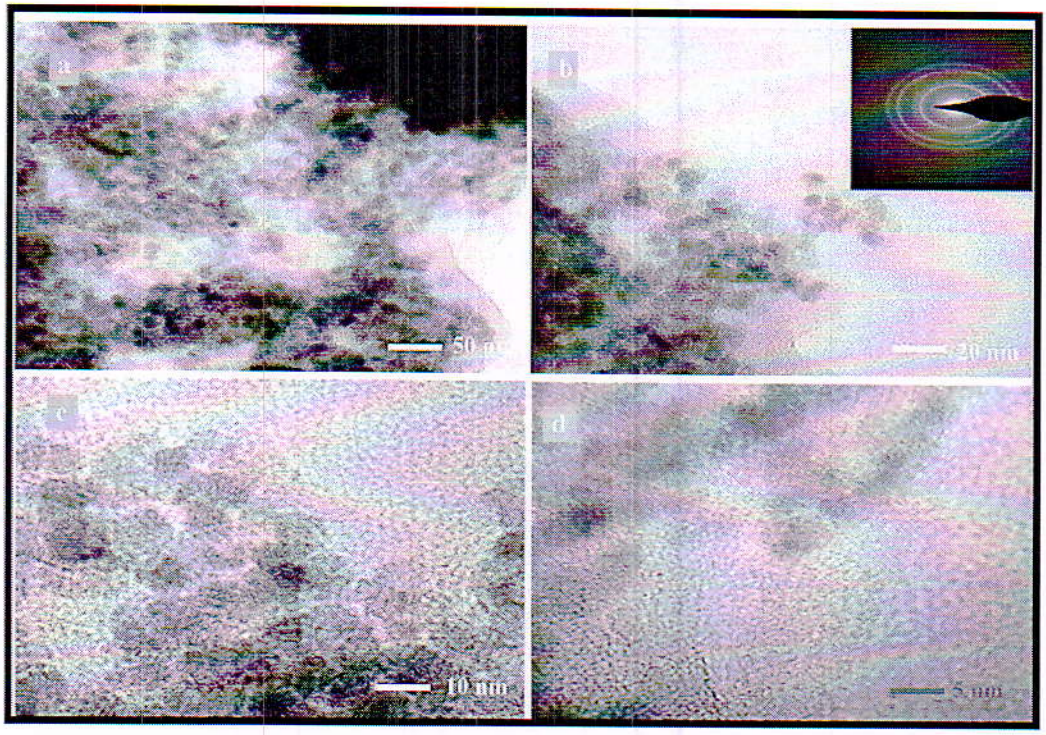

Figure 7. HR-TEM images of Cu@Ag-CeO_2/chitosan at (a) 50 nm, (b) 20 nm, (c) 10 nm, (d) 5nm (inset) SAED pattern.

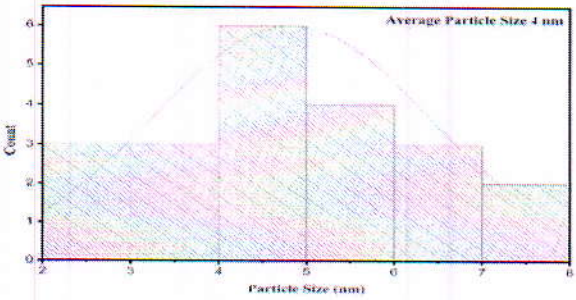

Figure 8. Average size distribution.

3.1.7. BET study

The N_2 adsorption/desorption isotherms of CeO_2 (Figure 9a), Ag-CeO_2 (Figure 9b), and Cu@Ag-CeO_2/chitosan nanocomposite (Figure 9c) were investigated. The isotherms obtained for CeO_2, Ag-CeO_2, and Cu@Ag-CeO_2/chitosan displayed a Type IV hysteresis loop, indicative of mesoporous materials. This characteristic pattern signifies narrow slit-like pores, particles with irregularly shaped

between larger particles, contributing to a more uniform and smoother surface. Additionally, the isotherms indicated the presence of hollow spheres with walls composed of ordered mesoporous ceria.

The BET surface area measurements for CeO_2, Ag-CeO_2, and Cu@Ag-CeO_2/chitosan were determined to be 47 $m^2\ g^{-1}$, 51 $m^2\ g^{-1}$, and 61 $m^2\ g^{-1}$, respectively. The total pore volume for CeO_2, Ag-CeO_2, and Cu@Ag-CeO_2/chitosan was found to be 0.03 $cm^3\ g^{-1}$, 0.11 $cm^3\ g^{-1}$, and 0.10 $cm^3\ g^{-1}$, respectively. The mean diameter of the pores was measured at 2.6 nm, 8.5 nm, and 6.8 nm for CeO_2, Ag-CeO_2, and Cu@Ag-CeO_2/chitosan, respectively. The decrease in pore diameter after nanocomposite formation can be attributed to the incorporation of nanoparticles into the composite material. Nanoparticles typically have a smaller size compared to the pores in the original material, and their presence can fill or block some of the pores. This filling effect reduces the overall pore size, leading to a decrease in pore diameter in the nanocomposite. Additionally, the interaction between the nanoparticles and the surrounding matrix may contribute to changes in the material's microstructure, influencing pore characteristics.

Table 2. BET analysis.

	BET surface area ($m^2\ g^{-1}$)	*Total pore volume* ($cm^3\ g^{-1}$)	*Mean pore diameter* (*nm*)
CeO_2	47	0.03	2.6
Ag-CeO_2	51	0.11	8.5
Cu@ Ag- CeO_2/chitosan	61	0.10	6.8

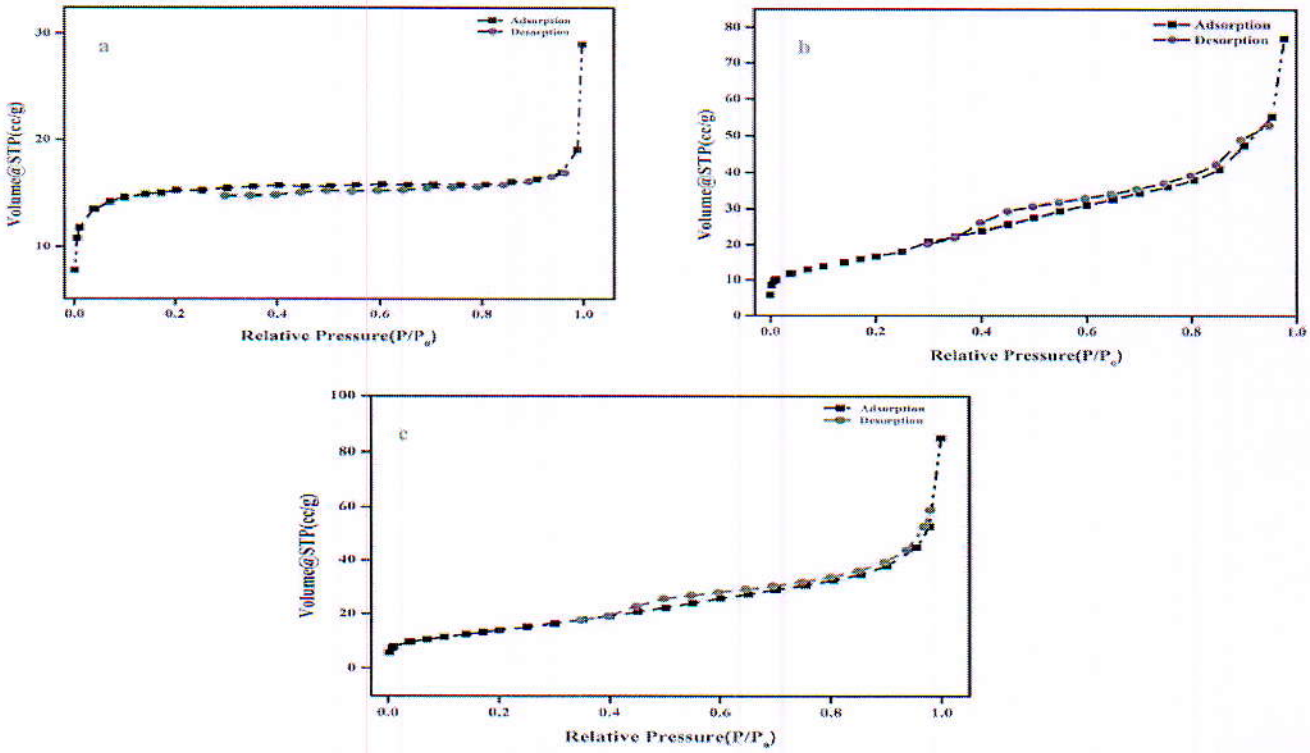

Figure 9. Adsorption–desorption spectrum of (a) CeO_2, (b) Ag-CeO_2, (c) Cu@Ag-

3.1.8. Optical properties of Cu@ Ag-CeO_2/chitosan nanocomposite

3.1.8.1. UV-vis spectrum

Figure 10 displays the diffuse reflectance spectra of the Cu@Ag-CeO_2/Chitosan nanocomposite. The band gap energy was calculated using the Kubelka–Munk equation, where the absorption (F(R)) is related to the reflectance (R) in DRS mode (equation 2).

$$F(R) = \frac{(1 - R)^2}{2R} \qquad \text{Equation 2}$$

In the equation, R represents the reflectance of the sample.

Figure 11 illustrates the Kubelka–Munk plot, revealing absorption peaks at 500 nm in the UV region. These peaks stem from charge transfer from O^{2-} 2p valence band to Ce^{4+} f-band. In CeO_2, the valence band has a width of 4 eV, and the conduction band is at the Ce 5d level, with the Ce 4f level situated between these two states and just above the Fermi level.

To determine the direct band gap, the plot of $[F(R)\ h\upsilon]^2$ against energy is plotted, and the linear segment of the curve is extended to $[F(R)^*\ h\upsilon]^2 = 0$ (refer to Figure 12). In this context, h represents Planck's constant, and ν denotes the ratio of the speed of light (c) to the wavelength (λ). The extrapolation results in a band gap value of 2.7 eV, which is smaller than the band gap of CeO_2 (3.1 eV). A comparison between the band gap of CeO_2 and the Cu@Ag-CeO2/chitosan nanocomposite indicates a red shift.

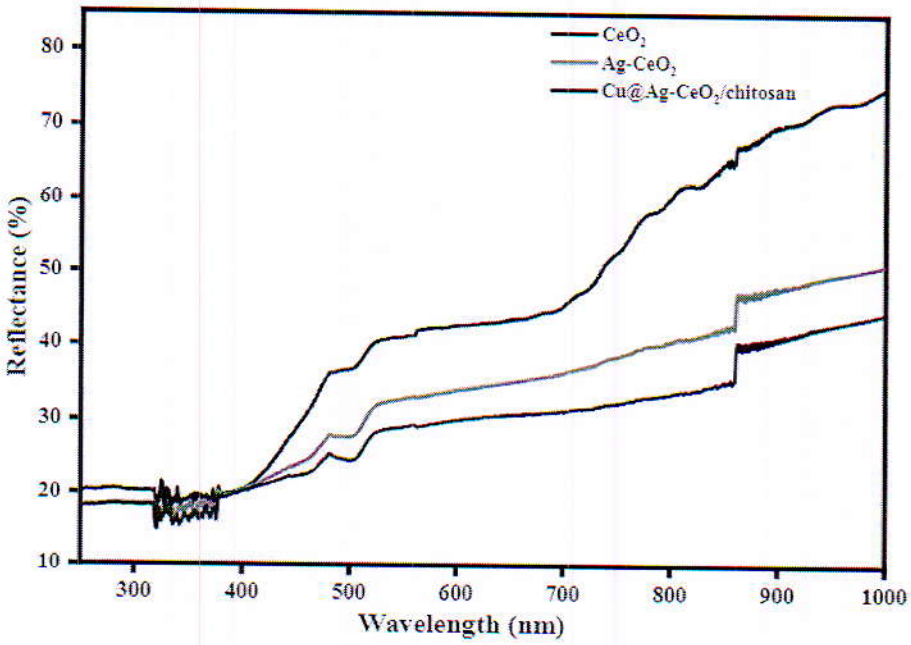

Figure 10. Diffuse reflectance spectrum of (a) CeO_2, (b) Ag-CeO_2, (c) Cu @Ag-CeO_2/chitosan.

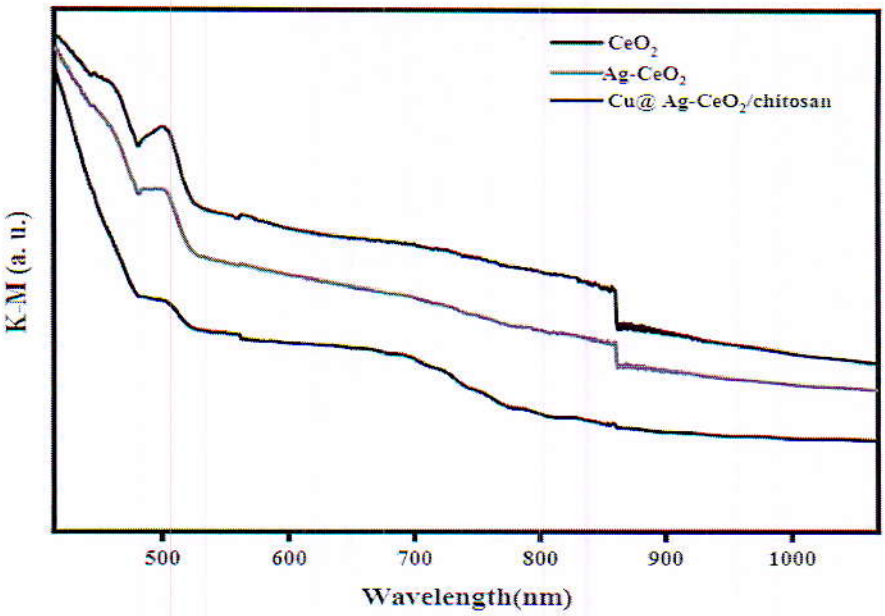

Figure 11. Kubelka–Munk plot of (a) CeO_2, (b) Ag-CeO_2, (c) Cu@Ag-CeO_2/chitosan.

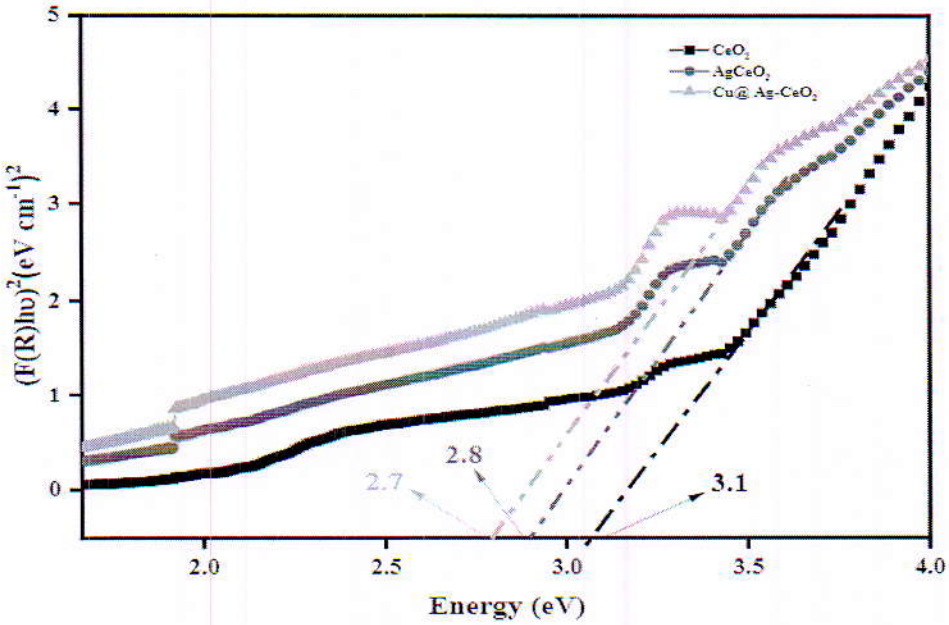

Figure 12. Band gap (direct) determination by plotting $[F(R)^* h\upsilon]^2$ vs. energy for (a) CeO_2, (b) Ag- CeO_2, (c) Cu@ Ag-CeO_2/chitosan.

3.1.8.2. Photoluminescence study

The photoluminescent (PL) spectra of the Cu@Ag-CeO_2/chitosan nanocomposite reveal that upon excitation at 425 nm, the emitted wavelength centres around 427 nm. This emitted peak corresponds to violet light, as depicted in Figure 13.

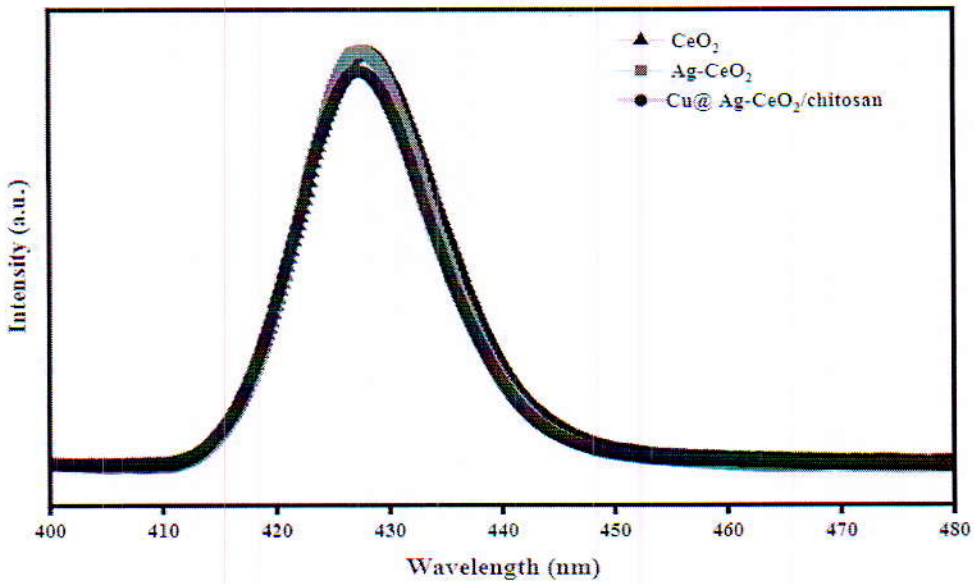

Figure 13. Photoluminescence spectra (a) CeO_2, (b) Ag-CeO_2, (c) Cu@Ag-CeO_2/chitosan.

3.2. Syntheses of 4-arylidene-isoxazolidinones and amidoalkyl naphthols

3.2.1. Synthesis of 4-arylidene-isoxazolidinones

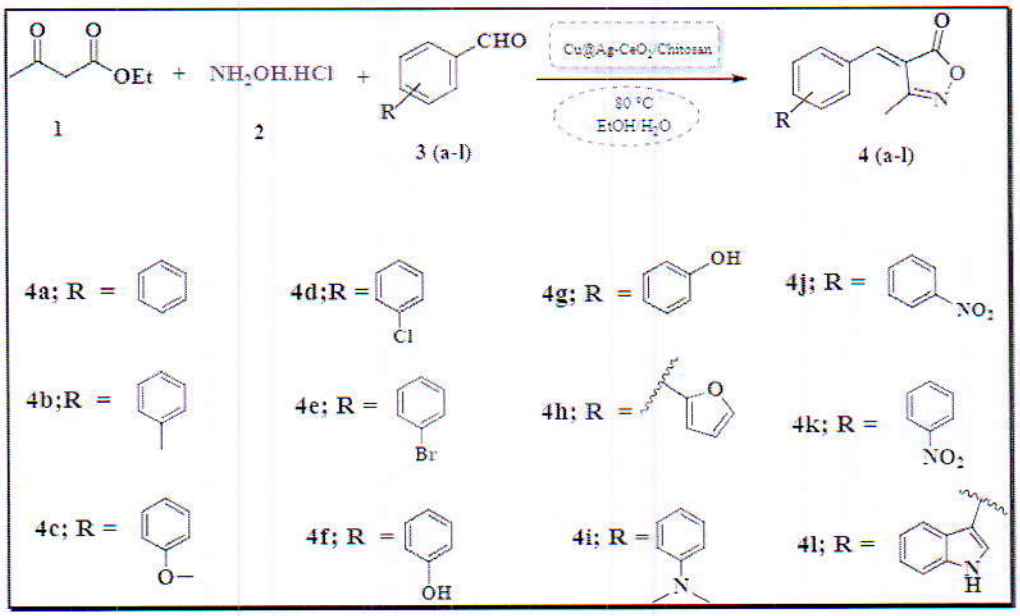

Scheme 1. Synthesis of 4-arylidene-isoxazolidinones.

The investigation focused on the reaction involving aldehydes, ethyl acetoacetate, and hydroxylamine hydrochloride in the presence of the heterogeneous catalyst Cu@Ag-CeO_2/chitosan (Scheme 1). The catalyst's role, along with factors such as reaction temperature, solvent, and reaction time, were systematically explored. In a model reaction with benzaldehyde (1 mmol, 106.1 mg), ethyl acetoacetate (1 mmol, 130.1 mg), and hydroxylamine hydrochloride (1 mmol, 69.49 mg), varying amounts of catalyst (5 mg, 10 mg, 15 mg, and 20 mg) were tested. Notably, 10 mg of Cu@Ag-CeO_2/chitosan proved to be sufficient, as higher amounts did not significantly improve the yield.

Further exploration of the model reaction indicated that employing Cu@Ag-CeO_2/chitosan as

in 95% yield of the desired product. Among various solvents tested, ethanol proved to be the most efficient, achieving product formation in just 10 minutes (refer to Tables S1–S4 in supporting information). With the optimized reaction conditions, the synthesis of 4-arylidene-isoxazolidinone derivatives was expanded to include various substrates, such as aromatic aldehydes. The catalyst showcased its versatility by producing significant quantities of products with aromatic aldehydes exhibiting diverse functional groups on the phenyl ring, as well as heterocyclic aldehydes. (Spectral data can be found in supporting Figures S1–S8).

Table 3. Substrate scope for the synthesis of 4-arylidene-isoxazolidinones[a] catalyzed by Cu@Ag-CeO_2/chitosan

Entry	Benzaldehyde	Time (min)	Yield (%)[b]	Product	Obs. M. pt. (°C) /Lit. M. Pt.
1 (4a)	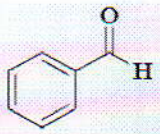	10	95	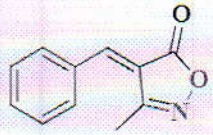	212-214/ 215-216[94]
2 (4b)	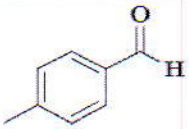	5	85	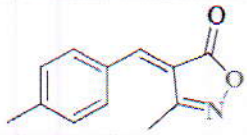	193-195/ 189–191[94]
3 (4c)	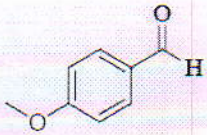	12	98	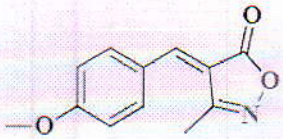	166-168/ 168-169[94]
5 (4e)	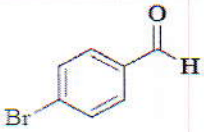	20	82	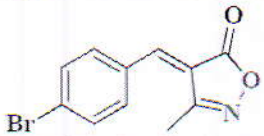	122-124/ 121–123[95]
6 (4f)	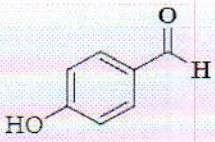	18	84	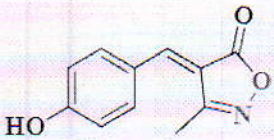	218-220/ 211–214[96]
7 (4g)	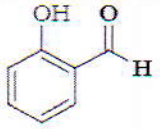	10	86	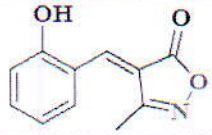	196-198/ 198–201[96]
8 (4h)	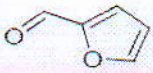	12	80	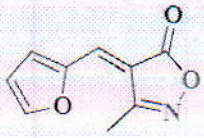	183-185/ 183-184[94]
9 (4i)		10	95	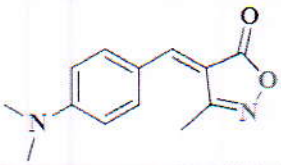	193-194/ 194–196[94]
10 (4j)	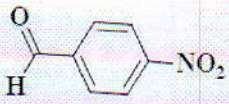	20	82	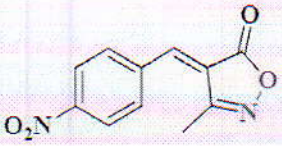	136-138/ 142–144[97]

11 (4k)	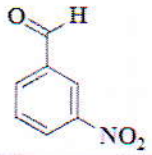	15	80	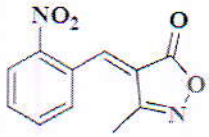	142-144/ 143-144[98]
12(4l)	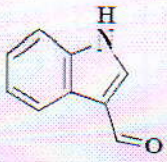	25	90	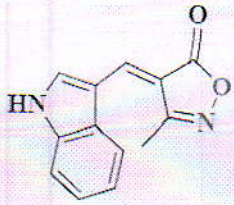	239-241/ 240-242[99]

[a]**Reaction conditions**: Benzaldehyde (1 mmol), ethyl acetoacetate (1 mmol), hydroxylamine hydrochloride (1 mmol), nanocatalyst (10 mg), and ethanol (2 ml) at 80 ℃.

[b]**Isolated yield** refers to yield obtained after crystallization with ethanol.

3.2.1.1. Proposed mechanism for the synthesis of 4-benzylidene-3-methylisoxazol-5(4*H*)-one

The proposed mechanism for the synthesis of 4-benzylidene-3-methylisoxazol-5(4*H*)-one catalyzed by the Cu@Ag-CeO_2/chitosan nanocomposite is illustrated in Scheme 2. In the initial phase of the reaction, Cu@Ag-CeO_2/chitosan activates the carbonyl groups within ethyl acetoacetate. Subsequently, the elimination of a water molecule results in the formation of oxime (A) through the condensation of ethyl acetate and hydroxylamine. The nanocatalyst facilitates the activation of oxime (A), leading to the cyclization of the intermediate (A) to form moiety (B). In the subsequent step, Knoevenagel condensation occurs between intermediate (B) and aldehyde in the presence of the catalyst, followed by the elimination of H_2O to yield 4-benzylidene-3-methylisoxazol-5(4*H*)-one.

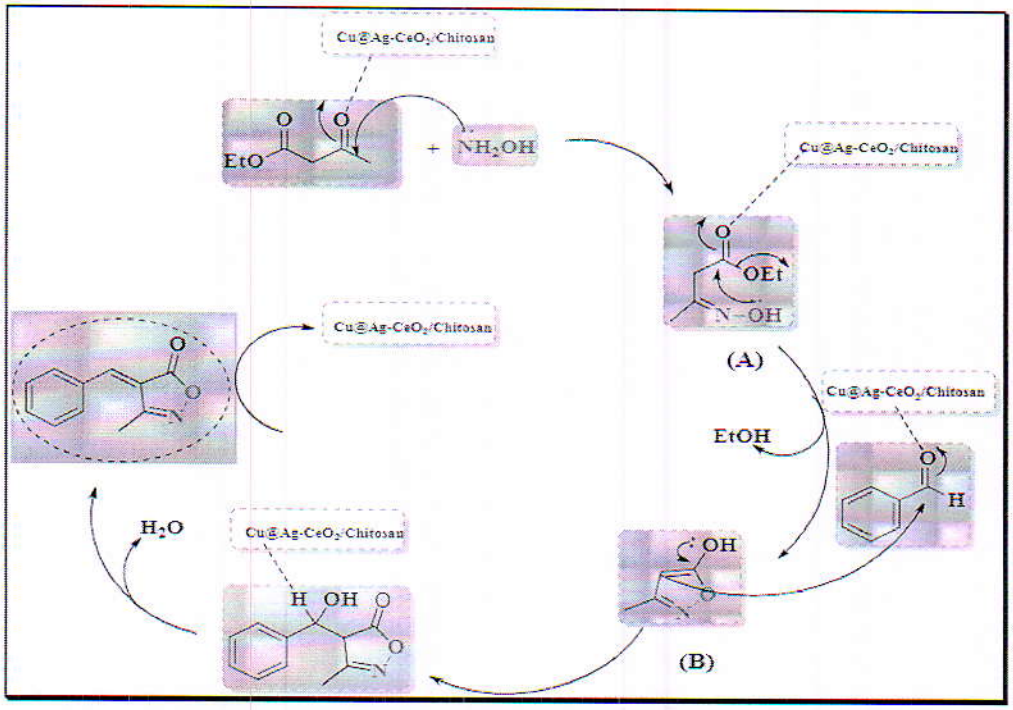

Scheme 2. Proposed mechanism for the synthesis of 4-benzylidene-3-methylisoxazol-5(4*H*)-one using Cu@Ag-CeO_2/chitosan.

3.2.2. Synthesis of amidoalkyl naphthols

The synthesis of amidoalkyl naphthol derivatives was used to examine the catalytic activity of Cu@ Ag-CeO_2/chitosan nanocomposite. As substrates, 2-naphthol, aromatic aldehydes, and amide were used (Scheme 3). The model reaction was carried out with varying amounts of catalyst and reactants benzaldehyde (1 mmol, 106.1 mg), 2-naphthol (1 mmol, 144.1 mg), and benzamide (1 mmol, 121.1 mg). The purpose of this reaction was to investigate the effect of reaction parameters such as reaction temperature, reaction time, and solvent. The catalyst amount was also tested, and 5 mg, 10 mg, 15 mg, and 20 mg of Cu@Ag-CeO_2/chitosan were chosen to study the reaction. It was discovered that 10 mg of catalyst was sufficient to achieve a high product yield. The reaction was carried out at several temperatures, including room temperature, 40, 60, 80, 100, and 120 °C, with the greatest yield of the primary product obtained at 100 °C under solvent-free conditions. The reaction time was then explored by monitoring the reaction with TLC; it was discovered that the reaction completed after 15 minutes. When the identical reactants were tested with different solvents under different conditions, it was revealed that the reaction progressed quite well solvent free, with 98 percent product achieved in 15 minutes when compared to other solvents refer to (Tables S5–S8 in supporting information). Ultimately, following the optimization of reaction conditions, the synthesis of amidoalkyl naphthol derivatives was carried out using a range of substrates, encompassing aromatic aldehydes and amides. The goal was to explore the catalyst's applicability, as depicted in Table 4. Aromatic aldehydes featuring diverse functional groups on the phenyl ring, along with heterocyclic aldehydes and different amides, consistently produced satisfactory to excellent yields (Table 4). (Spectral data can be found in supporting Figures S9–S16).

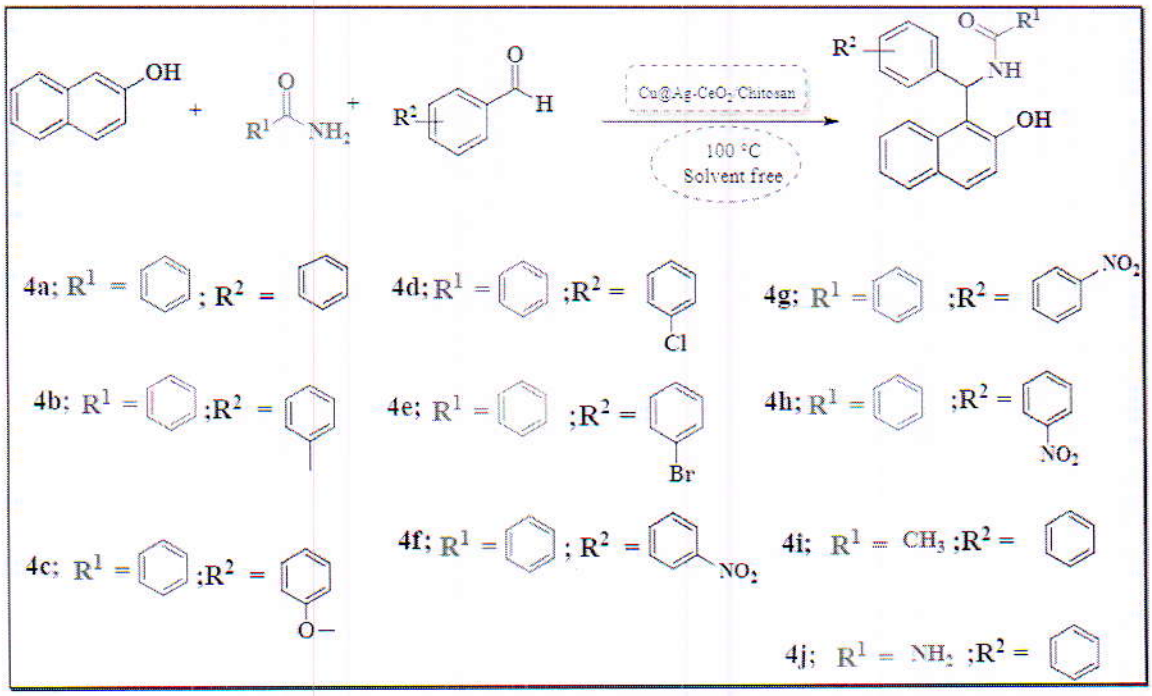

Scheme 3. Synthesis of 1-amidoalkyl-2-naphthols.

Table 4. Substrate scope for the synthesis of 1-amidoalkyl-2-naphthols catalyzed by Cu@Ag-CeO_2/chitosan.

Entry	Benzaldehyde (R^1)	Amide (R^2)	Time (min)	Yield (%)[b]	Obs. M. pt. (C) /Lit. M. Pt.
1 (4a)	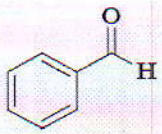	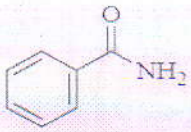	15	98	230-232/ 234-236[100]
2 (4b)	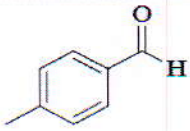	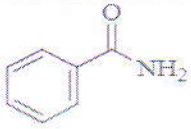	30	95	190-192/ 192–193[86]
3 (4c)	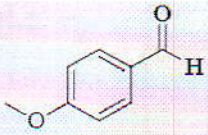	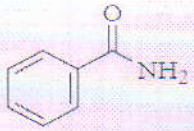	10	85	206-208/ 208–210[101]
4 (4d)	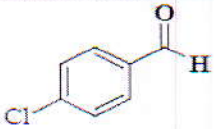	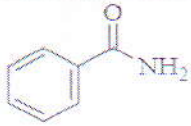	15	88	178-180/ 177-178[86]
5 (4e)	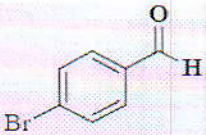	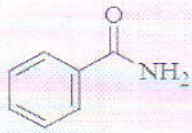	15	94	182-184/ 183–184[102]
6 (4f)	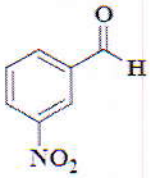	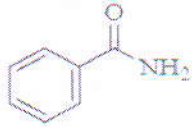	20	90	241-243/ 242–243[103]
7 (4g)		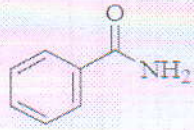	10	85	236-238/ 237–239[87]
8(4h)	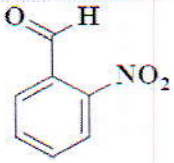	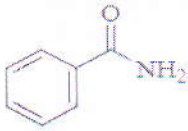	10	82	265-267/ 264–266[87]
9 (4i)	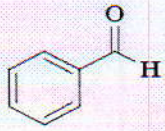	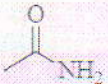	30	95	238-240/ 238-240[104]
10(j)	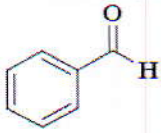	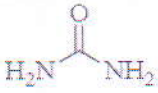	35	80	174-176/ 172–174[54]

[a]**Reaction conditions**: benzaldehyde (1 mmol), 2-naphthol (1 mmol), amide (1 mmol), nanocatalyst (10 mg), at 100℃.

[b]**Isolated yield** refers to yield obtained after purification.

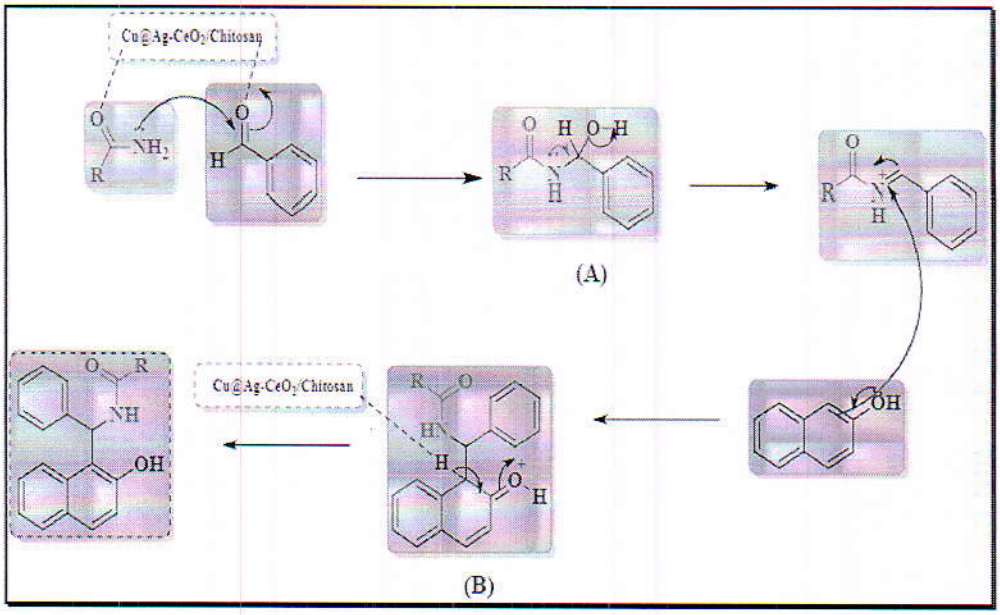

Scheme 4. Proposed mechanism for preparation of 1-amidoalkyl naphthol.

3.2.2.1. Proposed mechanism for preparation of amidoalkyl naphthol

The reaction mechanism for the synthesis of 1-amidoalkyl-2- naphthol is depicted in Scheme 4. A possible reaction mechanism was proposed. To begin, benzaldehyde was activated with Cu@Ag-CeO_2/chitosan. The benzaldehyde carbonyl group was then attacked by benzamide, giving intermediates (A). Furthermore, the intermediate (A) was employed to attack and condense 2-naphthol to give (B). Deprotonation of intermediates (B) yielded the desired product.

3.3. Recyclability of Cu@Ag-CeO_2/chitosan

The essential factors in the domain of green chemistry include the ability of the nanocatalyst to be recycled and reused. To demonstrate its sustained effectiveness, we examined model reactions involving benzaldehyde with ethyl acetoacetate and hydroxylamine hydrochloride (resulting in 4-benzylidene-3-methylisoxazol-5(4*H*)-one), as well as reactions with benzaldehyde, 2-naphthol, and benzamide (resulting in 1-amidoalkyl-2-naphthol), over five cycles. In each cycle, the reaction mixture was dissolved in ethyl acetate, and the catalyst was separated through filtration, washed with ethanol, and dried in an oven at 70°C for 60 minutes for subsequent use. Importantly, the model reaction proceeded smoothly with the recovered Cu@Ag-CeO_2/chitosan even after five cycles, demonstrating no prolongation of the reaction time or significant reduction in yield (Fig 14). Catalyst was checked with IR for any structural effects which shows no change (Fig 15).

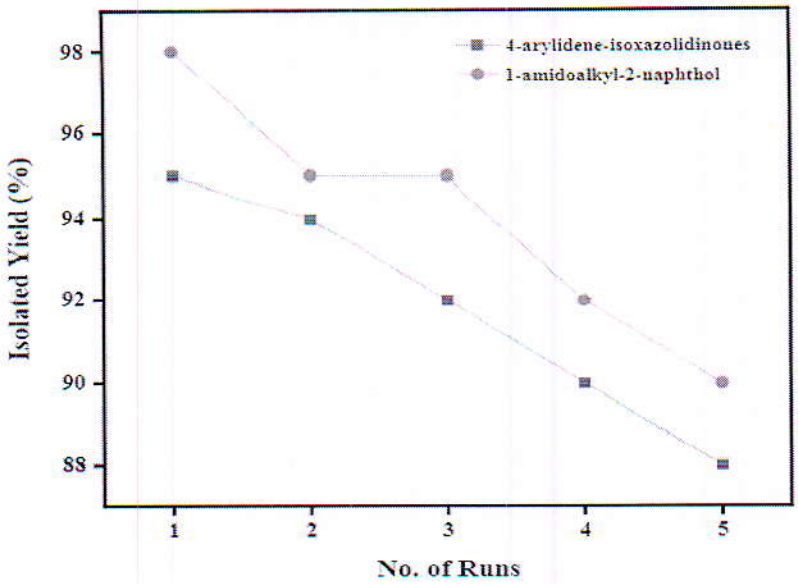

Figure 14. Recyclability diagram of Cu@Ag-CeO_2/chitosan. Reaction conditions (1) benzaldehyde (1 mmol), ethyl acetoacetate (1 mmol), hydroxylamine hydrochloride (1 mmol), nanocatalyst (10 mg), and ethanol (2 ml) at 80 ℃ (2) benzaldehyde (1 mmol), 2-naphthol (1 mmol), amide (1 mmol), nanocatalyst (10 mg), at 100 ℃.

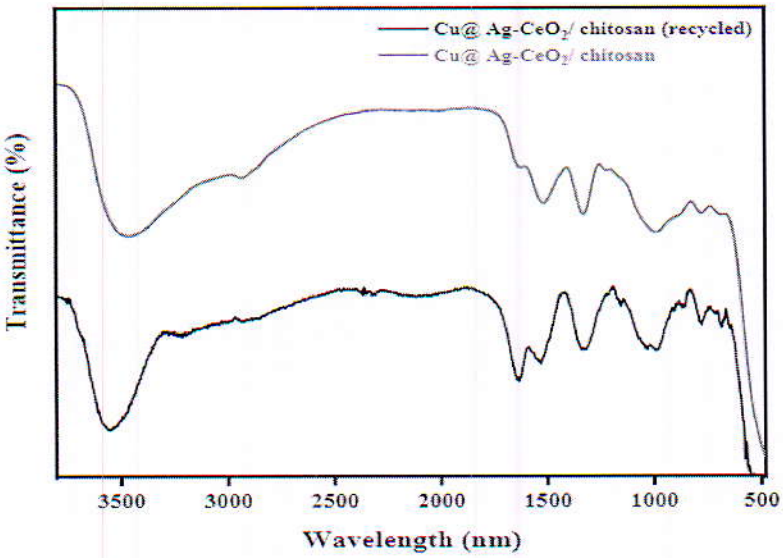

Figure 15. IR data for recyclability of Cu@Ag-CeO_2/chitosan.

3.4. Synergistic effects in Cu@Ag-CeO_2/chitosan

The FE-SEM analysis reveals a well-blended nanocomposite that significantly enhances catalytic performance. Clear and evenly dispersed Cu and Ag-CeO_2 particles were observed throughout the chitosan matrix, creating a substantial surface area. The introduction of copper and Ag-CeO_2 enhances the structural features of chitosan, evident in increased roughness and porosity on the surface of the resultant nanocomposite. This improvement signifies heightened dispersion and uniformity. The synergies occurring at the interface between the metal and support, along with the exchange of charges between the metal and metal oxide, could potentially enhance catalytic performance.

The antibacterial effectiveness of ceria (CeO_2), silver-doped ceria (Ag-CeO_2), silver-doped ceria/chitosan (Ag-CeO_2/chitosan), and copper plus silver-doped ceria/chitosan (Cu@Ag-CeO_2/chitosan) nanocomposite against Escherichia coli (gram-positive) and Klebsiella pneumoniae (gram-negative) bacteria was assessed through the agar well diffusion technique. Bacterial plates were prepared using the standard pour plate procedure, with glycerol stock cultures of bacteria revived and inoculated onto nutrient agar. The agar media, autoclaved for each experiment, was inoculated, and poured into petri plates. Wells were created, filled with various concentrations of nanoparticle samples, and controls (autoclaved distilled water and chloramphenicol) were included. Autoclaved distilled water and chloramphenicol were employed as negative and positive controls, respectively. The assessment of antibacterial efficacy involved the calculation of inhibition zones (ZOI), which were measured around the wells following a 24-hour incubation period at 37°C.

All four nanoparticles exhibited toxicity against the studied bacterial pathogens at different concentrations, as evidenced by the ZOI against Escherichia coli (Table 5) and Klebsiella pneumoniae (Table 6). Among them, Ag-CeO_2 demonstrated the strongest inhibitory effect against Escherichia coli, with a ZOI of 16 mm at the highest concentration (0.5 mg/ml) (Figure 16). Further investigation into the minimum inhibitory concentration (MIC) revealed that Ag-CeO_2 was most potent against Escherichia coli, with a MIC of 2.5%. Interestingly, the efficacy decreased when Ag-CeO_2 was added into chitosan (Ag-CeO_2/chitosan), having a 10% MIC. Copper and Ag-CeO_2/chitosan (Cu@Ag-CeO_2/chitosan) showed no anti-Escherichia coli activity (Figure 17).

Against Klebsiella pneumoniae, CeO_2 doped with silver (Ag-CeO_2) exhibited the strongest inhibitory activity, with a ZOI of 15 mm (Figure 15). The potency increased upon doping ceria with Ag, resulting in Ag-CeO_2 having a MIC of 2.5%. However, the MIC further decreased to 10% and 75% on adding Ag-CeO_2 to chitosan (Ag-CeO_2/chitosan) and Cu@Ag-CeO_2/chitosan, respectively.

Table 5. ZOI of different nanoparticles against *Escherichia coli*.

Zone of Inhibition (mm) against *Escherichia coli*					
	Positive control	100%	75%	50%	25%
CeO_2	24.0	12.0	11.5	11.0	-
Ag-CeO_2	25.0	16.0	15.0	14.0	13.0
Ag-CeO_2/chitosan	26.0	15.0	13.0	11.0	11.0
Cu@Ag-CeO_2/chitosan	23.0	-	-	-	-

Table 6. ZOI of different nanoparticles against Klebsiella pneumoniae.

Zone of Inhibition (mm) against *Klebsiella pneumoniae*					
	Positive control	100%	75%	50%	25%
CeO_2	24.0	12.5	12.0	11.0	-
Ag-CeO_2	25.0	15.0	15.0	13.0	13.0
Ag-CeO_2 chitosan	30.0	14.0	16.0	15.0	14.0
Cu@Ag-CeO_2 chitosan	29.0	0.9	-	-	-

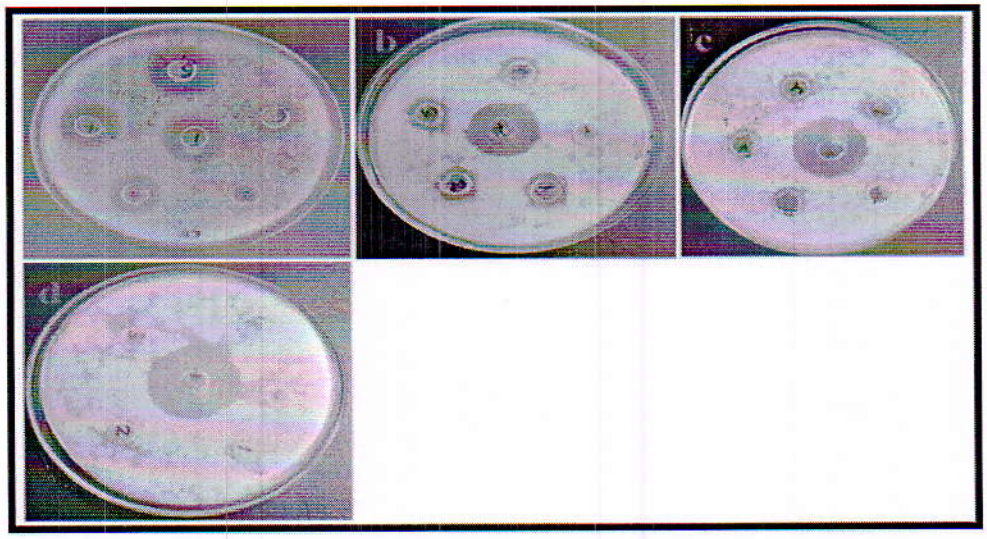

Figure 16. Antibacterial activity of (a) CeO_2, (b) Ag-CeO_2, (c) Ag-CeO_2/chitosan, (d) Cu@Ag-CeO_2/chitosan against *Escherichia coli*.

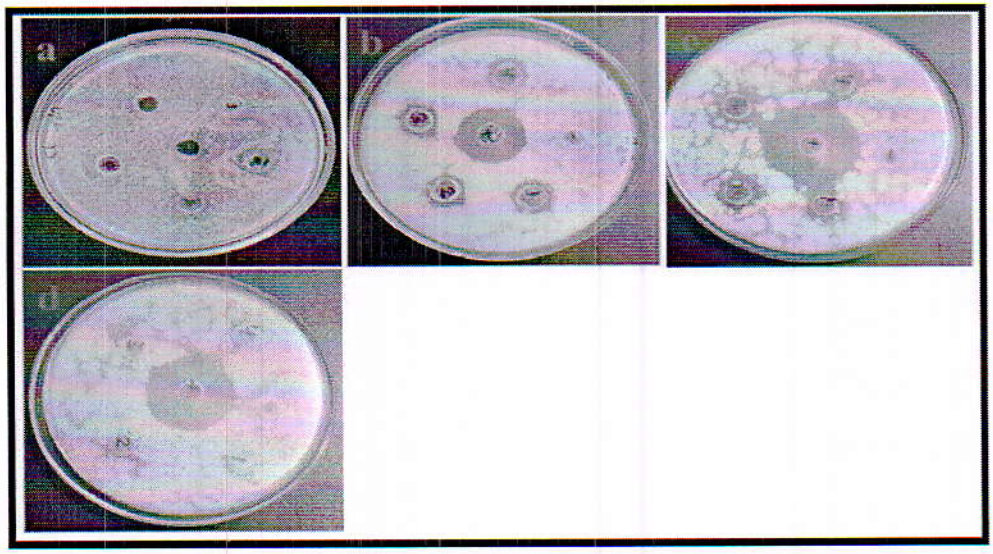

Figure 17. Antibacterial activity of (a) a) CeO_2, (b) Ag-CeO_2, (c) Ag-CeO_2/chitosan Cu@Ag-CeO_2/chitosan against *Klebsiella pneumoniae*.

3.6. Comparison of the catalytic activity of Cu@Ag-CeO_2/chitosan

Comparison of the catalytic activity of Cu@Ag-CeO_2/chitosan with recently published work has

Table 7. Comparison of catalytic activity of designed catalyst with recent published works.

Product	Catalyst	Reaction Time	Reaction conditions	Yield (%)	References
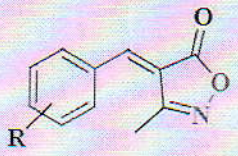	MnO_2@zeolite-Y	5 min	Solvent-free 100 °C	94	Kalhor et al. [105].
	10 mole % Tartaric acid	100 min	H_2O, RT	88	Khandebharad et al[106]
	6-methylguanamine @SCCFNPs	60	H_2O, 60 ℃	93	Saadati et al[81]
	Pyridine	60 min	Ethanol, reflux	77	Abhlajan et al.[80]
	Cu@ Ag-CeO_2/chitosan	10 min	EtOH, 80 ℃	95	This work
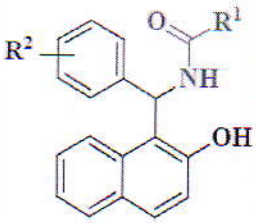	Schiff-base functionalized – core shell MNPs	70 min	Solvent free 80 ℃	94	Ghorbani et al. [107]
	Zinc oxide nanoparticles	35 min	Solvent-free, 120-130 °C	88	Singh et al. [108]
	10 mol% Hexanesulphonic acid	8 min	Microwave	92	Naryanan, et al. [109]
	Nickel-doped SnO_2	110 min	Solvent free, 100 °C	87	Dehbhashi et al. [110]
	Cu@ Ag-CeO_2/chitosan	15 min	Solvent free, 100 °C	90	This work

3.7. DFT Results

3.7.1. Structural features

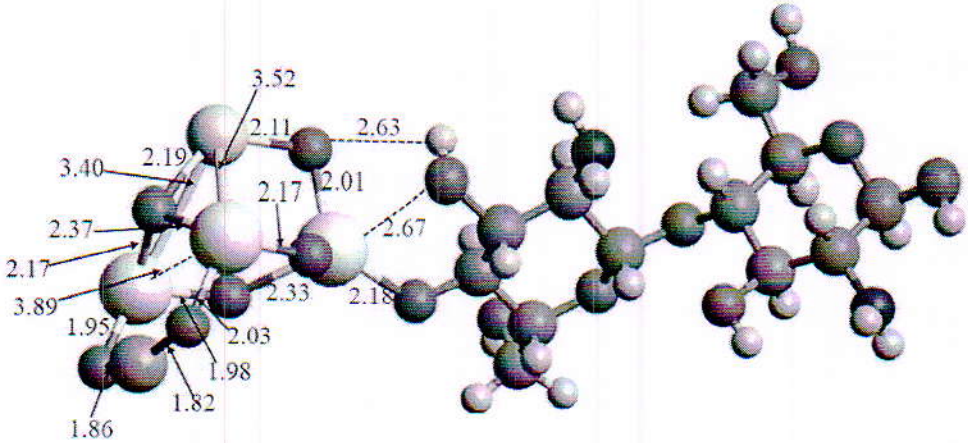

Figure 17. Structure of the model for the Cu@Ag-CeO_2/chitosan nanocomposite optimized at the B3LYP/SDD level in the gas phase. Selected bond distances are given in angstroms. Color coding: red for O, light grey for H, dark grey for C, dark blue for N, light yellow for Ce, silver-grey for Ag, and orange for Cu.

In Figure 17 the gas-phase B3LYP/SDD optimized model structure for the Cu@Ag-CeO_2/chitosan nanocomposite is provided. We chose for the Cu@Ag-CeO_2 NP the Ce_3CuAgO_7 model, which was connected through the oxo-bridge to two chitosan monomer units used to model the chitosan polymer. The ground state for this model structures was found to be doublet. From the optimized structure, it can be seen that in the metal-oxo nanocluster both Cu and Ag, along with the O-centers, are highly accessible for interactions with any molecules approaching the nanocomposite, thus supporting the observed high catalytic activity of the nanocomposite. From the optimized structure, it can be suggested also that along with the O-bridges the Cu@Ag-CeO_2 NP could be connected to the chitosan matrix by dipole-dipole interactions (exemplified by probable Ce···OH(chitosan) interactions) and hydrogen bonds (exemplified by probable O(NP)···HO(chitosan) interactions), see also discussion of Mulliken charges in the model structure below.

3.7.2. Mulliken charges

In Figure 18 the Mulliken charges and spins on selected atoms of the model structure of the nanocomposite are provided (it was not possible to perform Natural Bond Orbital analysis due to technical problems). As can be seen, the oxygens of the Ce_3CuAgO_7 NP carry significant negative charges, -0.359— -0.610e, whereas the Ce-centers carry significant positive charges, 0.942—0.998e, but the Ag- and Cu-centers have quite low positive charges, 0.088e and 0.005e, respectively. Furthermore, oxygen and nitrogen atoms of the chitosan matrix carry significant negative charges, which would facilitate their interactions.

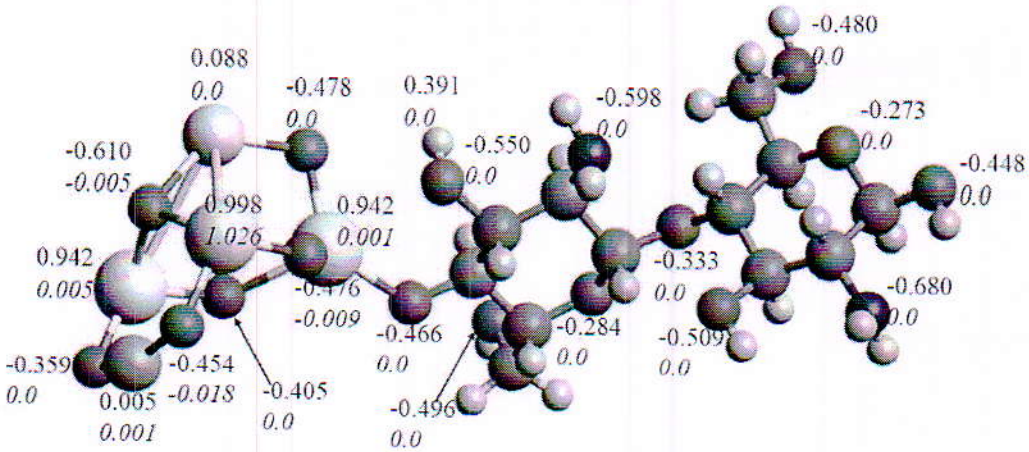

Figure 18. Mulliken charges, e, (regular font) and spins (italics) on the selected atoms of the model for the Cu@Ag-CeO_2/chitosan nanocomposite optimized at the B3LYP/SDD level in the gas phase.

with the Cu@Ag-CeO_2 NPs, as well as formation of hydrogen bonding with these NPs via H-atom of the OH and, possibly, NH_2 groups of the matrix. As expected, all unpaired spin density is concentrated at the Ce_3CuAgO_7 NP, with one Ce-center bearing almost all α-spin, 1.026e, with two other Ce-centers having negligible amounts of α-spin density, 0.001e and 0.005e, whereas the Ag-center does not have any unpaired spin on it at all, the Cu-center has negligible amount of α-spin density, 0.001e, and the oxygens carry none or very little of β-spin density, -0.009e and -0.018e. These results suggest quite high potential catalytic activity of the Cu@Ag-CeO_2 NPs, tentatively with the Ce-center(s) playing more significant role than the Ag- and Cu-centers. However, this issue requires further investigation which was not the subject of the current study.

3.7.3. Frontier molecular orbitals and molecular electrostatic potential (MEP)

Figure 19 presents the frontier molecular orbitals (MOs) (Fig. 19a) and plot of molecular electrostatic potential (Fig. 19b) for the model nanocomposite structure. As can be seen from fig. 19a, both HOMO and LUMO are dominated by the Ce_3CuAgO_7 NP, which implies the Cu@Ag-CeO_2 NP participation in the oxidation-reduction and other chemical processes and thus its catalytical activity. Furthermore, closer consideration of the frontier MOs shows that the HOMO is contributed by essentially all metal centers and most of the oxygen centers, whereas the LUMO is mostly contributed by the metal and oxygen centers located further away from the chitosan moieties, which might suggest ideas about space localization of oxidation-reduction processes occurring on the Cu@Ag-CeO_2 NP relative to the chitosan matrix. Further, the MEP plot (Fig. 19b) shows noticeable accumulation of positive electrostatic potential (as indicated by blue color) on the Ce_3CuAgO_7 NP, especially on its side located further away from the chitosan matrix, including the Ag-center. This accumulation renders the nanoparticles electrophilic properties, which supports suggested mechanisms of the

was suggested to occur. However, this issue also requires more detailed investigation, which should be the subject of the follow-up study.

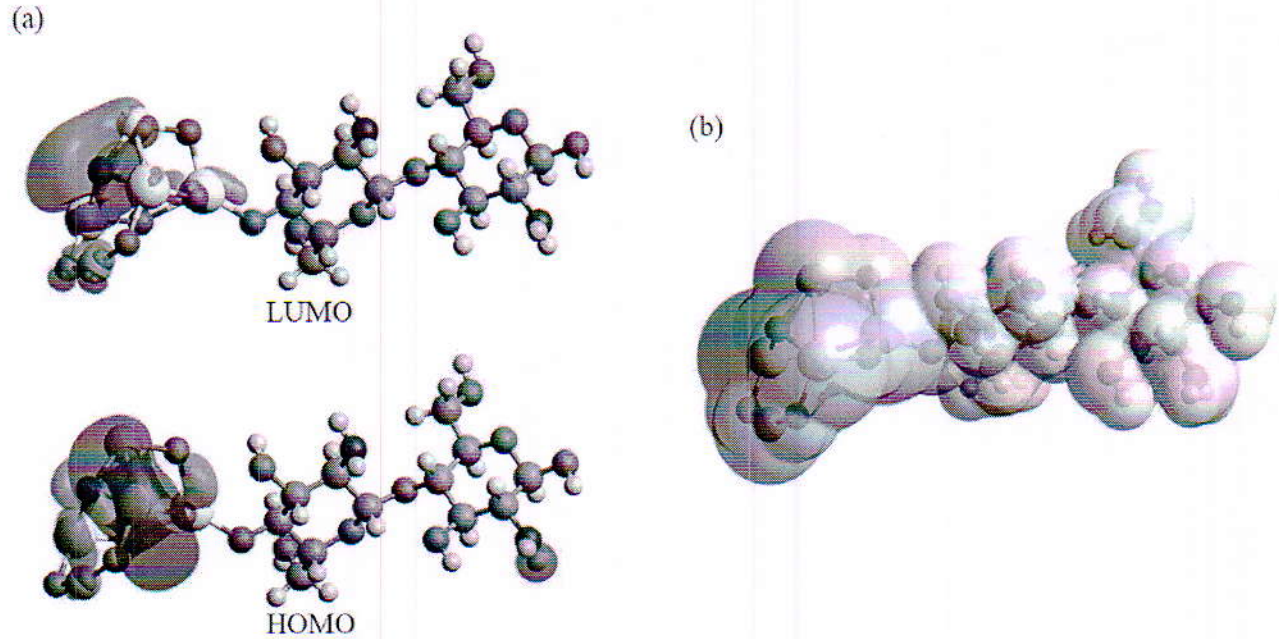

Figure 19. Frontier molecular orbitals (a) and MEP plot (b) for the model for the Cu@Ag-CeO_2/chitosan nanocomposite optimized at the B3LYP/SDD level in the gas phase.

Conclusions

We have reported the synthesis and characterization of the efficient polymer-based nanocomposite which has been studied using a variety of techniques, including FTIR, PXRD, FE-SEM, EDX, elemental mapping, and HRTEM, along with the computational approach. The nanocatalyst surface area was calculated. Its application as a nanocatalyst for the multicomponent synthesis of 4-arylidene-isoxazolidinones and 1-amidoalkyl naphthol has been demonstrated successfully. The various nanocomposite properties, including the bandgap, were studied in details. It was shown to be cost-effective and falls under the category of "green chemistry" because the nanocatalyst recyclability was tested over the course of up to five consecutive runs. The DFT results provided significant and comprehensive support for the experimental findings.

Associated content

Materials and characterization of synthesized nanocomposite, Tables, Spectral data, ^{1}HNMR, ^{13}CNMR, Mass and IR spectra of synthesized compounds

Acknowledgments

The authors express their gratitude to the Department of Chemistry, University of Jammu, Jammu, and the funding agencies supporting instrumental resources, including NMR (DST-PURSE), BET (RUSA 2.0), TGA (UGC-SAP), and PL (RUSA 2.0). Authors also thankful to University of Jammu for providing Research and Seed Money Grant. Additionally, the authors acknowledge IIT Roorkee

was suggested to occur. However, this issue also requires more detailed investigation, which should be the subject of the follow-up study.

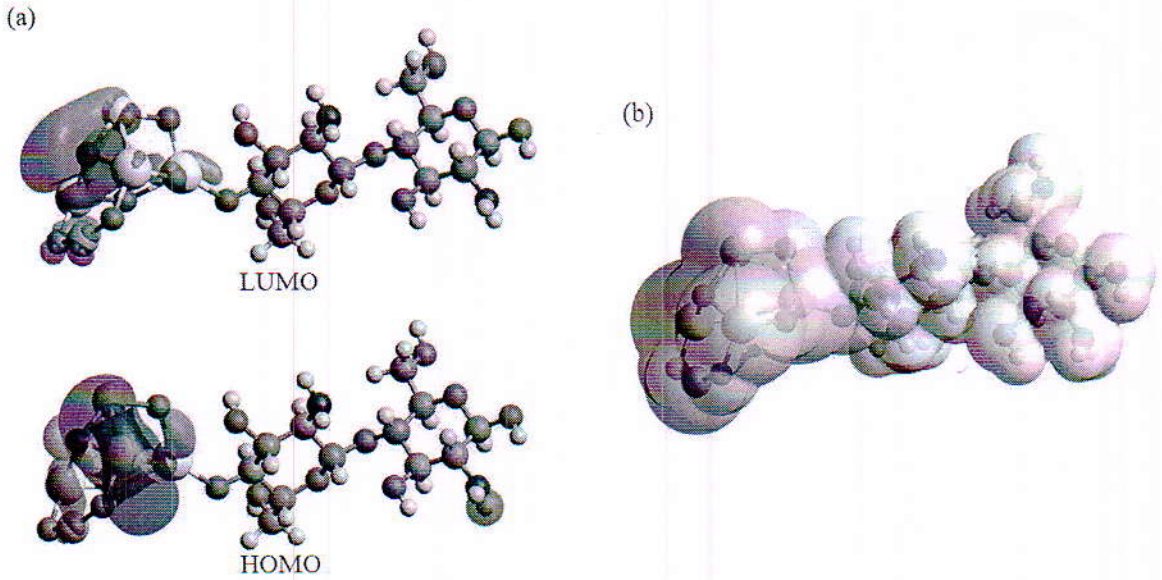

Figure 19. Frontier molecular orbitals (a) and MEP plot (b) for the model for the Cu@Ag-CeO_2/chitosan nanocomposite optimized at the B3LYP/SDD level in the gas phase.

Conclusions

We have reported the synthesis and characterization of the efficient polymer-based nanocomposite which has been studied using a variety of techniques, including FTIR, PXRD, FE-SEM, EDX, elemental mapping, and HRTEM, along with the computational approach. The nanocatalyst surface area was calculated. Its application as a nanocatalyst for the multicomponent synthesis of 4-arylidene-isoxazolidinones and 1-amidoalkyl naphthol has been demonstrated successfully. The various nanocomposite properties, including the bandgap, were studied in details. It was shown to be cost-effective and falls under the category of "green chemistry" because the nanocatalyst recyclability was tested over the course of up to five consecutive runs. The DFT results provided significant and comprehensive support for the experimental findings.

Associated content

Materials and characterization of synthesized nanocomposite, Tables, Spectral data, ^{1}HNMR, ^{13}CNMR, Mass and IR spectra of synthesized compounds

Acknowledgments

The authors express their gratitude to the Department of Chemistry, University of Jammu, Jammu, and the funding agencies supporting instrumental resources, including NMR (DST-PURSE), BET (RUSA 2.0), TGA (UGC-SAP), and PL (RUSA 2.0). Authors also thankful to University of Jammu for providing Research and Seed Money Grant. Additionally, the authors acknowledge IIT Roorkee for FE-SEM, EDX, and elemental mapping, IIT Jammu for P-XRD, and IIT Delhi for HR-TEM.

Aleksey Kuznetsov appreciates the financial support of USM. Powered@NLHPC: This research was partially supported by the supercomputing infrastructure of the NLHPC (ECM-02). Also, this research was supported by the high-performance computing system of PIDi-UTEM (SCC-PIDi-UTEM CONICYT - FONDEQUIP - EQM180180).

References

1. Fu, S.; Sun, Z.; Huang, P.; Li, Y.; Hu, N., Some basic aspects of polymer nanocomposites: A critical review. *Nano Mater. Sci.* **2019,** *1* (1), 2-30.

2. Bustamante-Torres, M.; Romero-Fierro, D.; Arcentales-Vera, B.; Pardo, S.; Bucio, E., Interaction between Filler and Polymeric Matrix in Nanocomposites: Magnetic Approach and Applications. *Polymers (Basel)* **2021,** *13* (17), 2998.

3. Müller, K.; Bugnicourt, E.; Latorre, M.; Jorda, M.; Echegoyen Sanz, Y.; Lagaron, J. M.; Miesbauer, O.; Bianchin, A.; Hankin, S.; Bölz, U., Review on the processing and properties of polymer nanocomposites and nanocoatings and their applications in the packaging, automotive and solar energy fields. *Nanomaterials* **2017,** *7* (4), 74.

4. Utracki, L. A.; Sepehr, M.; Boccaleri, E., Synthetic, layered nanoparticles for polymeric nanocomposites (PNCs). *Polym. Adv. Technol.* **2007,** *18* (1), 1-37.

5. Rangari, V. K.; Mohammad, G. M.; Jeelani, S.; Hundley, A.; Vig, K.; Singh, S. R.; Pillai, S., Synthesis of Ag/CNT hybrid nanoparticles and fabrication of their nylon-6 polymer nanocomposite fibers for antimicrobial applications. *Nanotechnology* **2010,** *21* (9), 095102.

6. Saini, R. K.; Bajpai, A. K.; Jain, E., " 13 Advances in bionanocomposites for biomedical applications. *Biodegradable and Biocompatible Polymer Composites: Processing, Properties and Applications* **2017,** pp *379*.

7. Binandeh, M.; Rostamnia, S.; Karimi, F., MNPs-IHSPN nanoparticles in multi-application with absorption of bio drugs in vitro. *Biochem. Biophys. Rep.* **2021,** *28*, 101159.

8. Rahman, A.; Ali, I.; Al Zahrani, S. M.; Eleithy, R. H., A review of the applications of nanocarbon polymer composites. *Nano* **2011,** *6* (03), 185-203.

9. Kausar, A.; Rafique, I.; Muhammad, B., Aerospace application of polymer nanocomposite with carbon nanotube, graphite, graphene oxide, and nanoclay. *Polym.-Plast. Technol. Mater.* **2017,** *56* (13), 1438-1456.

10. Fan, J.; Njuguna, J., An introduction to lightweight composite materials and their use in transport structures. In *Lightweight Composite Structures in Transport*, Elsevier: 2016; pp 3-34.

11. Kazemi, M.; Ghobadi, M.; Mirzaie, A., Cobalt ferrite nanoparticles (CoFe2O4 MNPs) as catalyst and support: magnetically recoverable nanocatalysts in organic synthesis. *Nanotechnol. Rev.* **2018,** *7* (1), 43-68.

12. Solomon, L.; Uzor, C. A.; Alalibo, I. K., Harnessing Green Technology for Ecological Sustainability and Healthy Citizenry. *J. Am. sci.* **2019,** *15* (8), 81-89.

13. Glaser, J. A., Green chemistry with nanocatalysts. Springer: 2012.

ACS Paragon Plus Environment